



Theses and Dissertations

2005-03-17

A Tool Wear Comparative Study in Turning Versus Computer Simulation in 1018 Steel

Woodrow D. Miner
Brigham Young University - Provo

Follow this and additional works at: <https://scholarsarchive.byu.edu/etd>



Part of the [Construction Engineering and Management Commons](#), and the [Manufacturing Commons](#)

BYU ScholarsArchive Citation

Miner, Woodrow D., "A Tool Wear Comparative Study in Turning Versus Computer Simulation in 1018 Steel" (2005). *Theses and Dissertations*. 277.
<https://scholarsarchive.byu.edu/etd/277>

This Thesis is brought to you for free and open access by BYU ScholarsArchive. It has been accepted for inclusion in Theses and Dissertations by an authorized administrator of BYU ScholarsArchive. For more information, please contact scholarsarchive@byu.edu, ellen_amatangelo@byu.edu.

A TOOL WEAR COMPARATIVE STUDY IN TURNING
VERSUS COMPUTER SIMULATION
IN 1018 STEEL

by

Woodrow D. Miner

A thesis submitted to the faculty of
Brigham Young University
in partial fulfillment of the requirements for the degree of
Masters of Science

School of Technology
Brigham Young University

April 2005

Copyright © 2005 Woodrow D. Miner

All rights reserved

BRIGHAM YOUNG UNIVERSITY

GRADUATE COMMITTEE APPROVAL

of a thesis submitted by

Woodrow D. Miner

This thesis has been read by each member of the following graduate committee and by majority vote has been found to be satisfactory.

Date

Kent E. Kohkonen

Date

Perry W. Carter

Date

Michael P. Miles

BRIGHAM YOUNG UNIVERSITY

FINAL READING APPROVAL

As chair of the candidate's graduate committee, I have read the thesis of Woodrow D. Miner in its final form and have found that (1) its format, citations, and bibliographical style are consistent and acceptable and fulfill university and department style requirements; (2) its illustrative materials including figures, tables, and charts are in place; and (3) the final manuscript is satisfactory to the graduate committee and is ready for submission to the university library.

Date

Kent E. Kohkonen
Chair, Graduate Committee

Approved for the Department

Thomas L. Erikson
Director, School of Technology

Accepted for the College

Douglas M. Chabries
Dean, Ira A. Fulton College of
Engineering and Technology

ABSTRACT

A TOOL WEAR COMPARATIVE STUDY IN TURNING VERSUS COMPUTER SIMULATION IN 1018 STEEL

Woodrow D. Miner

School of Technology

Masters of Science

The material removal process uses cutting tools in order to produce the desired shape of the workpiece. Tool wear has been a problem for cutting tools, since cutting tools wear and break. Research has been accomplished in the tool wear field for tool life and more recently tool wear. The computer generation has created a method to simulate the material removal process. These computer simulations model the cutting tool reaction with the workpiece. Many of the simulation models use finite element analysis to calculate the reaction of the cutting tool. Different finite element models are being used throughout the world for research. This thesis used an updated Lagrangian model in conjunction with Archard's law to predict the wear of the cutting tool.

This research used experimental data to correlate with simulation data to see whether or not Archard's law was a good approximation for tool wear. The research used different side rake angles and cutting surface speed to test the simulation. Shear angle, contact length, cutting ratio, and force are used to provide output values to compare the experimental and computer simulation data.

The comparative results showed good trends between the experimental and computer simulation data in every comparison. The results also showed a good approximation for the force and contact length values. Archard's law can be used to model wear on cutting tools with further research.

ACKNOWLEDGMENTS

First and foremost I would like to express deep gratitude for my wife, Erin; she has supported me through the years. My children, Jerusha, Syrus, Tavish and Arwynn have brought fun into my life during my school years. I would also like to thank my family for their support. I have many friends to thank as well for their help and support during this thesis. I would like to mention the staff at the PML for their help and technical support, especially Eric Bylund and Robert Perry. I would like to thank Clint Bybee for his help in reading amps and a person I could consult with. I would like to thank my committee members Mike Miles and Perry Carter for their understanding of my leave of absence. Lastly I would like to thank Kent Kohkonen for being my committee chair and friend.

TABLE OF CONTENTS

TITLE PAGE	i
COPYRIGHT PAGE	iii
GRADUATE COMMITTEE APPROVAL.....	v
FINAL READING APPROVAL.....	vii
ABSTRACT.....	ix
ACKNOWLEDGMENTS	xiii
LIST OF TABLES.....	xxi
LIST OF FIGURES	xxv
CHAPTER 1	1
1.1 COMPUTER SIMULATION INTRODUCTION.....	2
1.2 STATEMENT OF THE PROBLEM.....	3
1.2.1 NULL HYPOTHESES	3
1.2.2 THESIS STATEMENT	3
1.3 JUSTIFICATION	4
1.4 DELIMITATIONS	4
1.5 DEFINITION OF TERMS	5
CHAPTER 2	11
2.1 BACKGROUND INFORMATION	11
2.1.1 CUTTING TOOLS	11

2.1.2 TOOL WEAR	13
2.1.3 FINITE ELEMENT ANALYSIS	16
2.2 RESEARCH INFORMATION.....	22
2.2.1 ARCHARD’S LAW	22
2.2.2 COMPUTER SIMULATION CAPABILITIES	22
CHAPTER 3	25
3.1 EQUIPMENT	25
3.2 TEST PROCEDURES	26
3.3 TURNING EXPERIMENT	26
3.3.1 WORKPIECE PREPARATION.....	27
3.3.2 CUTTING TOOLS	28
3.3.3 TURNING PARAMETERS	29
3.3.4 PROGRAM SETUP.....	30
3.3.5 OUTPUT INFORMATION.....	30
3.3.6 PROCEDURES FOR THE TURNING EXPERIMENT.....	34
3.4 COMPUTER SIMULATION.....	37
3.4.1 PARAMETERS	37
3.4.2 MATERIAL LAW.....	38
3.4.3 FINITE ELEMENT ANALYSIS	39
3.4.4 FRICTION LAW	39
3.4.5 WEAR MODEL.....	39
3.5 COMPARITIVE STUDY OF DATA.....	40
CHAPTER 4	43

4.1 EXPERIMENTAL RESULTS.....	43
4.1.1 SIDE RAKE ANGLE COMPARISON FOR THE EXPERIMENTAL RESULTS	44
4.1.1.1 THE 0° SIDE RAKE ANGLE TOOLS	44
4.1.1.1.1 THE 0° SIDE RAKE ANGLE AT 25 M/MIN	44
4.1.1.1.2 THE 0° SIDE RAKE ANGLE AT 30 M/MIN	46
4.1.1.1.3 THE 0° SIDE RAKE ANGLE AT 35 M/MIN	48
4.1.1.1.4 COMPARISON OF THE 0° SIDE RAKE ANGLE TOOL.....	50
4.1.1.2 THE 5° SIDE RAKE ANGLE TOOLS	51
4.1.1.2.1 THE 5° SIDE RAKE ANGLE AT 25 M/MIN	51
4.1.1.2.2 THE 5° SIDE RAKE ANGLE AT 30 M/MIN	53
4.1.1.2.3 THE 5° SIDE RAKE ANGLE AT 35 M/MIN	55
4.1.1.2.4 COMPARISON OF THE 5° SIDE RAKE ANGLE TOOL.....	57
4.1.1.3 THE 10° SIDE RAKE ANGLE TOOLS	58
4.1.1.3.1 THE 10° SIDE RAKE ANGLE TOOL AT 25 M/MIN	58
4.1.1.3.2 THE 10° SIDE RAKE ANGLE TOOL AT 30 M/MIN	60
4.1.1.3.3 THE 10° SIDE RAKE ANGLE TOOL AT 35 M/MIN	61
4.1.1.3.4 COMPARISON OF THE 10° SIDE RAKE ANGLE TOOL.....	63
4.1.1.4 THE 15° SIDE RAKE ANGLE TOOLS	64
4.1.1.4.1 THE 15° SIDE RAKE ANGLE TOOL AT 25 M/MIN	64
4.1.1.4.2 THE 15° SIDE RAKE ANGLE TOOL AT 30 M/MIN	66
4.1.1.4.3 THE 15° SIDE RAKE ANGLE TOOL AT 35 M/MIN	68
4.1.1.4.4 COMPARISON OF THE 15° SIDE RAKE ANGLE TOOL.....	70

4.1.2 CUTTING SURFACE SPEED COMPARISON FOR THE EXPERIMENTAL RESULTS.....	71
4.1.2.1 CHIP THICKNESS	71
4.1.2.2 CRATER DEPTH.....	73
4.1.2.3 CONTACT LENGTH.....	73
4.1.2.4 SHEAR ANGLE.....	74
4.1.2.5 CUTTING RATIO.....	75
4.1.2.6 FORCE.....	76
4.2 SIMULATION RESULTS	77
4.2.1 SIDE RAKE ANGLE COMPARISON FOR THE SIMULATION DATA	77
4.2.1.1 THE 0° SIDE RAKE ANGLE TOOLS	78
4.2.1.2 THE 5° SIDE RAKE ANGLE TOOLS	80
4.2.1.3 THE 10° SIDE RAKE ANGLE TOOLS	81
4.2.1.4 THE 15° SIDE RAKE ANGLE TOOLS	82
4.2.2 CUTTING SURFACE SPEED COMPARISON FOR THE SIMULATION DATA.....	83
4.2.2.1 CHIP THICKNESS	83
4.2.2.2 CONTACT LENGTH.....	84
4.2.2.3 SHEAR ANGLE.....	85
4.2.2.4 CUTTING RATIO.....	86
4.2.2.5 FORCE.....	88
4.3 COMPARISON ANALYSIS.....	88
4.3.1 SHEAR ANGLE AND SIDE RAKE ANGLE.....	88
4.3.2 CUTTING RATIO AND SIDE RAKE ANGLE.....	91

4.3.3 CONTACT LENGTH AND SIDE RAKE ANGLE.....	93
4.3.4 FORCE AND SIDE RAKE ANGLE.....	95
CHAPTER 5	99
5.1 CONCLUSION.....	99
5.2 RECOMMENDATIONS	101
BIBLIOGRAPHY.....	103
APPENDIX.....	105
APPENDIX A:.....	107
APPENDIX B:.....	113
APPENDIX C:.....	123
APPENDIX D:.....	129
APPENDIX E:	135
APPENDIX F:	137
APPENDIX G:.....	139

LIST OF TABLES

Table 2.1 Various cutting tool geometry for HSS cutting tool in mild steel.	11
Table 2.2 The trend as a result of increasing the rake angle.....	12
Table 3.1 The ANSI tool signature and computer image of cutting tools used in this thesis.	29
Table 4.1 The 0° side rake angle cutting tool pictures at 25 m/min.	44
Table 4.2 The 0° side rake angle cutting tool pictures at 30 m/min.	47
Table 4.3 The 0° side rake angle cutting tool pictures at 35 m/min.	48
Table 4.4 The 0° side rake angle cutting tools results.	50
Table 4.5 The 5 ° side rake angle cutting tool pictures at 25 m/min.	52
Table 4.6 The 5° side rake angle cutting tool pictures at 30 m/min.	53
Table 4.7 The 5° side rake angle cutting tool pictures at 35 m/min.	56
Table 4.8 The 5° side rake angle cutting tools results.	58
Table 4.9 The 10° side rake angle cutting tool pictures at 25 m/min.	58
Table 4.10 The 10° side rake angle cutting tool pictures at 30 m/min.	60
Table 4.11 The 10° side rake angle cutting tool pictures at 35 m/min.	62
Table 4.12 The 10° side rake angle cutting tools results.	64
Table 4.13 The 15° side rake angle cutting tool pictures at 25 m/min.	65
Table 4.14 The 15° side rake angle cutting tool pictures at 30 m/min.	66
Table 4.15 The 15 ° side rake angle cutting tool pictures at 35 m/min.	68

Table 4.16 The 15° side rake angle cutting tools results.	70
Table 4.17 Simulation results for the 0° side rake angle tools.....	79
Table 4.18 Simulation results for the 5° side rake angle tools.....	80
Table 4.19 Simulation results for the 10° side rake angle tools.....	82
Table 4.20 Simulation results for the 15° side rake angle tools.....	83
Table 5.1 The trends from the results of experimental and simulation data as the side rake angle increases from 0 to 15°	100
Table B.1 The data sheet for the 0° side rake angle cutting tool at 25 m/min.....	113
Table B.2 The data sheet for the 5° side rake angle cutting tool at 25 m/min.....	113
Table B.3 The data sheet for the 10° side rake angle cutting tool at 25 m/min.....	114
Table B.4 The data sheet for the 15° side rake angle cutting tool at 25 m/min.....	114
Table B.5 The data sheet for the 0° side rake angle cutting tool at 30 m/min.....	115
Table B.6 The data sheet for the 5° side rake angle cutting tool at 30 m/min.....	116
Table B.7 The data sheet for the 10° side rake angle cutting tool at 30 m/min.....	117
Table B.8 The data sheet for the 15° side rake angle cutting tool at 35 m/min.....	118
Table B.9 The data sheet for the 0° side rake angle cutting tool at 35 m/min.....	119
Table B.10 The data sheet for the 5° side rake angle cutting tool at 35 m/min.....	119
Table B.11 The data sheet for the 10° side rake angle cutting tool at 35 m/min.....	120
Table B.12 The data sheet for the 15° side rake angle cutting tool at 35 m/min.....	120
Table B.13 The raw data for the force calculations.....	121
Table C.1 Chip Thickness measurements taken from experimental data chips.	123
Table C.1 continued	124
Table C.1 continued	125

Table C.1 continued	126
Table C.1 continued	127
Table C.1 continued	128
Table E.1 Raw data for the experimental results.	135
Table E.2 Raw data for the simulation results.	135
Table F.1 The 25 m/min cutting speed before and after tool wear images.....	137
Table F.2 The 30 m/min cutting speed before and after tool wear images.....	138
Table F.3 The 35 m/min cutting speed before and after tool wear images.....	138

LIST OF FIGURES

Figure 1.1 Tool Signature terms.	5
Figure 1.2 Orthogonal cutting terms.	8
Figure 3.1 Hardness test locations on sample 1018, distances are in mm.	27
Figure 3.2 The crater area defined where the crater depth measurement is taken.	31
Figure 3.3 The contact length measurement for the cutting tool.	31
Figure 3.4 The location of the shear angle with respect to the tool, chip, and workpiece.	33
Figure 4.1 Chip images from the first and last sampling for the 0° side rake tool at 25 m/min.	45
Figure 4.2 The average measurements from the six samplings taken for the 0° side rake tool at 25 m/min.	46
Figure 4.3 Chip images from the first and last sampling for the 0° side rake tool at 30 m/min.	47
Figure 4.4 The average measurements from the six samplings taken for the 0° side rake tool at 30 m/min.	48
Figure 4.5 Chip images from the first and last sampling for the 0° side rake tool at 35 m/min.	49
Figure 4.6 The average measurements from the six samplings taken for the 0° side rake tool at 35 m/min.	50
Figure 4.7 Chip images from the first and last sampling for the 5° side rake tool at 25 m/min.	52
Figure 4.8 The average measurements from the six samplings taken for the 5° side rake tool at 25 m/min.	53

Figure 4.9 Chip images from the first and last sampling for the 5° side rake tool at 30 m/min.	54
Figure 4.10 The average measurements from the six samplings taken for the 5° side rake tool at 30 m/min.	55
Figure 4.11 Chip images from the first and last sampling for the 5° side rake tool at 35 m/min.	56
Figure 4.12 The average measurements from the six samplings taken for the 5° side rake tool at 35 m/min.	57
Figure 4.13 Chip images from the first and last sampling for the 10° side rake tool at 25 m/min.	59
Figure 4.14 The average measurements from the six samplings taken for the 10° side rake tool at 25 m/min.	59
Figure 4.15 Chip images from the first and last sampling for the 10° side rake tool at 30 m/min.	61
Figure 4.16 The average measurements from the six samplings taken for the 10° side rake tool at 30 m/min.	61
Figure 4.17 Chip images from the first and last sampling for the 10° side rake tool at 35 m/min.	62
Figure 4.18 The average measurements from the six samplings taken for the 10° side rake tool at 35 m/min.	63
Figure 4.19 Chip images from the first and last sampling for the 15° side rake tool at 25 m/min.	65
Figure 4.20 The average measurements from the six samplings taken for the 15° side rake tool at 25 m/min.	66
Figure 4.21 Chip images from the first and last sampling for the 15° side rake tool at 30 m/min.	67
Figure 4.22 The average measurements from the six samplings taken for the 15° side rake tool at 30 m/min.	68
Figure 4.23 Chip images from the first and last sampling for the 15° side rake tool at 35 m/min.	69

Figure 4.24 The average measurements from the six samplings taken for the 15° side rake tool at 35 m/min.	70
Figure 4.25 Graph of the chip thickness versus cutting surface speed for the experimental results.	72
Figure 4.26 Graph of the crater depth versus cutting surface speed for the experimental results.	72
Figure 4.27 Graph of the contact length versus cutting surface speed for the experimental results.	74
Figure 4.28 Graph of the shear angle versus cutting surface speed for the experimental results.	75
Figure 4.29 Graph of the cutting ratio versus cutting surface speed for the experimental results.	76
Figure 4.30 Graph of the force versus cutting surface speed for the experimental results.	77
Figure 4.31 Sample image from computer simulation with outputs labeled, from the 15 ° side rake angle at 25 m/min cutting surface speed.	78
Figure 4.32 The computer simulation model of the 0° side rake angle cutting tool at 35 m/min cutting surface speed.	79
Figure 4.33 The computer simulation model of the 5° side rake angle cutting tool at 35 m/min cutting surface speed.	81
Figure 4.34 The computer simulation model of the 10° side rake angle cutting tool at 35 m/min cutting surface speed.	82
Figure 4.35 The computer simulation model of the 15° side rake angle cutting tool at 35 m/min cutting surface speed.	83
Figure 4.36 Graph of the chip thickness versus cutting surface speed for the simulation results.	84
Figure 4.37 Graph of the contact length verse cutting surface speed for the simulation results.	85
Figure 4.38 Graph of the shear angle verse cutting surface speed for the simulation results.	86

Figure 4.39 Graph of the cutting ratio verse cutting surface speed for the simulation results.	87
Figure 4.40 Graph of the force verse cutting surface speed for the simulation results.	87
Figure 4.41 A comparison of the shear angle with the side rake angle at 25 m/min cutting surface speed.	89
Figure 4.42 A comparison of the shear angle with the side rake angle at 30 m/min cutting surface speed.	90
Figure 4.43 A comparison of the shear angle with the side rake angle at 35 m/min cutting surface speed.	90
Figure 4.44 A comparison of the cutting ratio with the side rake angle at 25 m/min cutting surface speed.	92
Figure 4.45 A comparison of the cutting ratio with the side rake angle at 30 m/min cutting surface speed.	92
Figure 4.46 A comparison of the cutting ratio with the side rake angle at 35 m/min cutting surface speed.	93
Figure 4.47 A comparison of the contact length with the side rake angle at 25 m/min cutting surface speed.	94
Figure 4.48 A comparison of the contact length with the side rake angle at 30 m/min cutting surface speed.	94
Figure 4.49 A comparison of the contact length with the side rake angle at 35 m/min cutting surface speed.	95
Figure 4.50 A comparison of the force with the side rake angle at 25 m/min cutting surface speed.	96
Figure 4.51 A comparison of the force with the side rake angle at 30 m/min cutting surface speed.	96
Figure 4.52 A comparison of the force with the side rake angle at 35 m/min cutting surface speed.	97
Figure D.1 Chip images for the 0° side rake angle cutting tool at 25 m/min.	129
Figure D.2 Chip images for the 5° side rake angle cutting tool at 25 m/min.	129

Figure D.3 Chip images for the 10° side rake angle cutting tool at 25 m/min.	130
Figure D.4 Chip images for the 15° side rake angle cutting tool at 25 m/min.	130
Figure D.5 Chip images for the 0° side rake angle cutting tool at 30 m/min.	131
Figure D.6 Chip images for the 5° side rake angle cutting tool at 30 m/min.	131
Figure D.7 Chip images for the 10° side rake angle cutting tool at 30 m/min.	132
Figure D.8 Chip images for the 15° side rake angle cutting tool at 30 m/min.	132
Figure D.9 Chip images for the 0° side rake angle cutting tool at 35 m/min.	133
Figure D.10 Chip images for the 5° side rake angle cutting tool at 35 m/min.	133
Figure D.11 Chip images for the 10° side rake angle cutting tool at 35 m/min.	134
Figure D.12 Chip images for the 15° side rake angle cutting tool at 35 m/min.	134
Figure G.1 The computer simulation image for the 0° side rake angle cutting tool at 25 m/min.	139
Figure G.2 The computer simulation image for the 0° side rake angle cutting tool at 30 m/min.	139
Figure G.3 The computer simulation image for the 0° side rake angle cutting tool at 35 m/min.	140
Figure G.4 The computer simulation image for the 5° side rake angle cutting tool at 25 m/min.	140
Figure G.5 The computer simulation image for the 5° side rake angle cutting tool at 30 m/min.	141
Figure G.6 The computer simulation image for the 5° side rake angle cutting tool at 35 m/min.	141
Figure G.7 The computer simulation image for the 10° side rake angle cutting tool at 25 m/min.	142
Figure G.8 The computer simulation image for the 10° side rake angle cutting tool at 30 m/min.	142
Figure G.9 The computer simulation image for the 10° side rake angle cutting tool at 35 m/min.	143

Figure G.10 The computer simulation image for the 15° side rake angle cutting tool at 25 m/min.	143
Figure G.11 The computer simulation image for the 15° side rake angle cutting tool at 30 m/min.	144
Figure G.12 The computer simulation image for the 15° side rake angle cutting tool at 35 m/min.	144

CHAPTER 1

INTRODUCTION

A common method to manufacture parts to a specific dimension involves the removal of mass amounts of material by machining operations. This process involves the workpiece or material, the machine and cutting tools. The material removal process was performed when the machine uses the cutting tool to remove material from the workpiece. Specific dimensions and tolerances are defined by a drawing to give the workpiece its final shape. Metal removal machines today are controlled by computers for precise and repeatable positioning.

Turning machines have computer controls to monitor and allow changes in all operations of the machine. Turning machines are a popular method to remove material for cylindrical parts and some non-cylindrical parts with the newer machines that accommodate live tooling. The cutting tools used to remove material in a turning machine can cut parts accurately and within tolerance for a time before they wear or break.

Tool wear and breakage has been an issue with cutting tools since they were created. Tool wear weakens the cutting tool, increases the forces used in cutting and causes a lack of consistency in material removal. Parts and time lost to scrap and rework from tool wear are costly to companies. Companies spend money to grind and replace

cutting tools due to tool wear. There are many factors that contribute to the wear of cutting tools: the workpiece properties, cutting tool properties, cutting surface speed, cutting feedrate, depth of cut and machine rigidity.

1.1 COMPUTER SIMULATION INTRODUCTION

Computer simulation has been an expanding field being used in research studies and increasingly used in industrial applications for tool wear. Many companies have software on the market to simulate tool wear for a wide variety of machining operations. These simulations provide information on how the cutting tool will react and respond to the workpiece properties. The simulation outcome depends largely on the model and laws it follows. To use a simulation, there needs to be a model to predict the outcome of specific inputs to that model. Several different laws are applied to a model in order to describe the workpiece properties, cutting tool properties, cutting surface speed, and cutting feedrate. The model was used to describe and predict the outcome of orthogonal cutting. There are different criteria in simulating the orthogonal cutting process. These criterions are as follows: how the simulation controls the material being removed from the workpiece, tool wear rate evaluations, neural networks to predict the wear, wear maps to predict the amount of wear and several others. Many of the simulations use finite element analysis as a base to evaluate the phenomena.

Today with the ever-increasing capability of computers to compute equations quicker more of the criteria mentioned above are being combined to create a more accurate model for orthogonal cutting. Research continues in all facets of simulation with the main focus being on predicted metal chip shape, metal chip breakage, and

cutting forces. Recently there has been an increase in the research done in tool wear prediction on the cutting tool. Many papers use the results of existing data to reduce the time and cost of experimental data to evaluate the simulation.

1.2 STATEMENT OF THE PROBLEM

The combination of computer simulation and tool wear has been a growing source for research. This study examined whether there was any correlation between experimental tool wear and computer simulated tool wear using an updated Lagrangian finite element analysis with Archard's law. This study has compared experimental with computer simulated turning data to see if there are any correlations.

1.2.1 NULL HYPOTHESES

There is no significant difference between simulation wear and experimental cutting wear in metal cutting.

1.2.2 THESIS STATEMENT

Tool wear has been a critical issue in metal removal processes. In turning, tool wear can create parts that are out-of-tolerance and eventually cause tool failure. Research efforts have been initiated in computer simulation to model turning forces and tool wear. However, there has been no significant data relating the computer simulation to actual cutting data gathered from turning. This study has tested for the correlation between actual tool wear in turning and simulated results.

1.3 JUSTIFICATION

There was minimal data to correlate between Archard's law and experimental data for orthogonal cutting. This thesis has evaluated the use of Archard's law in the calculation of the tool wear phenomena in orthogonal cutting. Varying the side rake angle in this thesis has provided a larger sampling of data to compare the simulation and experimental results. This thesis does not validate Archard's law rather present evidence that Archard's law has been a functional approximation for calculating tool wear.

1.4 DELIMITATIONS

This thesis was limited to comparing the wear of a high speed steel (HSS) cutting tool with theoretically predicted tool wear based on Archard's law. Emphasis was placed on the effect of varying the side rake angle on the wear pattern on the tool. The following was a list of delimitations for this thesis.

1. The workpiece material will be 1018 cold rolled steel. No attempt was made to change the workpiece microstructure.
2. The tests were performed on an Okuma space turn LB300 – M CNC lathe.
3. All angles on the cutting tool remained constant except the side rake angles; the side rake angles will be 0, 5, 10, and 15 degrees (°).
4. The cutting conditions for this test were a depth of cut of 1.5 millimeters (mm) and the feed rate will be 0.2 millimeters per revolution (mm/r).
5. Constant cutting surface speeds were used during this experiment. The cutting surface speed was increased for each run in increments of 5 meters per minute (m/min) starting the first run at 25 m/min and ending at 35 m/min. If a tool broke before

completion of the run then the cutting surface speed was reduced 2.5 m/min.

6. This test was run without coolant.
7. The simulation model used Archard's law to predict tool wear.

1.5 DEFINITION OF TERMS

Tool Signature – This is the nomenclature that the American National Standards Institute (ANSI) standardized to define tool geometry. The nomenclature is as follows: Back rake angle, Side rake angle, End relief angle, Side relief angle, End cutting edge angle, Side cutting edge angle, and nose radius, shown in Figure 1.1. An example of how the tool geometry would be written would be [0, 0, 10, 10, 8, 0, 0.031].

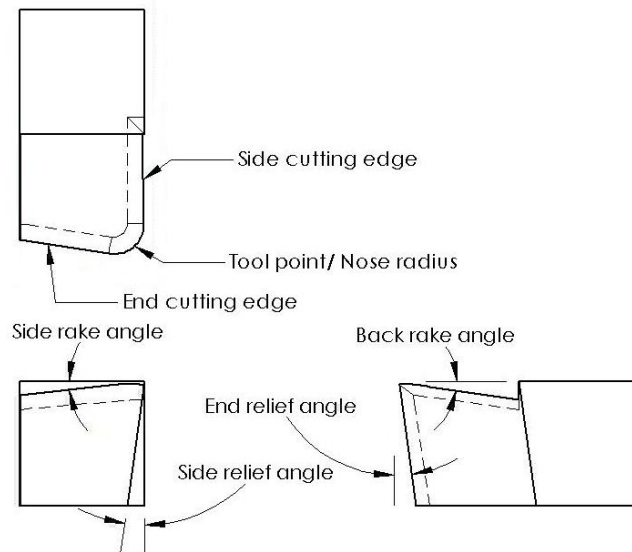


Figure 1.1 Tool Signature terms.

Back Rake Angle – “This is the angle between the face of the tool and a line that is parallel to the base of the toolholder. It is measured in a plane that is parallel to the side cutting edge and perpendicular to the base.” (Nee 1998)

Side Rake Angle – “This angle is defined as the angle between the tool face and a plane parallel to the tool base. It is measured in a plane perpendicular to both the base of the holder and the side cutting edge.” (Nee 1998)

End Relief Angle – “This is the angle between the end flank and a line perpendicular to the base of the tool. The purpose of this angle is to prevent rubbing between the workpiece and the end flank of the tool.” (Nee 1998)

Side Relief Angle – “This is the angle between the side flank of the tool and a line drawn perpendicular to the base. For turning operations, the side relief angle must be large enough to prevent the tool from advancing into the workpiece before the material is machined away.” (Nee 1998)

End Cutting Edge Angle – “This is the angle between the edge on the end of the tool and a plane perpendicular to the side of the tool shank. The purpose of the angle is to avoid rubbing between the edge of the tool and the workpiece.” (Nee 1998)

Lead Angle (Side Cutting Edge Angle) – “This is the angle between the straight cutting edge on the side of the tool and the side of the tool shank. This side edge provides the major cutting action and should be kept as sharp as possible.” (Nee 1998)

Nose Radius – “The nose radius connects the side and end cutting edges and dramatically affects tool life, radial force, and surface finish. Sharp pointed tools have a nose radius of zero.” (Nee 1998)

Face – “The face of the tool is the surface over which the chip passes during its formation.” (Nee 1998)

Flank – “The flank is the clearance face of the cutting tool, along which the major cutting edge is located.” (Nee 1998)

Face Wear – “Wear takes the form of a cavity or crater which has its origin not along the cutting edge but at some distance away from it and within the chip contact area.” (Nee 1998)

Cratering – Caused by the flowing metal chip which wears (thermo-chemical abrasion) a cup in the tool face behind the cutting edge which gradually grows larger and finally causes the cutting edge to crumble.

Chipping – Breaking out of small chips from the face or flank, at the cutting edge; usually due to mechanical or thermal shock on brittle tool materials.

Built-up Edge (BUE) – The material of the workpiece not removed with the chip but adhered to the cutting tool.

Workpiece – The test material in which the material was to be removed from.

Neutral Point – The area between the end cutting edge and the crater on the face of the cutting tool caused by a build up edge.

Contact Length – The distance the metal chip was in contact with the cutting tool, measured from the side cutting edge to the indicated contact.

Forces – There are 3 major forces when using a turning machine, they are the forces normal to the X axis, Z axis, and the chuck.

Depth of Cut – The measured distance that the tool was into the workpiece, for the removal of material. Depth of cut was mainly called out as the amount of material removed off of the diameter of the workpiece on a lathe.

Feedrate – The speed at which the cutting tool has traveled across the workpiece, measured in mm/r for turning shown in Figure 1.2.

Chip thickness – The measured thickness of the deformed metal chip that was removed

from the workpiece shown in Figure 1.2.

Cutting ratio – This was the ratio between the undeformed chip thickness and the thickness of the metal chip or the feedrate and the thickness of the metal chip in orthogonal cutting.

Cutting Surface Speed – The rate of speed the cutting tool was encountering the workpiece.

Constant Cutting Surface Speed – A method in turning to control the rate the cutting tool was encountering the workpiece to remain the same as the diameter of the workpiece changes. This was achieved by increasing the revolutions per minute of the workpiece as the diameter decreases.

Volume – In turning the volume of material removed was the depth of cut, length of cut, and the circumference around the workpiece.

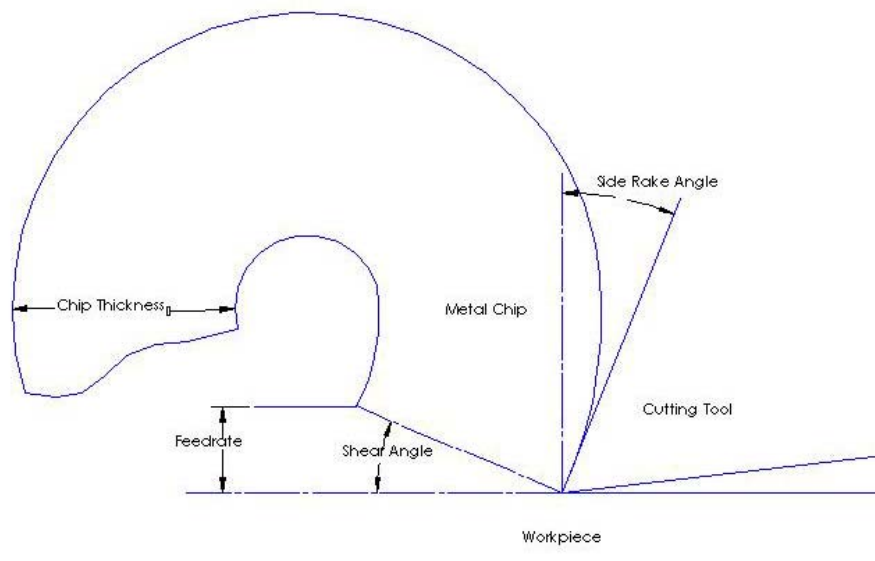


Figure 1.2 Orthogonal cutting terms.

Shear angle – This was the angle that was created between the chip, workpiece and cutting tool that the shearing action happens as the chip was removed from the workpiece by the cutting tool shown in Figure 1.2.

CHAPTER 2

LITERATURE REVIEW

2.1 BACKGROUND INFORMATION

Background information was gathered on cutting tools, tool wear and finite element analysis to highlight some of what has occurred in tool wear studies. Research for this thesis was done on Archard's law and computer simulation capabilities.

2.1.1 CUTTING TOOLS

In this thesis, background on cutting tools was done in order to understand what tool geometry has been used before with HSS tools. HSS cutting tool geometry has been studied to arrive at the current tool geometry. Over the past few years cutting geometry has changed slightly for HSS tooling. In Table 2.1 the various tool geometries found in different books are listed. Also added was the tool geometry that this thesis will use.

Table 2.1 Various cutting tool geometry for HSS cutting tool in mild steel.

Material	back rake	side rake	end relief	side relief	references
1020, 1035, 1040	10 to 12	10 to 12	8 to 10	8 to 10	Nee (1998)
carbon steels wrought	10	12	5	5	MDH (1980)
1020, 1035, 1040	0-12(0)	8-12(8)	8-10(8)	8-10(8)	Drozda (1983)
1018	0	0,5,10,15	10	10	thesis

In a study by Albert J. Shih he used annealed 1020 carbon steel along with HSS cutting tools to study the effects of the rake angle of the cutting tool. The initial finite element used perfectly sharp cutting tools to identify what the differences and similarities of the deformation of the work material. A later finite element used worn cutting tools to examine residual stresses under the cut surface. The finite element mesh used ten layers to model the chip formation, four layers for under the cut surface, and four layers for distributions of the residual stresses. However the lengths and heights of these layers vary depending on the rake angle used. “As the cutting tool proceeds, the mesh rezoning technique is applied to add, refine, combine, and delete columns of elements in front of and behind the cutting tool until the steady-state chip formation is achieved”(Shih 1996). The research used finite element to understand what occurred when the rake angle changed from -2, 0, 5, and 15°. The trends that occurred in this study are shown in Table 2.2. A conclusion reached for this research was that the deformed finite element mesh was still not adequate for the work-material model.

Table 2.2 The trend as a result of increasing the rake angle

Trend in rake angle -2° to 15°	
Chip thickness	Decreased
Cutting ratio	Increased
Shear angle	Increased
Contact length	Decreased
Averaged cutting force	Decreased
Averaged feed force	Decreased
Resultant force	Decreased

2.1.2 TOOL WEAR

Tool wear mechanisms –most studies agree that there are 5 basic causes of wear. Tool wear mechanisms are divided into 5 categories and can occur in combination with the others or singly. “The causes of wear do not always behave in the same manner, nor do they always affect wear to the same degree under similar cutting conditions.” (Nee 1998) The 5 categories are listed below with a brief explanation.

1. Abrasive wear was a mechanical action that occurs when hard particles found within the workpiece cut, chip, groove, or dislodge sections of the cutting tool surface.
2. Plastic deformation of the cutting edge was caused by the extreme pressure imposed on the cutting edge that causes a depression or bulging of the edge. The more the tool deforms the greater the pressure and temperature on the tool resulting in more deformation and possible edge wipe out.
3. A chemical reaction between the tool and the workpiece occurs at elevated temperature. The tool has tiny sections that are weakened due to the pressure and temperature of the cutting process. These tiny sections have smaller particles within them that react to the workpiece material thus forming a bond between the tool and the workpiece. As the bond strengthens the weakened particles from the tool are carried away with the chip or stay with the workpiece.
4. Diffusion between work and tool material occurs when a section of the tool reaches a critical temperature and a change in composition happens between the tool and the chip interface. This composition change usually induced by elevated temperature and the bond between the section and the chip strengthen as the section was torn away from the tool.

5. The welding of asperities between workpiece and the tool occur at lower temperatures than the diffusion and chemical reaction. These asperities are joined to the workpiece material as it was removed in the work-hardened chip. The high pressure in the cutting process enables the asperities to be pulled away from the tool as the chip removed from the workpiece.

Research has been done in tool wear in many different categories. A few of these categories are finite element analysis, neural networks, and predictive mapping. The majority of research in tool wear uses the finite element analysis method to predict tool wear. Further background for finite element analysis for this thesis can be found later in this chapter.

A study by J.H. Lee and S.J Lee was conducted in South Korea that used S45C as a workpiece and uncoated carbide cutting tools. This researched used a neural network model from a force ratio and readings from a dynamometer to predict flank wear in turning. Two different force ratios and a force increment were incorporated into neural networks to predict tool wear. The first force ratio was the ratio between the feed force and the tangential force, while the second was a modification that includes the radial force. A force increment of the tangential and the feed forces were used for learning in another neural network. This research stated that the second force ratio was more accurate ratio because of the three forces used. The model the neural network used to predict the tool wear was “based on a multi-layer perception which consists of input, hidden, and output layers and uses error-back-propagation algorithm for learning”(Lee 1999). To train the neural networks 3 of the 9 tests were used to train all three of the networks. The force increment’s average prediction error was about 10.3%. When force

ratio 1 was used for prediction the average error was about 11.9%. The average of the prediction errors when force ratio 2 was used was about 8.0%. The study showed that force ratio 2 was more accurate than force ratio 1 and the force increment in predicting flank wear. The results of the study predicted that as the cutting distance increased the flank wear also increased.

In a predictive mapping study by X.P. Li, H.H. Ng, and S.C. Lim from the National University of Singapore, estimated tool wear using 1050 steel as the workpiece and uncoated tungsten carbide cutting tools. This study used the theoretical model of Kannatey-Asibu that takes the heat generated from the tool flank-workpiece interface. Li, Ng, and Lim modify the model by adding in the heat transfer from the shear zone and the tool-chip interface along with the frictional heat from the flank-workpiece to create an accurate model of the heat transfer phenomena. This modified model was then used to predict the rate of flank wear on the tool. Next the wear maps are generated off of the predicted tool wear rates. This wear-rate model system was explained in the study by going through a series of steps. These steps are to specify variables for the wear-rate map and the steps are: specifying conditions to be input into the simulator, running the simulator to obtain the required outputs, converting the output data to pressures and temperature at the tool tip, calculating the wear-rate from the pressures and temperature for the diffusion and adhesion wear parameters, gather the results of the wear rate and generate a wear-rate map. Once the maps were generated they were compared to experimental data that showed good agreement. This study did not base its wear maps on the experimental data because of the lack of data points; they instead imposed the experimental data onto the predicted wear-rate maps (Li 1999).

2.1.3 FINITE ELEMENT ANALYSIS

There has been a great deal of research done on the cutting process using finite element analysis. The first step in the analysis process has been to simplify the cutting phenomenon; this was done by using the orthogonal cutting theory. Orthogonal cutting occurs when a cutting situation has been modeled into a simplified two-dimensional problem. Most cutting research relating to simulation has been done with orthogonal cutting or two-dimensional cutting in order to simplify equations. However there are a couple of simulation models that depict 3-dimensional cutting. Orthogonal cutting takes the relationship of a tool with the workpiece at an instance. The instances of the relationship between the tool and the workpiece are combined into a finite element analysis.

The finite element analysis then takes the relationship of the cutting tool and the workpiece and evaluates the instances into a flowing analysis of the material removal. In the finite element analysis there are different approaches to combining the instances of the orthogonal cutting occurrences. These different methods to combine the orthogonal cut are called models. These models are used to predict what the cutting tool will do to the workpiece at specified cutting conditions. There are several different models used to create the necessary method and calculations to approximate the phenomenon that occurs during the machining process. Many of the formulations are used in conjunction with each other in order to better predict the material properties and to model different conditions of the material removal process. These formulations are Lagrangian, Eulerian, Arbitrary Lagrangian Eulerian, and the updated Lagrangian formulas.

The Lagrangian model has been used to predict the chip geometry from the beginning until the simulation reaches a steady state. The chip separation criteria must be provided for this model. The model worked with a finite element mesh of material elements that cover the region of analysis exactly. The elements are attached to the material and deformed with the deformation of the workpiece.

The Eulerian model was used from the steady state condition that avoided the chip separation criteria, but the shape of the chip must be known. This model was more suitable for fluid-flow problems with a controlled volume. The mesh used in this model consisted of elements fixed in space that cover the controlled volume. The material properties are calculated at fixed special locations as the material flowed through the mesh.

The Arbitrary Lagrangian Eulerian (ALE) model used a finite element mesh that was not attached to the material or fixed in space, but has a motion independent of the material. The ALE Model has several key items for modeling the cutting tool workpiece interaction. It was derived using two velocities the material and a grid point. The model established mapping between velocities through time derivatives. It has supplementary equations provided by assigning grid velocities in incremental steps. As the solution has been converged in incremental steps the nodal points are updated to reflect the new points. Material and grid displacements points are computed instead of using geometric extrapolation. The last of the key items was a transfinite method used to account for boundary motions of the patch element in the mesh generation, and applied at the end of each incremental step.

The updated Lagrangian model was similar to the Lagrangian model for the formulations. The difference with the updated Lagrangian model can begin the formulation at a given time while the Lagrangian model must begin at time zero. Therefore when the calculations are being made the updated Lagrangian model utilizes the current state rather than the initial.

Along with modeling what effects the cutting tool has on the workpiece research has now been done on the effect the workpiece has had on the cutting tool. Within the program that utilizes these models to predict how the chip has been removed from the workpiece, there are wear theories being applied to the program. These wear theories predict how the cutting tool has been effected by the process. The two main wear models being used are Usui's and Takeyama and Murata's for orthogonal cutting simulation. Usui's wear model was derived from adhesive wear. Takeyama and Murata's wear model has been derived from abrasive and diffusive wear. Usui's wear rate was incorporated more frequently into the prediction of wear on cutting tools than Takeyama and Murata's wear model especially with finite element formulations.

There are many different studies available in finite element analysis evaluating the workpiece, cutting tool interaction. Many of these studies are done using different finite element formulations, workpiece material, or cutting tool material. Below are some of the researches done using these models to predict effects the workpiece and the cutting tool generate in respect to each other.

In a technical paper by Joon-Dong Oh and Gunter Warnecke, they used finite element analysis to study chip formation in orthogonal cutting. Their material was modeled using the Anand's material model that has two parts to it, the thermo-

viscoplastic flow stress and the strain hardening evolution. This material model was modified to begin the modeling at room temperature since Anand's model was not accurate from room temperature to the phase transition. They used a nonlinear stress equation to model the friction between the workpiece, chip, and cutting tool. The finite element analysis method that they used to calculate the chip formation was the Lagrangian and the Eulerian formulations. The Lagrangian model was used to predict the events of cutting from the beginning of the cut to steady state. They used the Lagrangian model to calculate the deformed chip and the temperature in the cutting zone. Once the chip formation reaches a steady state the Eulerian model calculates the temperature within the cutting tool. To improve their results they used shorter element lengths to produce finer remeshing of the model. Oh and Warnecke found that the tool stability at high temperatures was important to tool wear. They found that their calculated cutting forces were 15% smaller than their measured ones. The cutting tool that was modeled was assumed to be perfectly sharp. The study conducted showed that the Anand's model could be used to predict the material at a lower temperature. They used both the Lagrangian and Eulerian to model the chip formation. The workpiece material was 4140 steel and the cutting tool was a carbide insert. This research looked into what modeling was done before in finite element analysis and improved it by combining the Lagrangian and Eulerian formulations to open new methods of prediction (Oh 2000).

In 2000 M. Movahhedy, M.S. Gadala, and Y. Altintas take the Lagrangian and Eulerian formulations that have been utilized in orthogonal cutting and combined them into simulating the cutting process efficiently. In this study the material was modeled using an elasto-plastic analysis with linear strain-hardening. The software used to

perform the calculations was Deform-2D. The wear was not researched in this study. This research used the advantages of the two formulations to create this ALE finite-element method to simulate the orthogonal cutting process. The ALE formulation used the features of the Lagrangian to model the unconstrained flow of the material that defined the shape and size of the chip. The Eulerian formulation was used to analyze the region close to the tool tip. The material and the workpiece have individual mesh motion and the tool was neither attached to the material nor fixed in space. The ALE approach used two velocities, the material points and the grid points, these velocities were used to gather and track the incremental relationship between them. The mesh motion was then gathered from the calculation from these velocities and the positions of the nodal points were updated. In this study the initial chip size was assumed, however it was not a requirement of the ALE. The conclusions were that a node separation criterion was not required. Chip formation around the tool occurred by continuous plastic flow of material. The mesh motion becomes a part of the solution so frequent remeshing was avoided (Movahhedy 2000).

Published in 2001, this research performed by A.G. Mamalis, M. Horvath, A.S. Branis, and D.E. Manolakos modeled mild steel workpiece with a tungsten carbide cutting tool. The finite element analysis for this study utilized the commercial finite element code MARC to perform the calculations for the simulation. The material was modeled as an isotropic elastic-plastic, with isotropic strain-hardening. The friction force was modeled as a distributed tangential force. Heat transfer was also modeled during the analysis using the friction force and the plastic work created at the tool and chip interaction region. The MARC code used the updated Lagrangian formula however, the

chip-separation criteria was implemented into the MARC code for this study. The chip-separation criterion was defined as the distance when the node separated the chip from the workpiece. The defined distance for the chip-separation was the undeformed chip thickness. Upon separation the node splits and the rezoning of the now two nodes occurred and chip-separation was allowed to occur continuously in front of the tool. “The model was able to predict the stress, strain, strain-rate and temperature distribution in the chip, the workpiece and the tool, as well as the developed cutting forces” (Mamalis 2001). The predicted and experimental results showed a good agreement.

From the Ohio State University Yung-Chang Yen, Jorg Sohner, Blaine Lilly and Taylan Altan made modifications to the commercial available finite element method, Deform 2D to estimate tool wear in uncoated carbide inserts machining carbon steel ANSI 1045. In this study Usui’s wear rate model was used to continually update the tool wear that occurred on the cutting tool during the cutting process. Once the tool wear calculations were made the tool geometry was then updated to predict the new tool geometry. Then new tool geometry was then evaluated and the wear rate applied to the new geometry and the cycle to predict and update the tool geometry began again. The tool geometry may not update continuously, therefore the updates were performed at individual nodal movements. This study also looked into starting the evaluation with a predetermined wear on the cutting tool. The research shows that a cutting tool can have constantly updated wear during the cutting operation using the finite element method simulation. The results showed that the simulation that constantly updated the worn tool underestimated the wear of the crater and flank (Yen 2002).

2.2 RESEARCH INFORMATION

Research was done in the fields of Archard's law and computer simulation to understand what had been accomplished before in these fields. The research showed that there was little material available for the use of Archard's law in calculating tool wear in orthogonal cutting simulation. The majority of the computer simulation software utilizes other methods to calculate tool wear or none at all.

2.2.1 ARCHARD'S LAW

Archard's law states where a volume of material has been removed during a given increment of time, a coefficient which was a function of tool hardness, microstructure, and lubrication conditions, the normal contact load, and the sliding distance during a given time increment for a contact area. Archard's law in research has been used for wear; however, it has been utilized minimally in tool wear prediction with respect to orthogonal cutting. Some examples of Archard's law being utilized for wear studies are extrusion, punches, shears, railroad tracks, computer hard disks, and knee replacements.

2.2.2 COMPUTER SIMULATION CAPABILITIES

In industry there are several companies producing cutting tool simulation software. The software has been available for many different machining operations. The major machining operations that are simulated are milling, turning, forging, drawing, and material flow. The majority of the software that looks at the turning operation study coated and uncoated carbide insert cutting tools. The software in the turning operations uses finite element analysis to evaluate the workpiece, chip and tool interface. These software packages offer a reasonable look at the forces, temperature, stresses and strains involved in the turning operation. In the last several years wear rates have been applied

to the finite element analysis to predict the size, shape and location of the wear on the cutting tool. Usui's wear rate was the most popular equation being utilized to capture the effect of the workpiece and cutting tool interaction.

In this thesis the finite element formulation has utilized the updated Lagrangian model for the cutting tool workpiece interaction and Archard's law to predict wear on the cutting tool.

CHAPTER 3

METHODS OF RESEARCH

This research was accomplished in two sections; first the experimental turning of the workpiece for material removal to gather actual tool wear data and second the computer simulation of the cutting phenomena. This evaluation will determine whether tool wear from an actual experiment has been comparable with tool wear from a computer simulation using Archard's law. The test consists of turning a workpiece of cold-rolled 1018 steel H_{r_b} 80.36 while using the DoALL ½ inch square M2 high speed steel H_{r_c} 66.4 cutting tools for a constant cubic centimeter of material removed, feedrate, and depth of cut for all cutting tools.

3.1 EQUIPMENT

1. Turning Center – Okuma Space Turn LB300–M CNC lathe
2. Wire EDM – Sodick 325L Wire EDM Linear Servo Controller
3. Microscope – Brown & Sharpe
4. Optical comparator – Starrett HB400
5. Optical Camera – ROI optical camera
6. Hardness Tester – Mitutoyo ARK–510 Hardness Tester
7. Stereoscope – Olympus Stereoscope SZH
8. Digital Camera – Olympus DP11

9. Coordinate measurement machine (CMM) – Brown & Sharpe
10. Computer simulation software – Forge 2[®] [xx]
11. Grinder – Blanchard No. 22 Serial # 11691
12. Grinder – Chevalier FSG–1020AD II
13. Multimeter – Fluke 177 True RMS Multimeter
14. Current Clamp – Fluke i200 AC Current Clamp

3.2 TEST PROCEDURES

Procedures are important to follow in order to eliminate as much error as possible within the experiment. The turning experiment and computer simulation were programmed with the same cutting conditions and parameters where applicable. The computer simulation will utilize information from the software material database to reduce additional experiments, in order to model the cutting tool and the workpiece material.

3.3 TURNING EXPERIMENT

In order to begin the turning experiment, the workpiece, cutting program and cutting tools were prepared. These procedures establish the method followed from preparation to experiment completion including information gathered. The testing procedures for this research were designed to remove a constant cubic centimeter (cm³) removal rate for each tool tested in the turning operation. The constant cubic centimeter removal rate ensured that each cutting tool removes the same amount of material as the workpiece diameter decreases. A variable will be placed in the cutting program to indicate the correct number of passes for the cutting tool to ensure that the correct amount

of material was removed from the workpiece. To maintain the other constants of the experiment requires the cutting program to maintain the cutting surface speed, feedrate, and depth of cut while changing tools in order for each tool to cut along different sections of the workpiece. To begin the experiment the workpiece, cutting tools and cutting program were prepared.

3.3.1 WORKPIECE PREPARATION

To prepare the workpiece for the experiment several operations were performed. Two lengths of 381 mm stock were prepared by mounting them on a manual lathe with a 4-jaw chuck. In order to support the size and weight of the stock material a center drill was used to create a location for a live spindle to seat. The end of the stock material was faced to create a flat surface on the end of the workpiece. This procedure was done on the opposite side and then repeated for the second piece of 1018 cold rolled steel stock.

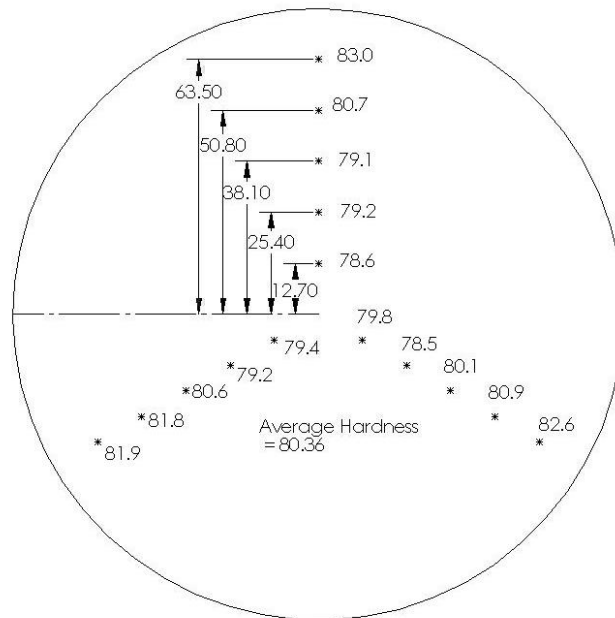


Figure 3.1 Hardness test locations on sample 1018, distances are in mm.

A section about 19 mm was taken off of the stock in order to perform a hardness test. The material for the hardness test was taken from the same billet as the stock material being tested and will have both faces rough ground using the Blanchard surface-grinding machine. The Chevalier grinding machine then finish ground the material. The hardness test started at 12.7-mm from the outside of the stock and moved toward the center by 12.7-mm increments. The hardness test was repeated on the material at 120 and 240° from the original test line as shown in Figure 3.1. The hardness values were averaged and the hardness of the stock piece was H_{rb} 80.36.

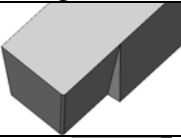
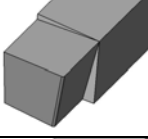
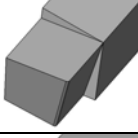
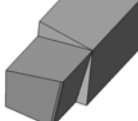
3.3.2 CUTTING TOOLS

The cutting tools are DoALL ½ inch square M2 tool steel blanks. To obtain the correct tool signature for the test the cutting tools angles were cut on a Sodick 325L wire EDM with linear servo controller. Two programs were used to cut the tool angles, the first program cut the side (0°) and end cutting edge (8°) along with the side relief angle (10°) and end relief angle (10°). The second program cut the side rake angle (5, 10 or 15°). The cutting tools were marked according to their number and specified side rake angle. The four cutting tool signatures are listed below in Table 3.1.

In order for the DoALL cutting tools to align properly in the Okuma lathe tool holders, four tool holder inserts were manufactured from 25.4 mm aluminum square stock. The 25.4 mm square stock was cut to a length of 133.35 mm on the band saw. One side of the inserts was undersized with a skim cut to ensure that the Okuma lathe tool holders held the cutting tool. A recess of 12.7 mm square was cut into the 25.4 mm stock to provide a shelf for the cutting tool to seat in. A groove was cut in the corner of the shelf to remove the radius left from the milling operation, so that the cutting tool

would seat squarely into the tool holder inserts. Lastly the tool holder inserts were deburred.

Table 3.1 The ANSI tool signature and computer image of cutting tools used in this thesis.

Tool Signature	Computer Image of Tool
[0, 0, 10, 10, 8, 0, 0.254]	
[0, 5, 10, 10, 8, 0, 0.254]	
[0, 10, 10, 10, 8, 0, 0.254]	
[0, 15, 10, 10, 8, 0, 0.254]	

3.3.3 TURNING PARAMETERS

There are several constants for the turning experiment in order to evaluate the relationship between the side rake angle and cutting surface speed: the feedrate, depth of cut and volume of material removed from the workpiece. The parameters of the experiment that changed are the side rake angle and the cutting surface speed.

The feedrate for this study was .2 mm/r. This value was selected from a preliminary experiment conducted with similar workpiece and cutting tool. A depth of cut of 1.5 mm was utilized during this study. The volume of material removed from the workpiece by the cutting tool was 1047 cm³. Each tool will remove the same volume of material in this study to provide an accurate comparison of the tool wear obtained.

During this thesis the side rake angle has been four different values being 0, 5, 10, and 15°. Constant cutting surface speed has been utilized during the study to ensure each tool had always removed material at the same cutting surface speed as the other tools. The constant cutting surface speed adjusts the revolutions per minute of the workpiece to compensate for the reduction of the workpiece diameter. The cutting surface speed will start with 25 m/min and increase by 5 m/min to 35 m/min.

3.3.4 PROGRAM SETUP

The test consisted of removing 1047 cm³ for each cutting tool tested. The program for the experimental data was run three times for each of the different cutting surface speed. Each program tested the four different side rake angles, with each of the different side rake angles being tested within the same pass. The program changed the order of the tools at each pass, so that each tool cut along the different locations throughout the program. The starting diameter of the workpiece determined the number of passes made by the program. The 25 m/min and 35 m/min cutting surface speed took 12 passes to remove 1047 cm³ and the 30 m/min took 20 passes to remove the same volume of material. To decrease the time it takes tool wear to occur the test was performed in dry conditions.

3.3.5 OUTPUT INFORMATION

- A. Time – The accumulated amount of time that the cutting tool was removing material. The time will be taken from the Okuma lathe cutting time.
- B. Tool wear – The two different tool wear types that were measured are the crater size and the contact length. The crater size consists of the tool wear on the face

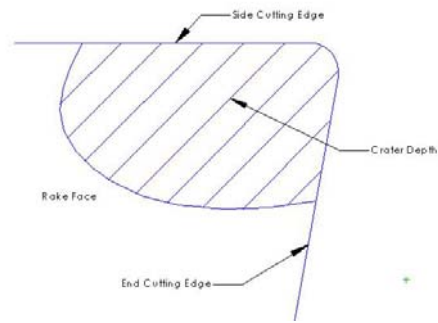


Figure 3.2 The crater area defined where the crater depth measurement is taken.

of the tool shown in Figure 3.2. The crater depth was measured from the rake face to the bottom of the crater. The contact length was the distance that the workpiece stayed in contact with the face of the cutting tool while the chip was formed. This was normally measured from the side cutting edge to the indicated contact, shown in Figure 3.3.

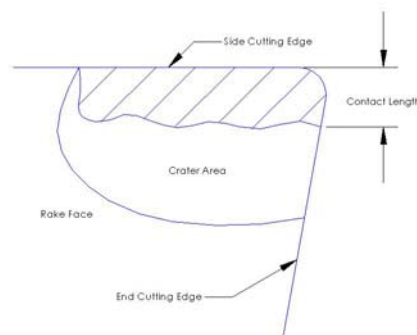


Figure 3.3 The contact length measurement for the cutting tool.

C. Chip thickness – This was the measurement of the thickness of the metal chip formed in the cutting process. The chip thickness will be measured using

calipers, and average of 60 measurements for each cutting tool has been used to express the chip thickness for the various cutting tools. The chip thickness was used to calculate cutting ratio and shear angle.

- D. Chip style – This was an effective output in monitoring the cutting process. The different styles of the chips indicated how effective the cutting tool has been performing. There are several different styles of chips that were removed from the workpiece. The chips were gathered six times for each cutting tool at the different side rake angles and the different cutting surface speeds. In general, as the cutting tool sheared metal, chip color changes from a color similar to the workpiece material to a dark blue, purplish color. The darker color signified that more heat was being removed from the workpiece into the chip. The more heat that was generated from the workpiece and cutting tool strengthens the bond between the metal chip formed from the workpiece and cutting tool section at the elevated temperature causing the section to be removed from the cutting tool with the chip.
- E. Cutting Ratio – The cutting ratio r was the relationship of the feedrate t_1 over the thickness of the chip t_2 shown in equation 3.1 (Nee 1998).

(Equation 3.1)
$$r = \frac{t_1}{t_2}$$

- F. Shear Angle – The shear angle changes with the SIDE RAKE ANGLE where the metal chip separated from the workpiece material shown in Figure 3.4. To

calculate the tangent of the shear angle ϕ , cutting ratio r , was multiplied by the cosine of the side rake angle α , this product was divided by 1 minus the cutting ratio r multiplied by the sine of the rake angle, see equation 3.2.

(Equation 3.2)
$$\tan \phi = \frac{r \cos \alpha}{1 - r \sin \alpha}$$

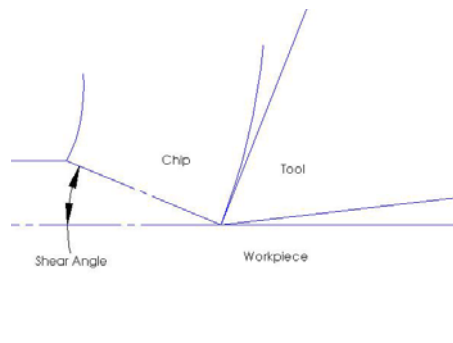


Figure 3.4 The location of the shear angle with respect to the tool, chip, and workpiece.

Force – The forces for the experiment were measured from the percent of load on the motor during turning operations. The percent of load on the motor has the load from the cutting tool and also the torque to turn the workpiece. To gather the amount of force that the machine was using for cutting a current meter was attached to the power line. The ampere was read at the beginning of the cut before any force from the cutting tool was used. This current was used to subtract out the current draw from torque of turning the material. The current I was then multiplied by the volts V from the machine and divided by a constant used to calculate the horsepower (HP) see

equation 3.3. Utilizing the equations 3.4 and 3.5 to calculate torque, the force can be solved for as shown in equation 3.6 and will be used to calculate the force.

$$(Equation 3.3) \quad HP = \frac{V * I}{746}$$

$$(Equation 3.4) \quad Torque = \frac{HP * 5252}{rpm}$$

$$(Equation 3.5) \quad Torque = Force * radius$$

$$(Equation 3.6) \quad Force = \frac{HP * 5252}{radius * rpm}$$

G. Tool wear images – Images of the surface of the cutting tool to visually show the wear of the tool pictures are a .jpeg format taken with the digital camera attached to the stereoscope.

3.3.6 PROCEDURES FOR THE TURNING EXPERIMENT

The procedures for the experiment were established in order to maintain continuity between the different cutting conditions, parameters and tool angle. The procedures are followed to reduce the variation that can occur during experiments.

1. Lathe setup.
 - A. Load program, the program had the specific G and M codes to run at the desired cutting variables and stops to take measurements and collect chips. The complete program can be found in Appendix A.
 - B. Load stock, Adjust the 3-jaw chuck to clamp on the diameter of the workpiece. Then extend the tailstock to the end of the workpiece to support the weight of the workpiece.
 - C. Tools were calibrated to the workpiece parameter.
2. Run program
 - A. While the program was running the percent of load in the X, Z, and spindle on the machine was recorded during each tool and each different cut along the sections of the workpiece. After each pass was complete the BUE will be broken off with a file.
 - B. The program was stopped at each tool change during the pass that 99 or 143 cm³ had been removed to collect chip samples. Depending on the starting diameter of the workpiece the chips were taken during passes 1 or 2 respectively.
 - C. The program was stopped at each tool change during the pass that 290 or 277 cm³ had been removed to collect chip samples. Depending on the starting diameter of the workpiece the chips were taken during passes 3 or 4 respectively.
 - D. The program was stopped at each tool change during the pass that 383 or 403 cm³ had been removed to collect chip samples. Depending on the starting diameter of the workpiece the chips were taken during passes 4 or 6 respectively.

- E. The program was stopped at each tool change during the pass that 562 or 577 cm³ had been removed to collect chip samples. Depending on the starting diameter of the workpiece the chips were taken during passes 6 or 9 respectively.
 - F. The program was stopped at each tool change during the pass that 732 or 730 cm³ had been removed to collect chip samples. Depending on the starting diameter of the workpiece the chips were taken during passes 8 or 12 respectively.
 - G. The program was stopped at each tool change during the final pass that 1047 cm³ had been removed to collect chip samples. Depending on the starting diameter of the workpiece the chips were taken during passes 12 or 20 respectively.
3. Repeat the program for 3 more sets of tools starting at step 2.
 4. Collect data on the cutting tools
 - A. Pictures of the tool wear were taken with a digital camera mounted to the stereoscope. The cutting tool was placed under the stereoscope with an angle block to bring the surface of the tool parallel with the stereoscope. This was to allow the normal surface of the face and flank of the tool to be the true view. The picture was previewed first to verify a clear image and the tool was actually in the screen of the camera. After the preview was verified the picture was recorded. Each cutting tool has two pictures, the face and the flank.
 - B. To measure the tool wear of the cutting tools the optical camera measured the crater depth and contact length. The crater depth was measured with the CMM. The tools were scanned with the probe on the CMM and the resulting scan saved as a drawing file. The scan of the cutting tool was saved as a drawing file (.dwg) to be transferred into a CAD program to gather the necessary crater depth

measurements. The contact length was measured with the optical comparator.

The cutting tool was held in a vice and the surface lights used to examine the worn area for the contact length. The length was measured from the side cutting edge to the end of where the abrasive wear occurred.

5. The chips were analyzed by taking chips from several pre-selected values of volume of material removed. There were several chips measured for chip thickness and an average was used in the calculations. Images of the chip style were taken by a digital camera to compare the change in the chip as the volume of material removed increased.
6. The output variables were calculated by placing the collected data onto a spreadsheet with the correct formulas to produce the output values.

3.4 COMPUTER SIMULATION

The computer simulation used for this thesis was the commercial software Forge 2[®] [xx]. The software analysis the orthogonal cutting in turning; the cutting conditions and parameters used in the software was the same as the turning experiment. The computer simulation also evaluates the effect the side rake angle has on tool wear; the side rake angle will be varied from 0 to 15° by 5°, the same as the turning experiment. In this software application there are formulas used to simulate the turning phenomena for the material, the finite element analysis, the friction law, and the wear model the next sections cover theses formulas (Miles 2002).

3.4.1 PARAMETERS

The computer simulation tests have the feedrate, depth of cut, side rake angle, and cutting surface speed input into the program. The feedrate for the simulation were the

same as the experiment at 0.2 mm/r. The side rake angles are from 0 to 15° by 5°. The test was run for each of the side rake angles at the cutting surface speeds of 25, 30, and 35 m/min. The data was collected from the turning operation and compared to the data from the computer simulation. The computer simulation utilizes several other parameters in order to calculate and model the cutting tool and workpiece. These different laws and models are described below.

3.4.2 MATERIAL LAW

In this work we used the commercial software Forge2[®] [xx] to simulate the orthogonal machining process. Here the material was modeled using the Norton-Hoff law

$$\text{(Equation 3.7)} \quad \dot{s} = 2K(\sqrt{3}\dot{\bar{\epsilon}})^{m-1} \dot{\bar{\epsilon}}$$

shown in equation 3.7, where the stress deviator $\dot{\mathbf{S}}$ was a function of strain rate $\dot{\bar{\epsilon}}$, the effective strain rate $\dot{\bar{\epsilon}}$, the strain rate sensitivity index m , and the strength coefficient K . The strength coefficient accounts for temperature and strain hardening, as shown in

$$\text{(Equation 3.8)} \quad K = K_o (\bar{\epsilon}_o + \bar{\epsilon})^n \exp\left(\frac{\beta}{T}\right)$$

equation 3.8, where K_o is a base strength coefficient, $\bar{\epsilon}$ was the effective strain, n was the strain hardening exponent, and $\bar{\epsilon}_o$ and β are fitting parameters.

3.4.3 FINITE ELEMENT ANALYSIS

Linear 3-noded triangular elements were employed in a plane strain configuration. The plane-strain assumption was reasonable for orthogonal cutting, because there was little variation in strain or temperature in the direction normal to the plane of the cutting tool. The software employs an updated Lagrangian approach, which allows for prediction of the evolution of chip formation, as well as calculation of stresses, strain rates, and temperatures.

3.4.4 FRICTION LAW

The friction between the cutting tool and the workpiece was modeled using a

(Equation 3.9)
$$\tau = -\alpha K \|v_s\|^{q-1} v_s$$

power law where τ was the shear stress at the interface between the cutting tool and the workpiece, α was the friction coefficient, v_s was the sliding velocity of the tool on the workpiece, and q was the sensitivity of the shear stress to the sliding velocity shown in equation 3.9.

3.4.5 WEAR MODEL

Abrasive tool wear can be estimated using Archard's law shown in equation 3.10,

(Equation 3.10)
$$\delta V = kP \delta l$$

where δV was the volume of material removed during a given increment of time, k was a wear coefficient which was a function of tool hardness, microstructure, and lubrication

conditions, P was the normal contact load, and δl was the sliding distance during a given time increment. For a contact area A , the contact pressure and wear depth are given by equations 3.11 and 3.12.

$$\text{(Equation 3.11)} \quad \sigma_n = \frac{P}{A}$$

$$\text{(Equation 3.12)} \quad \delta h = \frac{\delta V}{A}$$

The sliding distance of the tool for a given increment of time was given by equation 3.13 where Δv_s is the sliding velocity during time increment δt . The material removed at a point on the tool, at a given point in time, was then estimated using an explicit integration scheme.

$$\text{(Equation 3.13)} \quad \delta l = \Delta v \delta t$$

3.5 COMPARITIVE STUDY OF DATA

The data between the simulation and the experiment was compared graphically to see if there are any trends that may occur with the cutting surface speed and the side rake angle. There are several comparisons made with how the outputs are related to the side rake angles. The study made four comparisons they are as follows:

1. Shear angle versus side rake angle as the cutting surface speed increased.

2. Cutting ratio versus side rake angle as the cutting surface speed increased.
3. Contact length versus side rake angle as the cutting surface speed increased.
4. Force versus side rake angle as the cutting surface speed increased.

CHAPTER 4

RESULTS AND ANALYSIS

Data gathered during this thesis has been used to evaluate the functionality of tool wear prediction from a computer simulation using Archard's law. Experimental data has been gathered to compare with computer simulation data for tool wear. The data has been examined in three sections. These sections are experimental results, simulation results and a comparison analysis. The first two sections compared similar side rake angle and then examined the entire set of data for that side rake angle. The data gathered for the same cutting surface speed was compared after the side rake angle comparisons for the first two sections. The comparison analysis section has been used to compare the effect the side rake angle had in relationship to the outputs. The comparisons are side rake angle versus shear angle, cutting ratio, contact length and force.

4.1 EXPERIMENTAL RESULTS

The results from the experiment were gathered and recorded onto data sheets, the complete data sheets can be found in Appendix B. The tool wear data was presented by showing the data by the same side rake angle and then analyzed by the same cutting surface speed. The chip thickness measurement results are based on an average of 60 samples the complete measurements are in Appendix C. Images of the cutting tools were examined with the chip images, and output data to better understand the dynamics of the

cutting process. Appendix D contains the entire images of the chips formed by the cutting tool, in this chapter only the first and last samples are shown.

4.1.1 SIDE RAKE ANGLE COMPARISON FOR THE EXPERIMENTAL RESULTS

The results in this section are compared to the same side rake angle cutting tools as the cutting surface speed increased. The results showed images of the cutting tools as well as chips formed during the material removal process.

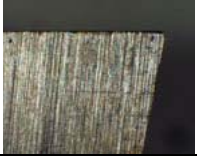
There were several different styles of chips that were removed from the workpiece. The chips were gathered six times for each cutting tool at the different side rake angles and the different cutting surface speeds. The evaluation for the chip styles was observed with similar side rake angles. In general as the cutting tools removed more material the chip color was expected to get darker. The darker color signified that more heat has been removed from the workpiece into the chip.

4.1.1.1 THE 0° SIDE RAKE ANGLE TOOLS

4.1.1.1.1 THE 0° SIDE RAKE ANGLE AT 25 M/MIN

The cutting tool tested for the 0° side rake angle tool at a cutting surface speed of 25 m/min as shown in Table 4.1. These images show the cutting tool before and after

Table 4.1 The 0° side rake angle cutting tool pictures at 25 m/min.

0° Side Rake Angle Tool at 25 m/min Rake Face	
Before	After
	

the cutting process and the wear that occurred. The rake face of the tool can be seen in Table 4.1, which showed the contact length and the crater size that occurred due to tool wear. The contact length measured 0.625 mm and the lighter color steel can be seen on the rake face. A measurement of 0.0508 mm was the depth of the crater. The crater depth was created from the wear of the chip being formed against the rake face of the cutting tool. The chips from the first and last pass show the progression of the chips formed as the volume of material removed increased. These chips are seen in Figure 4.1. Observations from the chips show that the last pass (pass 12) chips are darker than

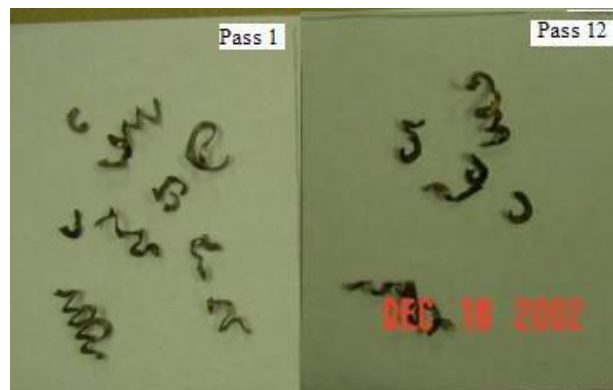


Figure 4.1 Chip images from the first and last sampling for the 0 ° side rake tool at 25 m/min.

those collected in pass 1. The darker color of the chips indicates greater heat caused from increased contact from the chip with the cutting tool. The chips had tight curls throughout the cutting operations but show some evidence that the chip may become stringy. In conjunction with the chip color and style the chip thickness was used to gather information. The chip thickness for the 0° side rake angle tool at 25 m/min had an average of 0.671 mm. The average chip thickness taken from six different sampled measurements can be seen in Figure 4.2. The chip thickness for this cutting tool showed

a general increase in chip thickness as the volume of material removed was increased. The chip thickness was used to calculate the shear angle and cutting ratio, these values are 16.72° and 0.300 respectively. The force calculated for this cutting tool was 219 pounds of force used to remove material from the workpiece by the cutting tool.

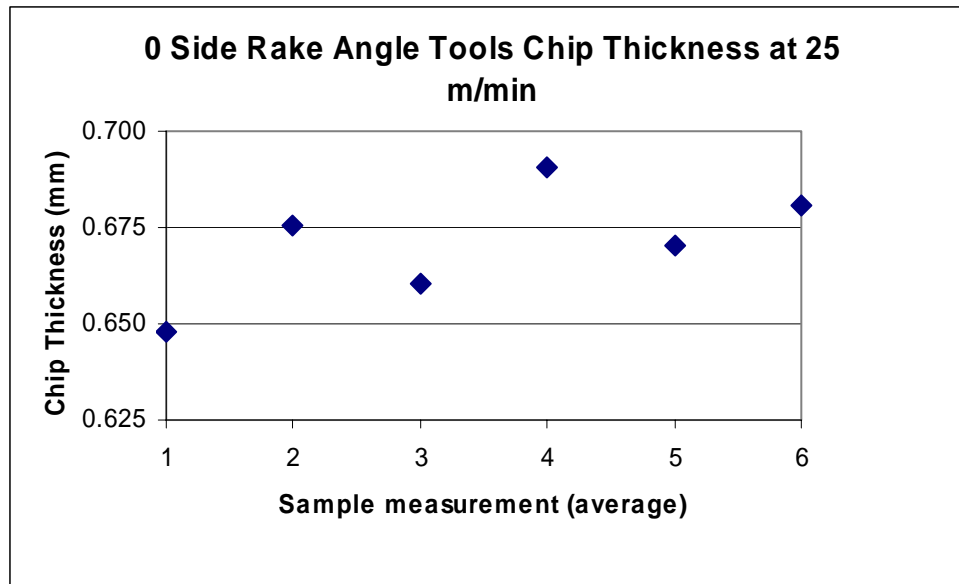


Figure 4.2 The average measurements from the six samplings taken for the 0° side rake tool at 25 m/min.

4.1.1.1.2 THE 0° SIDE RAKE ANGLE AT 30 M/MIN

The images for the 0° side rake angle tool cutting at the 30 m/min cutting surface speed are shown in Table 4.2. The contact length for this cutting tool measured 0.559 mm and the crater depth was 0.0686 mm. The chips formed during the beginning of the cutting process had tight curls and some discoloration. However at the end of the cutting process the chips became stringier and darker as seen in

Table 4.2 The 0° side rake angle cutting tool pictures at 30 m/min.

0° Side Rake Angle Tool at 30 m/min Rake Face	
Before	After
	

Figure 4.3. The stringer chip formed was caused from a BUE or less than ideal cutting conditions. The average measurement from all of the chips measured from this cutting tool was 0.713 mm. The average measurements from the six different sampling at the

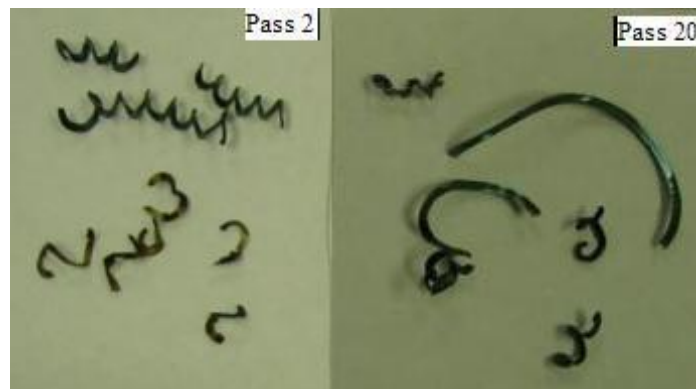


Figure 4.3 Chip images from the first and last sampling for the 0° side rake tool at 30 m/min.

select volumetric material removal value can be seen in Figure 4.4. As the cutting tool removed more material the chip thickness decreased, however the last sampling of chips are thicker by 0.200 mm from the other 5 samples taken. The stringier the chip the thicker the chip thickness becomes. The increased chip thickness for the last sampling correlates with the images of the chip. The shear angle measured for this cutting tool was 15.67°. The calculation for the cutting ratio was 0.281. A force of 213 lbs was

calculated for the material removal by the 0° side rake angle cutting tool at the 30 m/min cutting surface speed.

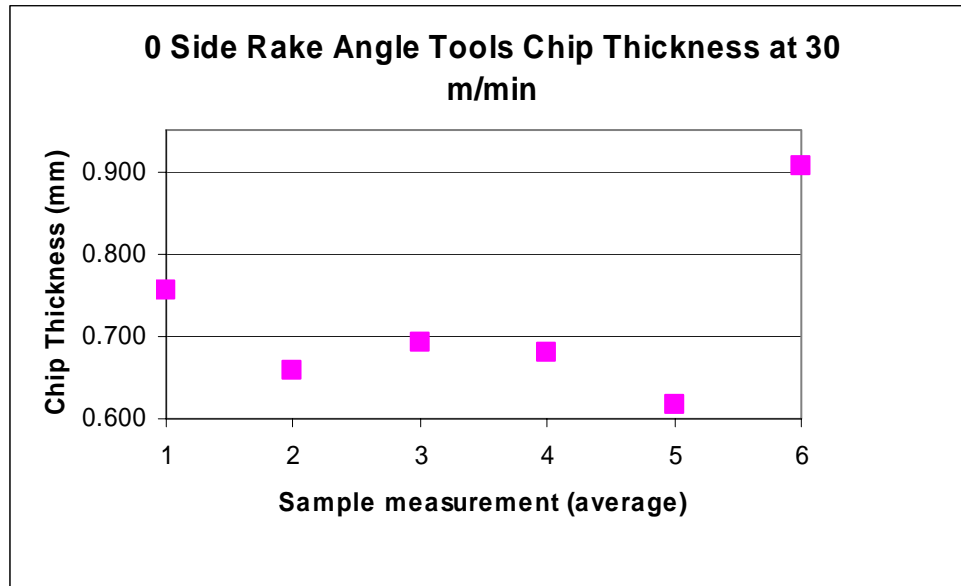


Figure 4.4 The average measurements from the six samplings taken for the 0° side rake tool at 30 m/min.

4.1.1.1.3 THE 0° SIDE RAKE ANGLE AT 35 M/MIN

The 0° side rake angle cutting tool that cut at 35 m/min had a prominent crater on the rake face of the cutting tool as seen in Table 4.3. The crater depth measured

Table 4.3 The 0° side rake angle cutting tool pictures at 35 m/min.

0° Side Rake Angle Tool at 35 m/min Rake Face	
Before	After

0.0762 mm and the contact length was 0.400 mm. The chips that were formed by this cutting tool show a stringy, loose curled chip at the beginning of the cutting. The chips formed at the end of cutting are less stringy and have a tighter curl than at the

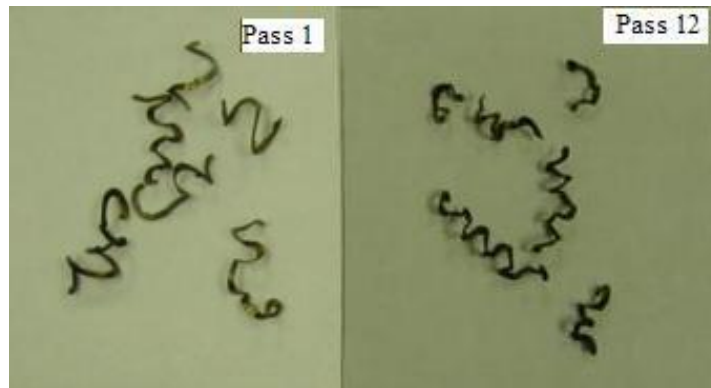


Figure 4.5 Chip images from the first and last sampling for the 0° side rake tool at 35 m/min.

beginning as seen in Figure 4.5. Looking at the chip thickness average measurements in Figure 4.6 the trend agrees with the images of the chips. The color of the chips increased in darkness from the first sample to the last. In Figure 4.6 the second average measurements taken show an increased thickness that could be from a BUE. A force of 224 lbs was calculated for the cutting tool, while the shear angle was calculated at 16.92°. The cutting ratio for the 0° side rake angle tool cutting at 35 m/min was calculated at 0.304.

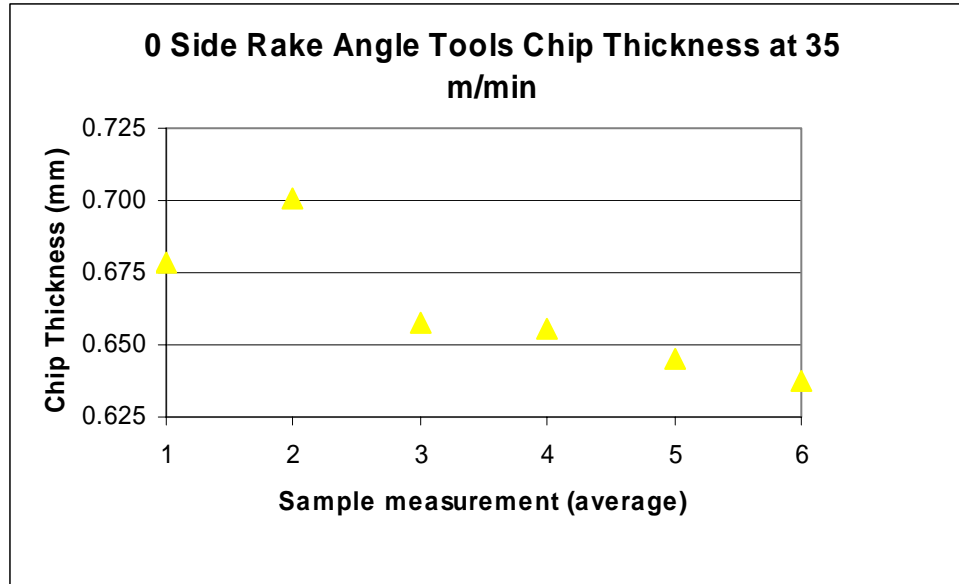


Figure 4.6 The average measurements from the six samplings taken for the 0° side rake tool at 35 m/min.

4.1.1.1.4 COMPARISON OF THE 0° SIDE RAKE ANGLE TOOL

In this section the comparison of the 0° side rake angle tools with the increasing cutting surface speed will be examined. In looking at the data gathered from these cutting tools, as seen in Table 4.4, there was a common pattern with the shear angle, cutting ratio and force. This pattern was that the data at the 30 m/min cutting surface

Table 4.4 The 0° side rake angle cutting tools results.

0° Side Rake Angle Cutting Tools						
Cutting Speed (m/min)	Chip Thickness avg. (mm)	Crater Depth (mm)	Contact Length (mm)	Shear Angle (degrees)	Cutting Ratio	Force (lbs)
25	0.671	0.0508	0.625	16.72	0.300	219
30	0.718	0.0686	0.559	15.67	0.281	213
35	0.663	0.0762	0.400	16.92	0.304	224

speed had a lower value than the other two cutting surface speeds. The chip thickness data had a similar trend except that the 30 m/min cutting surface speed was larger than the other two. The average chip thickness for the 30 m/min cutting tool had elevated chip thickness values for the last sampling taken. The average chip thickness without the last sampling was 0.681 mm still above the other two values. The chips formed at 30 m/min were thicker and stringier than the other two cutting surface speeds. The appearance of the chips from the 30 m/min cutting tool provided an explanation for the elevated chip thickness value. The tool wear data showed different trends, the crater depth increased as the cutting surface speed increased. However, the contact length decreased as the cutting surface speed increased. The data showed that as the cutting surface speed increased there was a decrease in contact length made from the chip but an increased crater on the rake face.

4.1.1.2 THE 5° SIDE RAKE ANGLE TOOLS

4.1.1.2.1 THE 5° SIDE RAKE ANGLE AT 25 M/MIN

The cutting tool for the 5° side rake angle with a 25 m/min cutting surface speed had a contact length of 0.456 mm. The contact length indicated by the lighter color material can be seen in the image of the cutting tool shown in Table 4.5. The image taken after the cutting process shows discoloration due to the temperatures of cutting. The crater depth on this tool measured 0.0432 mm. The first and last samples of chips are shown in Figure 4.7. The chips from the first sample are long and have a tight curl to them. In the last sample taken the chips still have a tight curl but are darker and shorter than those from the first sample. The average chip thickness from the average of the 6 samples was 0.554 mm. As the volume of material removed increased the chip thickness

increased in general as seen in Figure 4.8. The cutting ratio was calculated at 0.364 and the shear angle 20.52° . The force measured 216 pounds for the 5° side rake angle cutting tool at 25 m/min

Table 4.5 The 5° side rake angle cutting tool pictures at 25 m/min.

5° Side Rake Angle Tool at 25 m/min Rake Face	
Before	After
	

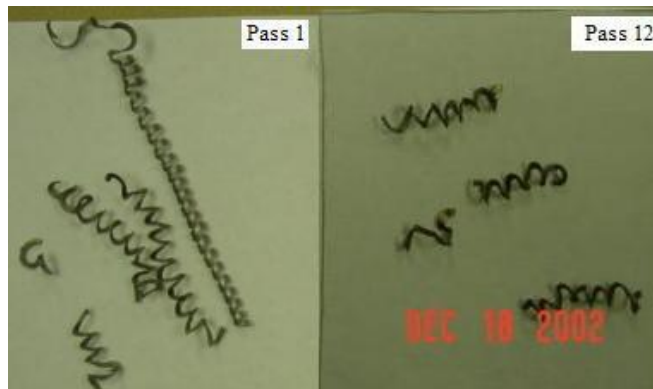


Figure 4.7 Chip images from the first and last sampling for the 5° side rake tool at 25 m/min.

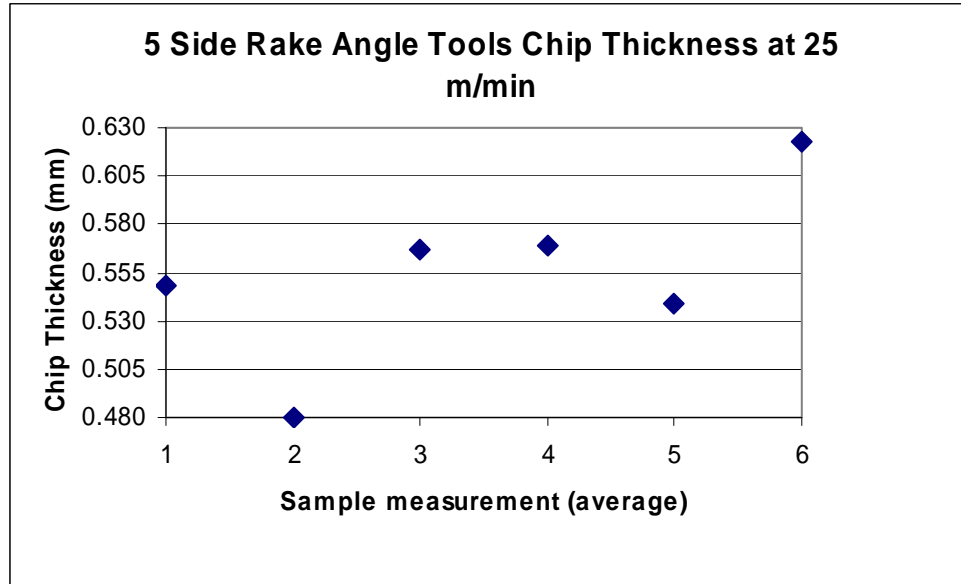


Figure 4.8 The average measurements from the six samplings taken for the 5° side rake tool at 25 m/min.

4.1.1.2.2 THE 5° SIDE RAKE ANGLE AT 30 M/MIN

The cutting tool image showed a similar area for the contact length and the overall wear area on the rake face of the tool as the previous cutting tool. The before and after images of the 5° side rake angle cutting tool at 30 m/min cutting surface speed can be

Table 4.6 The 5° side rake angle cutting tool pictures at 30 m/min.

5° Side Rake Angle Tool at 30 m/min Rake Face	
Before	After
	

seen in Table 4.6. The area around the crater where the contact length was measured was a couple shades lighter than the area around it. The contact length measured 0.352 mm in length and the crater measured 0.0305 mm in depth. The chips formed at the start of the material removal process had a tight curl and showed some stringiness of the chip. The chips taken at the end of the material removal process are darker in color, had a tight curl and were short stringy chips too. The chips of the first and last sampling can be seen in Figure 4.9. The stringy chips decreased in length as the material removed increased.

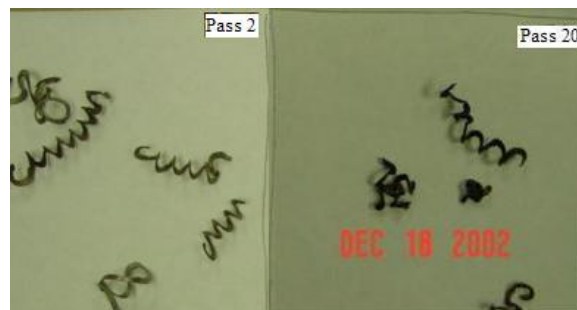


Figure 4.9 Chip images from the first and last sampling for the 5° side rake tool at 30 m/min.

The average chip thickness for the chips measured for the 5° side rake angle cutting tool at 30 m/min was 0.630 mm. The general trend of the chip thickness increased the more material was removed by the cutting tool as shown in Figure 4.10. The greater increase for the last sample chip thickness are from a BUE, the change in color of the latter chip also explains the chip was being removed at a higher temperature than the earlier chips, this would account for the increased chip thickness. The force measured for this cutting tool as it removed material was 202 pounds. The shear angle was calculated at 18.15° while the cutting ratio was 0.320.

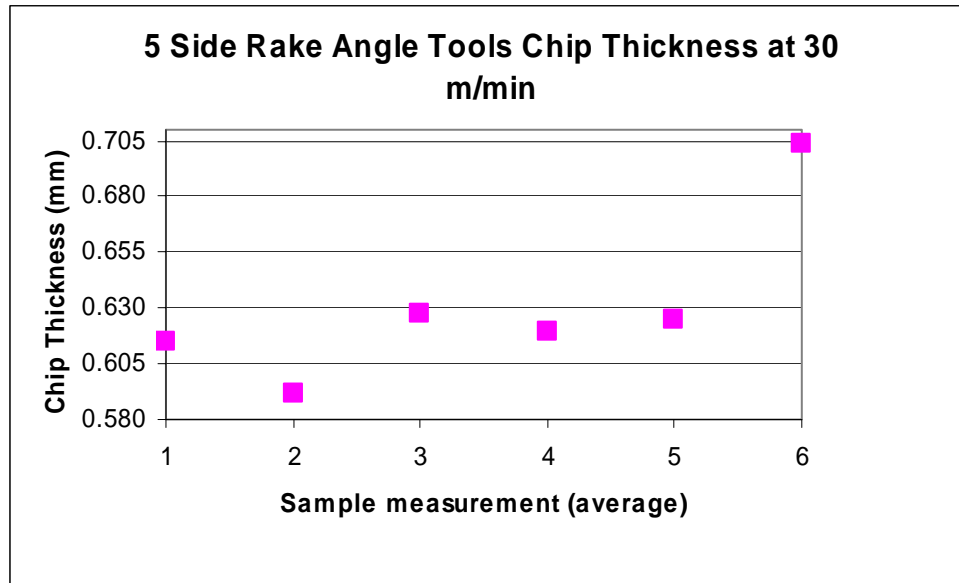


Figure 4.10 The average measurements from the six samplings taken for the 5° side rake tool at 30 m/min.

4.1.1.2.3 THE 5° SIDE RAKE ANGLE AT 35 M/MIN

The 5° side rake angle cutting tool at 35 m/min cutting surface speed had a contact length that measured 0.325 mm. The image of the cutting tool showed the contact length as the lighter color material near the top of the cutting tool and can be seen in Table 4.7. The depth of the crater on the rake face measured 0.0508 mm. The average chip thickness for the cutting tool averaged out to be 0.638 mm. The first and last sample of chips can be seen in Figure 4.11; the chips from the first sample are curled and have some chips that are short and stringy. The chips from the last sample taken are darker and had a tighter curl. However the data gathered from the different samples of the chip thickness are shown in Figure 4.12, they showed no real trend. The thickest

Table 4.7 The 5° side rake angle cutting tool pictures at 35 m/min.

5° Side Rake Angle Tool at 35 m/min Rake Face	
Before	After
	



Figure 4.11 Chip images from the first and last sampling for the 5° side rake tool at 35 m/min.

measurement from the chip came from the second sampling. There was no obvious explanation for the data provide in Figure 4.12. The shear angle and the cutting ratio for this cutting tool are 17.93° and 0.316 respectively. The force calculated for the 5° side rake angle cutting tool at 35 m/min was 173 pounds.

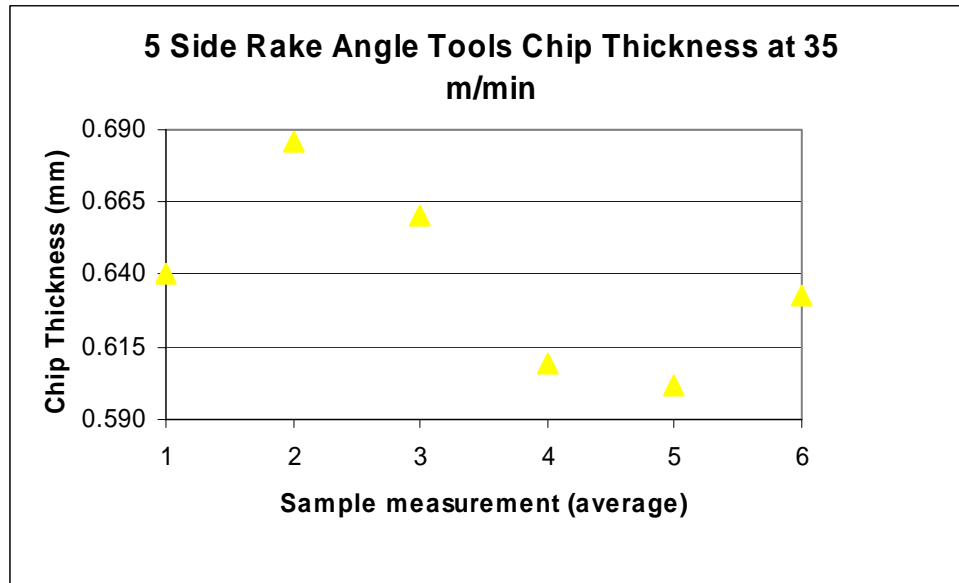


Figure 4.12 The average measurements from the six samplings taken for the 5° side rake tool at 35 m/min.

4.1.1.2.4 COMPARISON OF THE 5° SIDE RAKE ANGLE TOOL

In looking at the entire 5° side rake angle cutting tools against each other, showed some trends as the cutting surface speed increased. The contact length, shear angle, cutting ratio and force all decreased as the cutting surface speeds increased. The chip thickness increased as the cutting surface speed increased. However there was no trend for the crater depth, it did follow a similar pattern that occurred at the 0° side rake angle cutting tool data. There was no substantial data to explain the reason for the crater depth outcome. The data for the 5° side rake angle cutting tools can be seen in Table 4.8.

Table 4.8 The 5° side rake angle cutting tools results.

5° Side Rake Angle Cutting Tools						
Cutting Speed (m/min)	Chip Thickness (mm)	Crater Depth (mm)	Contact Length (mm)	Shear Angle (degrees)	Cutting Ratio	Force (lbs)
25	0.554	0.0432	0.456	20.52	0.364	216
30	0.630	0.0305	0.352	18.15	0.320	202
35	0.638	0.0508	0.325	17.93	0.316	173

4.1.1.3 THE 10° SIDE RAKE ANGLE TOOLS

4.1.1.3.1 THE 10° SIDE RAKE ANGLE TOOL AT 25 M/MIN

The tool wear images showed that the contact length for the 10° side rake angle cutting tool at 25 m/min cutting surface speed was not as light as the cutting tools from the previous two side rake angles. However the contact length as seen in Table 4.9 and the color of the crater region was more consistent of a color with the remainder of the material on the cutting tool rake face. The contact length measured 0.423 mm and the crater depth measured 0.0279 mm. The chips from the first sample had curls that were loose and tight, and long. The looser curl chips from the first sample were also stringy. The chips from the last sample were darker, the curl was tighter and the length of the chip

Table 4.9 The 10° side rake angle cutting tool pictures at 25 m/min.

10° Side Rake Angle Tool at 25 m/min Rake Face	
Before	After
	

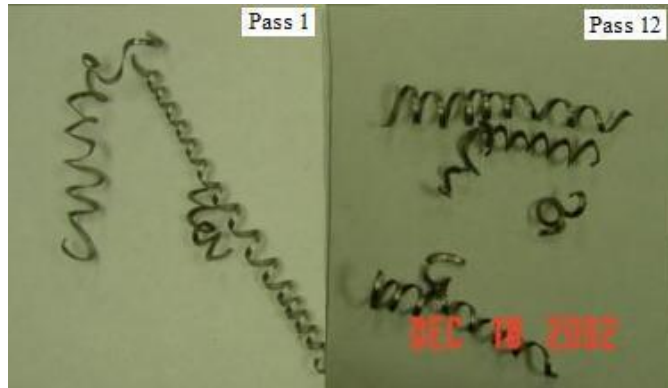


Figure 4.13 Chip images from the first and last sampling for the 10° side rake tool at 25 m/min.

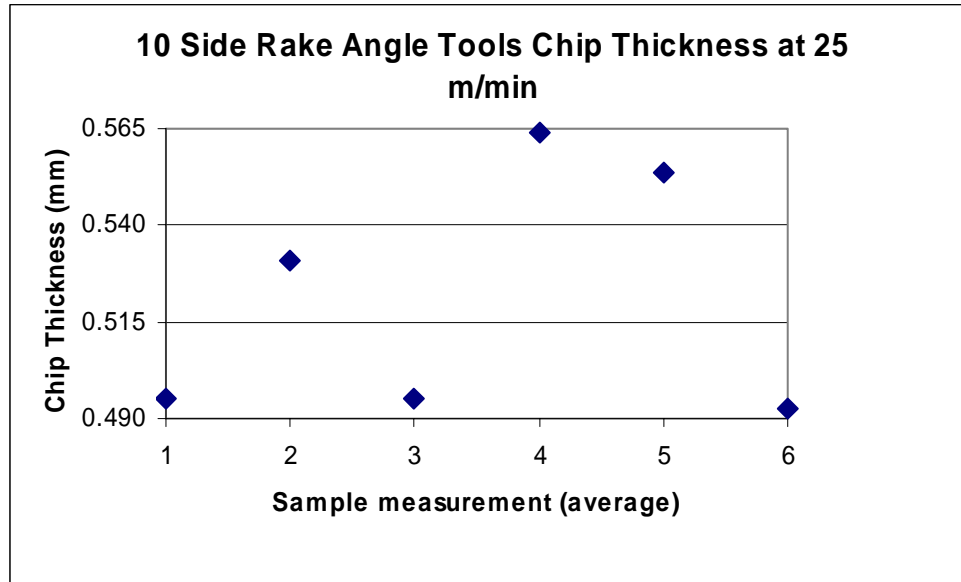


Figure 4.14 The average measurements from the six samplings taken for the 10° side rake tool at 25 m/min.

was shorter, as shown in Figure 4.13. Some of the chips from the last sample were categorized as short and stringy. The average chip thickness measures 0.522 mm for the entire set of chips sampled. The data from the averages of each of the 6 samples of chip thickness are shown in Figure 4.14. The shear angle calculation was 22.18° and the

cutting ratio was calculated at 0.386. The force calculated for the 10° side rake angle cutting tool at 25 m/min was 200 pounds.

4.1.1.3.2 THE 10° SIDE RAKE ANGLE TOOL AT 30 M/MIN

The 10° side rake angle cutting tool at 30 m/min had tool wear that measured 0.444 mm and 0.0254 mm for the contact length and crater depth respectively. The cutting tool before and after images are shown in Table 4.10, the area on the rake face showed little difference between color of the rake face and the crater region. The chips that were formed by the cutting tool showed that as the increased material removed the chips formed a tighter curl, shorter chips and the color darkens. Some of the chips from the first sampling are short and stringy; these chips are shown in Figure 4.15. The average measurement for the entire sample chips for the 10° side rake angle cutting tool at 30 m/min was 0.580 mm. The general trend for the six chip samples showed an increase in the chip thickness as the material removed was increased. However there was a decrease in the chip thickness on the fifth sample set. The values for the chip thickness averages are shown in Figure 4.16. The force was calculated at 177 pounds for the 10° side rake angle cutting tool at 30 m/min. The shear angle and the cutting ratio were calculated at 20.00° and 0.347 respectively.

Table 4.10 The 10° side rake angle cutting tool pictures at 30 m/min.

10° Side Rake Angle Tool at 30 m/min Rake Face	
Before	After
	

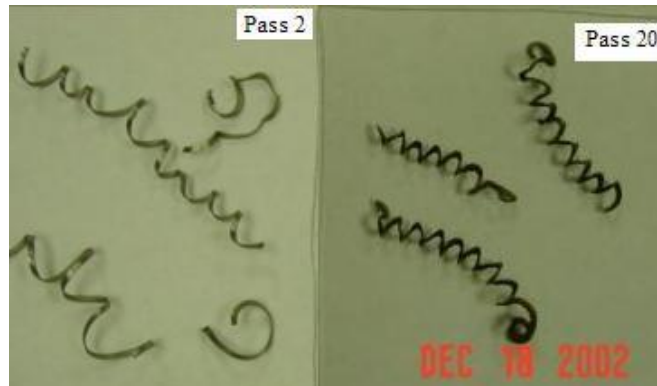


Figure 4.15 Chip images from the first and last sampling for the 10° side rake tool at 30 m/min.

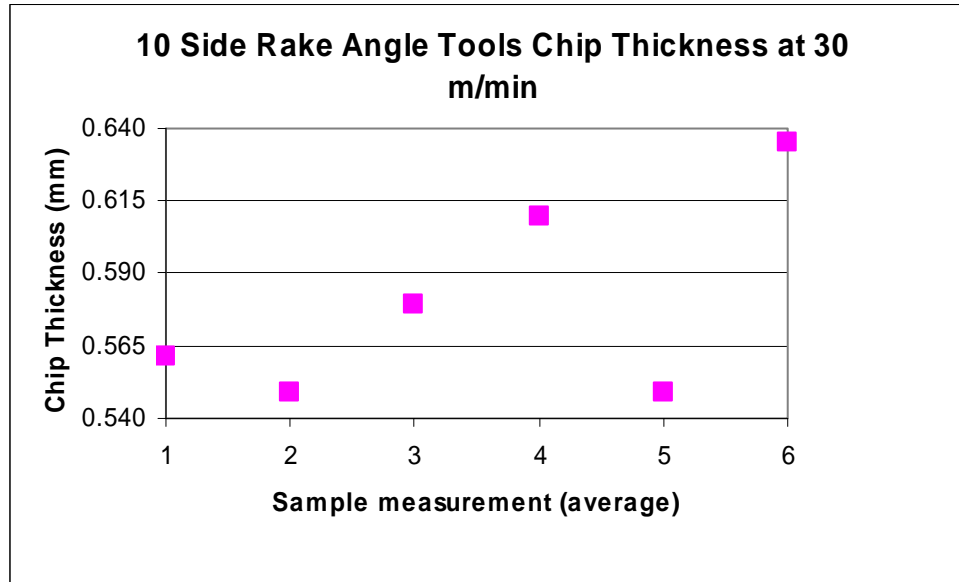


Figure 4.16 The average measurements from the six samplings taken for the 10° side rake tool at 30 m/min.

4.1.1.3.3 THE 10° SIDE RAKE ANGLE TOOL AT 35 M/MIN

The rake face of the 10° side rake angle tool at 35 m/min cutting surface speed had a similar color pattern on the entire rake face. The area where the contact length was measured was darker than the rest of the rake face. This cutting tool was different than

the previous cutting tools in the area of the contact length was darker than the rest of the rake face shown in Table 4.11. The contact length for this tool measured 0.453 mm in

Table 4.11 The 10° side rake angle cutting tool pictures at 35 m/min.

10° Side Rake Angle Tool at 35 m/min Rake Face	
Before	After
	

length. The depth of the crater measured 0.0356 mm in depth. The average chip thickness measured 0.565 mm and the formed chips during the material removal process are similar between the different samples taken. The chips from this cutting tool are tightly curled. The main difference between the first and last sample of chips was that the last sample are darker, shown in Figure 4.17. There was some indication at the

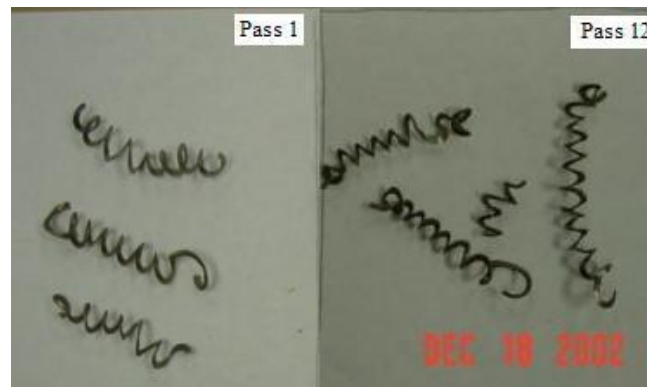


Figure 4.17 Chip images from the first and last sampling for the 10° side rake tool at 35 m/min.

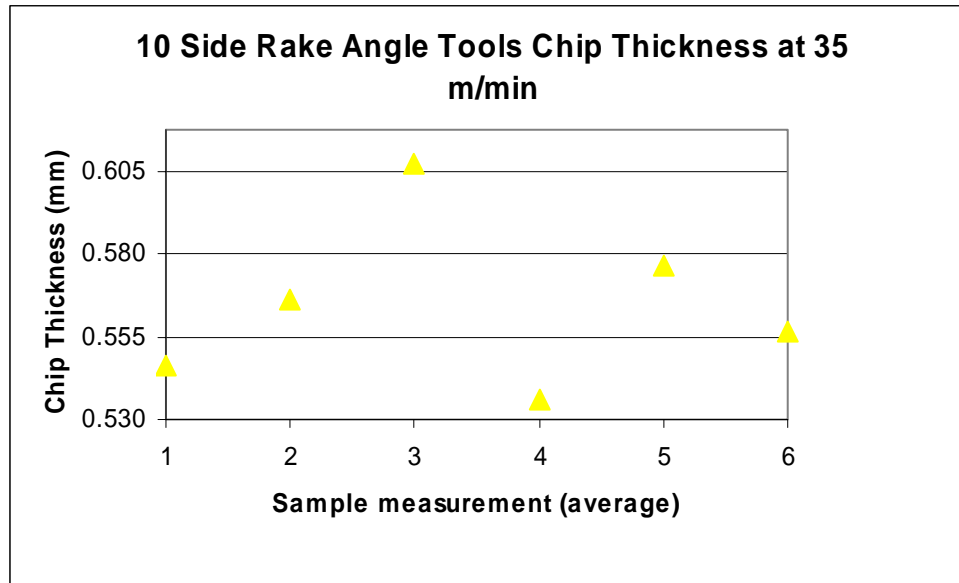


Figure 4.18 The average measurements from the six samplings taken for the 10° side rake tool at 35 m/min.

beginning and end of each chip that the chip might become stringy but actually did not. The pattern for the chip thickness increased between the first three samples taken then decreased to a thickness below that of the first sample. The pattern for the first three samples was repeated over the last three. The average chip thicknesses by sample are shown in Figure 4.18. The shear angle for this cutting tool was calculated at 20.54° and the cutting ratio was 0.357. The force calculated for the 10° side rake angle tool at 35 m/min was 162 pounds.

4.1.1.3.4 COMPARISON OF THE 10° SIDE RAKE ANGLE TOOL

In evaluating the data for the 10° side rake angle cutting tools there were trends and patterns that were seen. The first trend was as the cutting surface speed increased the contact length also increased. The next trend was the force decreased as the cutting

surface speed increased. A similar pattern can be seen in the crater depth, shear angle and cutting ratio. The pattern that was followed for those three measurements was that the 30 m/min cutting surface speed data was less than the 25 and 35 m/min cutting surface speed. The pattern with the chip thickness was opposite of the pattern previously stated, the 30 m/min cutting surface speed chip thickness was larger than the 25 and 35 m/min cutting surface speed. The data for the 10° side rake angle cutting tools are shown in Table 4.12.

Table 4.12 The 10° side rake angle cutting tools results.

10° Side Rake Angle Cutting Tools						
Cutting Speed (m/min)	Chip Thickness (mm)	Crater Depth (mm)	Contact Length (mm)	Shear Angle (degrees)	Cutting Ratio	Force (lbs)
25	0.522	0.0279	0.423	22.18	0.386	200
30	0.580	0.0254	0.444	20.00	0.347	177
35	0.565	0.0356	0.453	20.54	0.357	162

4.1.1.4 THE 15° SIDE RAKE ANGLE TOOLS

4.1.1.4.1 THE 15° SIDE RAKE ANGLE TOOL AT 25 M/MIN

The cutting tool with the 15° side rake angle at the 25 m/min cutting surface speed had less discoloration than the previous tools as seen in Table 4.13. The after image of the cutting tool was discolored but not as dark as the previously examined cutting tools. The contact length area had a dark outline around the area. The contact

Table 4.13 The 15° side rake angle cutting tool pictures at 25 m/min.

15° Side Rake Angle Tool at 25 m/min Rake Face	
Before	After
	

length measured 0.371 mm and the crater depth measured 0.0152 mm. The chips created during the material removal process are shown in Figure 4.19. The only difference between the chips was that the chips increased in darkness as the material removed increased. The chips however did not darken to the purple color as seen with the 0 and 5° side rake angle cutting tools. The chips had long curls and some of the chips were stringy throughout the material removal process. The average chip thickness for this cutting tool was 0.470 mm. There was no trend or pattern for the average chip thickness between each of the 6 samples taken as shown in Figure 4.20. The force calculated for this cutting tool was 193 pounds. The shear angle and the cutting ratio were calculated and the results were 24.99° and 0.429 respectively.

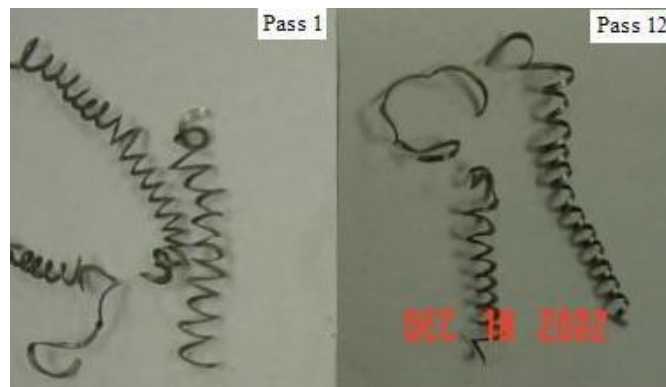


Figure 4.19 Chip images from the first and last sampling for the 15° side rake tool at 25 m/min.

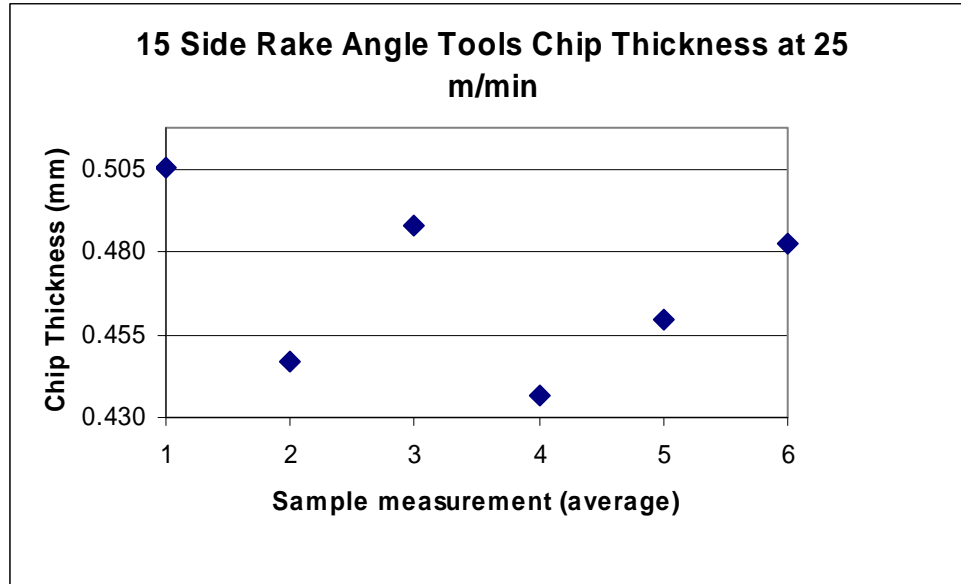


Figure 4.20 The average measurements from the six samplings taken for the 15° side rake tool at 25 m/min.

4.1.1.4.2 THE 15° SIDE RAKE ANGLE TOOL AT 30 M/MIN

The images from the 15° side rake angle cutting tool at 30 m/min cutting surface speed are shown in Table 4.14. The lighter area at the top of the after image was the contact length that measured 0.396 mm. The crater depth for this cutting tool measured

Table 4.14 The 15° side rake angle cutting tool pictures at 30 m/min.

15° Side Rake Angle Tool at 30 m/min Rake Face	
Before	After
	

0.0076 mm. The average chip thickness for this cutting tool was 0.521 mm. The chips formed during the first and last sampling can be seen in Figure 4.21. The chips sampled at the beginning are long and stringy and when a curl did form the curls were sporadic. The chips sampled at the end of the material removal process were shorter but stringy at the ends and had tighter curled chip. The color of the last chips sample were darker but had not went to the purple color. The general trend for the average chip thickness increased over the six samples shown in Figure 4.22. A shear angle of 22.55° and a cutting ratio of 0.387 were calculated for this cutting tool. The force for the material removal was measured at 174 pounds.

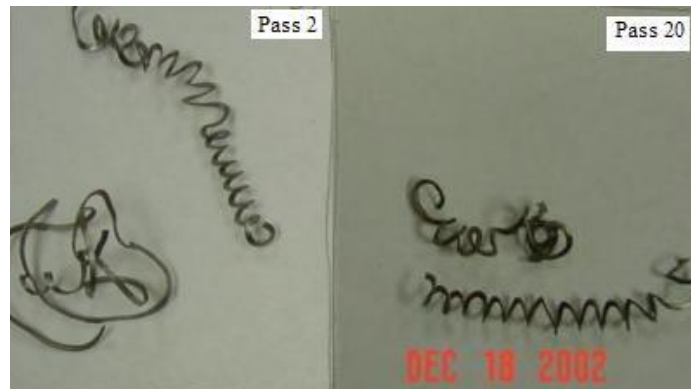


Figure 4.21 Chip images from the first and last sampling for the 15° side rake tool at 30 m/min.

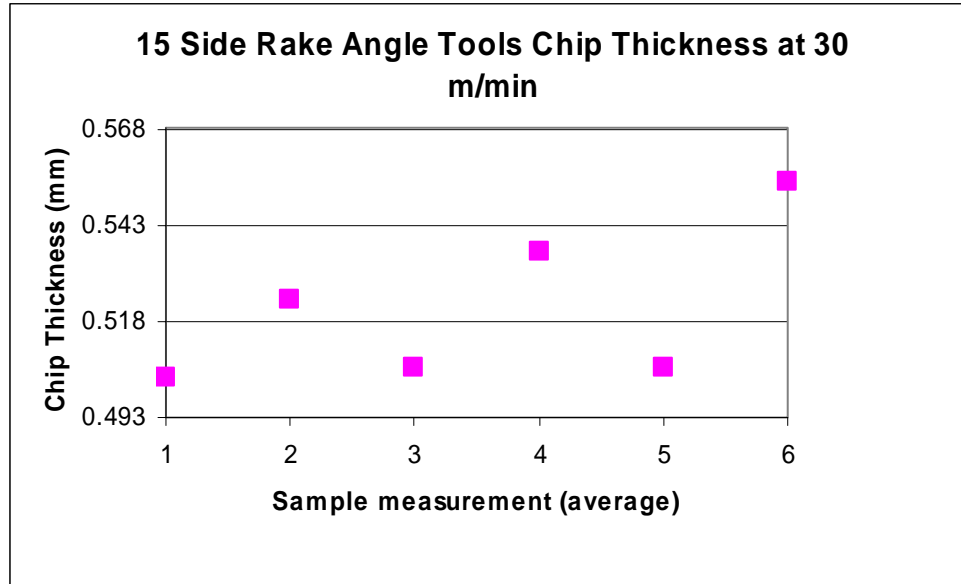


Figure 4.22 The average measurements from the six samplings taken for the 15° side rake tool at 30 m/min.

4.1.1.4.3 THE 15° SIDE RAKE ANGLE TOOL AT 35 M/MIN

A crater depth of 0.0305 mm and a contact length of 0.435 mm were measured for the 15° side rake angle cutting tool at 35 m/min cutting surface speed. The rake face images of the cutting tool are shown in Table 4.15. The contact length region appeared

Table 4.15 The 15 ° side rake angle cutting tool pictures at 35 m/min.

15 ° Side Rake Angle Tool at 35 m/min Rake Face	
Before	After
	

lighter in color than the remainder of the rake face. The rake face, other than the contact length region were darker than the heat generated between the cutting tool and the removed chip. The chips formed from this cutting tool were short and stringy and never formed curls. The main difference between the first and the last chips sampled, shown in Figure 4.23, were the later chips were darker in color. The average chip thickness for this cutting tool was 0.555 mm. The trend for the six samples for the average chip thickness increased as the material removed increased as shown in Figure 4.24. The force measured for the 15° side rake angle cutting tool at 35 m/min was 141 pounds. The shear angle and the cutting ratio were calculated at 21.19° and 0.364 respectively.

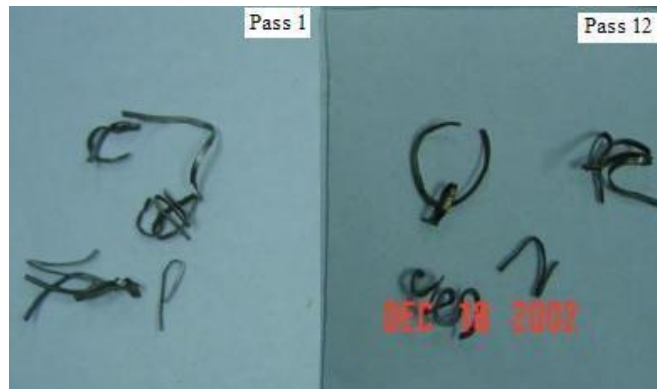


Figure 4.23 Chip images from the first and last sampling for the 15° side rake tool at 35 m/min.

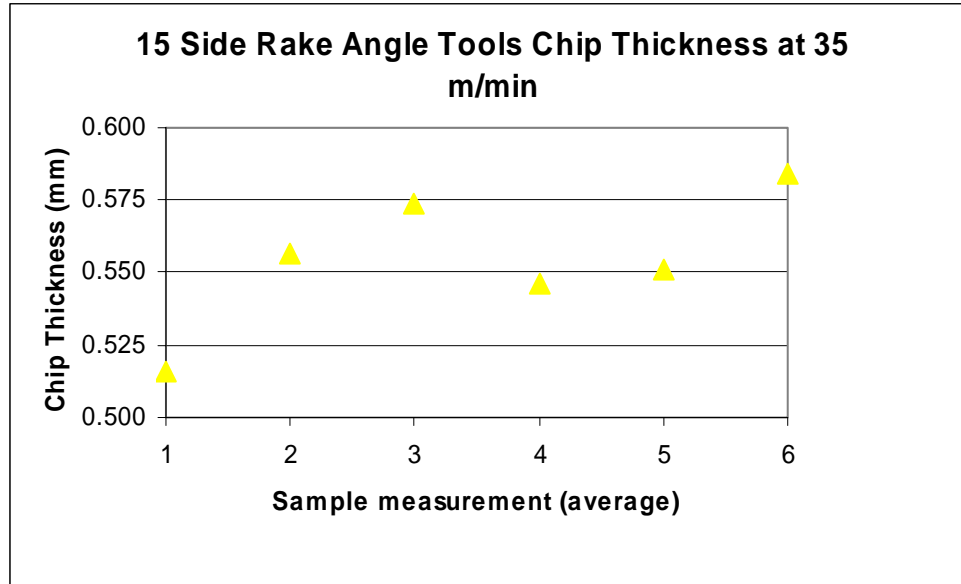


Figure 4.24 The average measurements from the six samplings taken for the 15° side rake tool at 35 m/min.

4.1.1.4.4 COMPARISON OF THE 15° SIDE RAKE ANGLE TOOL

The calculated shear angle, cutting ratio and force decreased as the cutting surface speed increased for the 15° side rake angle cutting tools. The chip thickness and contact length values increased as the cutting surface speed increased. The crater depth did not have a significant pattern to compare with the other output data. The data gathered for the 15° side rake angle tools are shown in Table 4.16.

Table 4.16 The 15° side rake angle cutting tools results.

15° Side Rake Angle Cutting Tools						
Cutting Speed (m/min)	Chip Thickness (mm)	Crater Depth (mm)	Contact Length (mm)	Shear Angle (degrees)	Cutting Ratio	Force (lbs)
25	0.470	0.0152	0.371	24.99	0.429	193
30	0.521	0.0076	0.396	22.55	0.387	174
35	0.555	0.0305	0.435	21.19	0.364	141

4.1.2 CUTTING SURFACE SPEED COMPARISON FOR THE EXPERIMENTAL RESULTS

In this comparison the different outputs were compared to the three cutting surface speeds on one graph. The side rake angle cutting tools were plotted with the same symbol throughout this section. Having the data plotted on the graph in this manner allowed the entire set of data was available on one plot, rather than three separate plots for the different cutting surface speeds. The different outputs that have been examined were the chip thickness, crater depth, contact length, shear angle, cutting ratio and force.

4.1.2.1 CHIP THICKNESS

The trend for the three cutting surface speeds chip thickness data showed that as the side rake angle increased from 0 to 15° the chip thickness decreased. This trend can be seen because the pattern of the symbols was the same going down from top to bottom of the graph for each cutting surface speed as shown in Figure 4.25. The chip thickness values at the 30 m/min cutting surface speed appeared to be elevated. The cutting tools used for the 30 m/min cutting surface speed removed material at a smaller diameter of the workpiece than the cutting tools used for the 25 and 35 m/min cutting surface speed. The images of the chips at 30 m/min did not provide enough similarities to correlate the increased values of the chip thickness to the chip style.

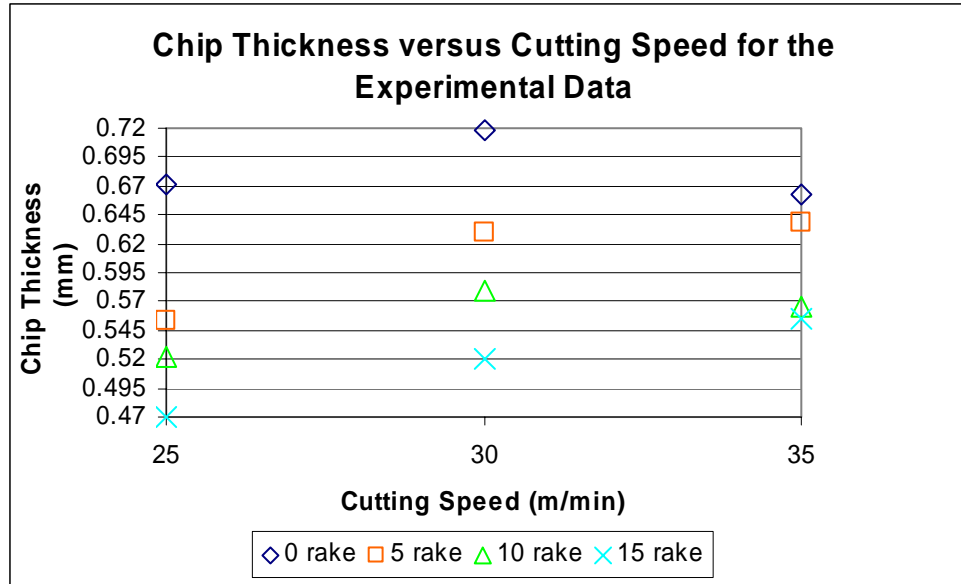


Figure 4.25 Graph of the chip thickness versus cutting surface speed for the experimental results.

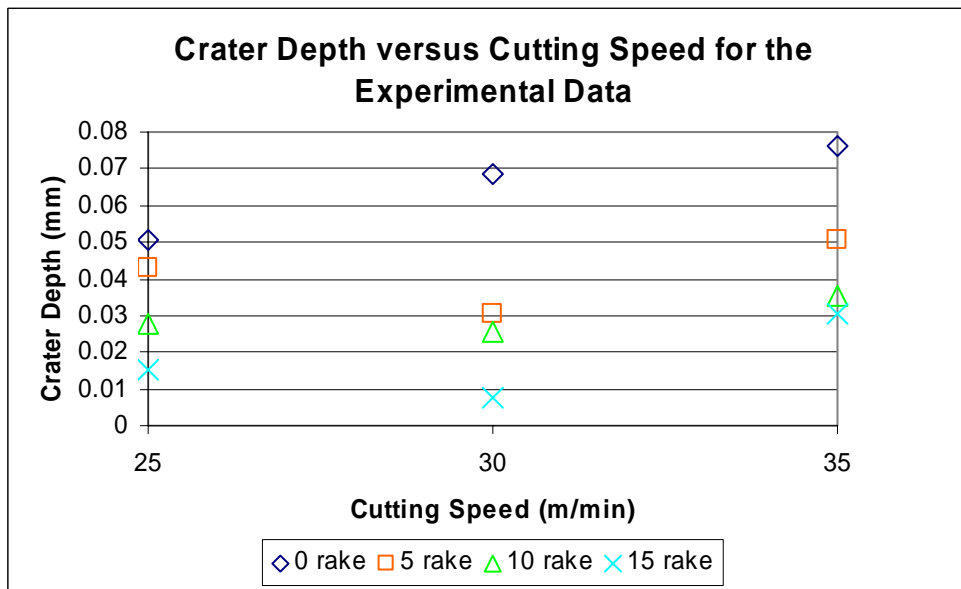


Figure 4.26 Graph of the crater depth versus cutting surface speed for the experimental results.

4.1.2.2 CRATER DEPTH

As the side rake angle increased the crater depth decreased, this trend was followed by the three cutting surface speeds. Figure 4.26 shows the trend for the crater depth. A pattern appeared with the 5, 10 and 15° side rake angle, that the 30 m/min cutting surface speed data was lower than the data for the 25 and 35 m/min cutting surface speed. The crater depth pattern showed at the 30 m/min cutting surface speed could be linked to the pattern shown with the chip thickness at 30 m/min cutting surface speed. The 0° side rake angle cutting tools had an increased crater depth as the cutting surface speed increased as stated in section 4.1.1.4.

4.1.2.3 CONTACT LENGTH

There were different results for the contact length data than the previous two. At the 25 m/min cutting surface speed the increased side rake angle results in a contact length that decreased. The 5° side rake angle cutting tool at the 30 m/min cutting surface speed did not follow the previous trend because its value was the lowest, as shown in Figure 4.27. At the 35 m/min cutting surface speed the 0 and 5° side rake angle cutting tools contact length value fall below both the 10 and 15° side rake angle cutting tools contact length. Having all of the values of contact length plotted on one graph, there are two different trends as the cutting surface speed increased. The 0 and 5° side rake angle cutting tools contact length values decreased as cutting surface speed increased while the 10 and 15° side rake angle cutting tools contact length increased as cutting surface speed increased.

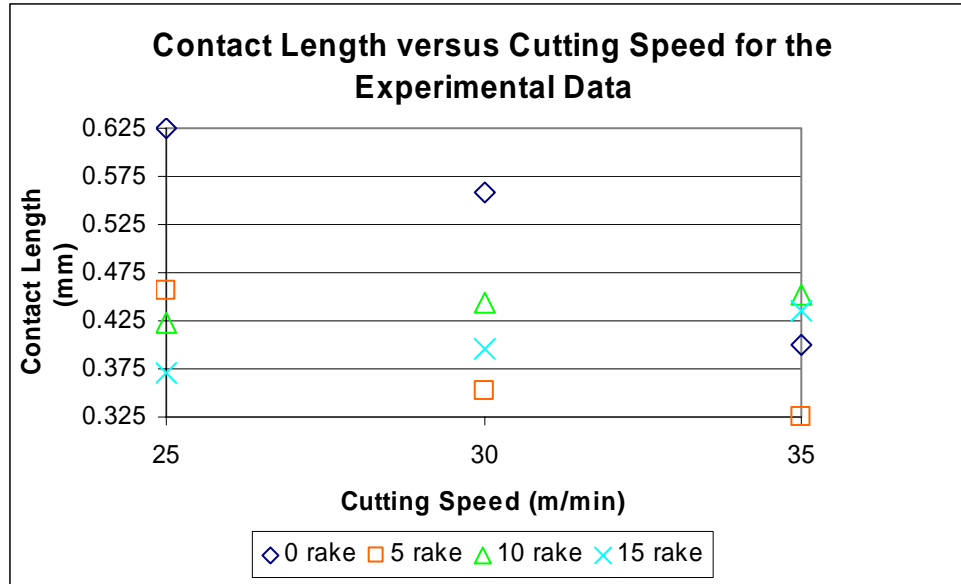


Figure 4.27 Graph of the contact length versus cutting surface speed for the experimental results.

4.1.2.4 SHEAR ANGLE

The trend for the shear angle value as the side rake angle increased was the same for the three cutting surface speeds. That trend was that as the side rake angle increased the shear angle increased. There was a pattern similar with the 0 and 10° side rake angle cutting tools as shown in Figure 4.28. The pattern shown was that the 30 m/min cutting surface speed values were lower than those at 25 and 35 m/min. The 5 and 15° side rake angle cutting tools shear angle decreased as the cutting surface speed was increased.

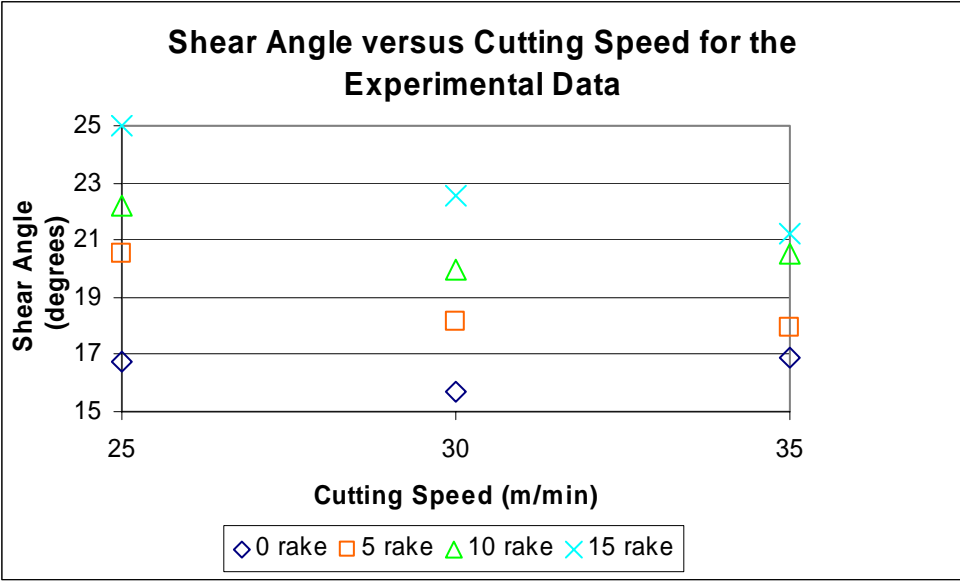


Figure 4.28 Graph of the shear angle versus cutting surface speed for the experimental results.

4.1.2.5 CUTTING RATIO

The cutting ratio and shear angle had the same trends and patterns since the shear angle was calculated with the cutting ratio as shown in equation 3.1. The cutting ratio increased as the side rake angle increased. The patterns shown in Figure 4.29 are the same as stated above in section 4.1.5.4 with the shear angle.

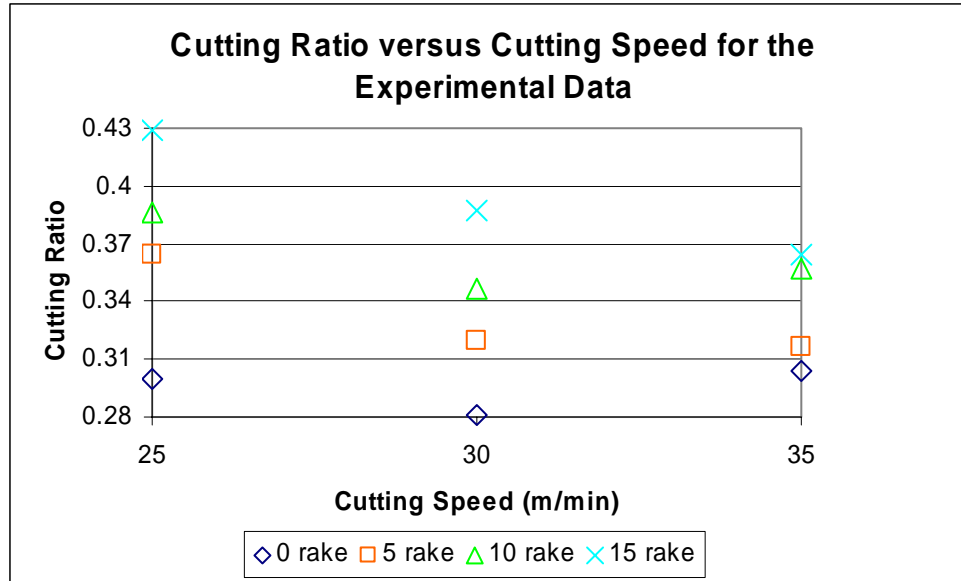


Figure 4.29 Graph of the cutting ratio versus cutting surface speed for the experimental results.

4.1.2.6 FORCE

The force data in Figure 4.30 showed the same trend for the three cutting surface speeds. As the side rake angle increased the force decreased. When looking at the data as the cutting surface speed was increased the force decreased, except for the 0° side rake angle cutting tool. The force data for the 0° side rake angle cutting tool at 35 m/min increased from 30 to 35 m/min.

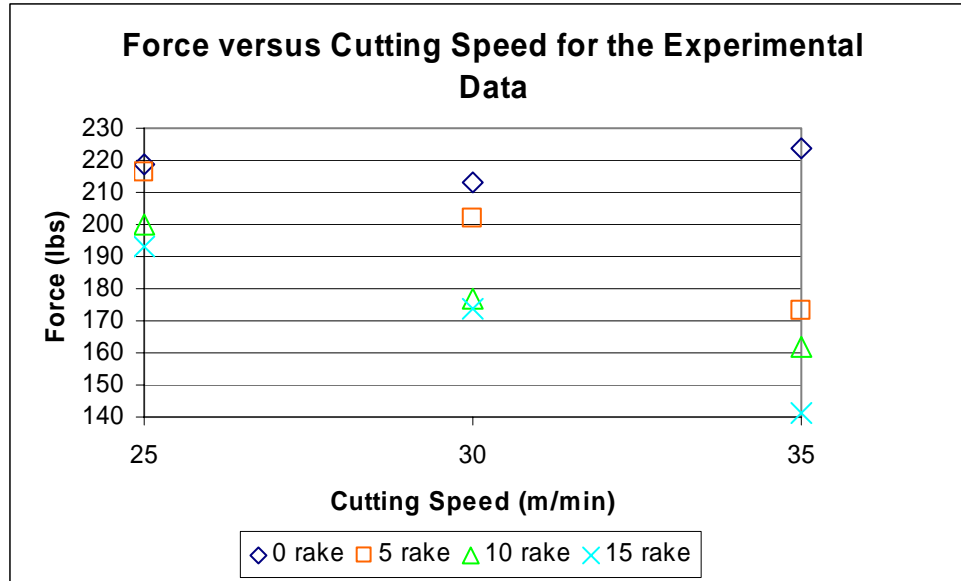


Figure 4.30 Graph of the force versus cutting surface speed for the experimental results.

4.2 SIMULATION RESULTS

The simulation program was run for each of the different side rake angles and cutting surface speeds, the data was gathered from two sources, the first being from the formed chip as shown in Figure 4.31. These results from the chip provided the information for the shear angle, cutting ratio and contact length. The second source was a plot of the force information that the force was calculated from.

4.2.1 SIDE RAKE ANGLE COMPARISON FOR THE SIMULATION DATA

The data for this section has been prepared in tabular format. A computer image from the simulation showed where the results of the computer simulation were measured. The shear angle area in the computer images were different colors than the cutting tool or the workpiece. The contact length in the image has been shown as well, the contact length was measured from the side cutting edge to where the chip curled away from the

cutting tool. Figure 4.31 shows a sample of the computer image from the computer simulation; since the images appeared similar only the images for the 35m/min cutting surface speed will be shown in this section. The complete computer simulation images are shown in Appendix G. This section will not highlight the individual cutting tools as

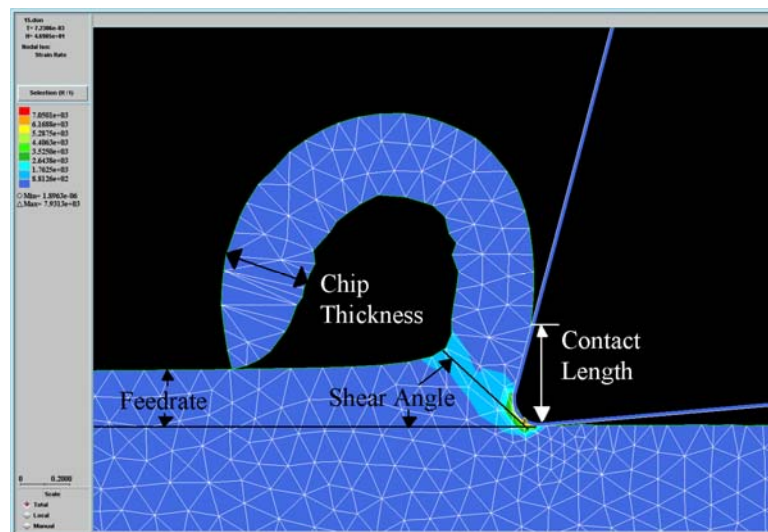


Figure 4.31 Sample image from computer simulation with outputs labeled, from the 15 ° side rake angle at 25 m/min cutting surface speed.

the experimental data section did, because of the lack of data from chip thickness measurements. The computer simulation generated one chip and did not model the rake face since the simulation modeled the orthogonal cutting process. Therefore the results do not include a multiple sampling of chips or the crater depth.

4.2.1.1 THE 0° SIDE RAKE ANGLE TOOLS

The results for the 0° side rake angle cutting tools do not show any significant trends as shown in Table 4.17. Since the chip thickness at the 30 and 35 m/min cutting surface speed were the same value the cutting ratio and shear angle were the same

because of the equations 3.1 and 3.2 that were used for the calculations. The computer simulation image for the 0° side rake angle tool at 35 m/min showed the chip was formed along the rake angle, shown in Figure 4.32. The simulation model showed that the contact length for the 0° side rake angle tools had a large area of interface with the rake face and had the largest value of the various side rake angles.

Table 4.17 Simulation results for the 0° side rake angle tools.

0° Side Rake Angle Cutting Tools					
Cutting Speed (m/min)	Chip Thickness (mm)	Contact Length (mm)	Shear Angle (degrees)	Cutting Ratio	Force (lbs)
25	0.351	0.430	29.68	0.570	216
30	0.380	0.380	27.76	0.526	257
35	0.380	0.385	27.76	0.526	224

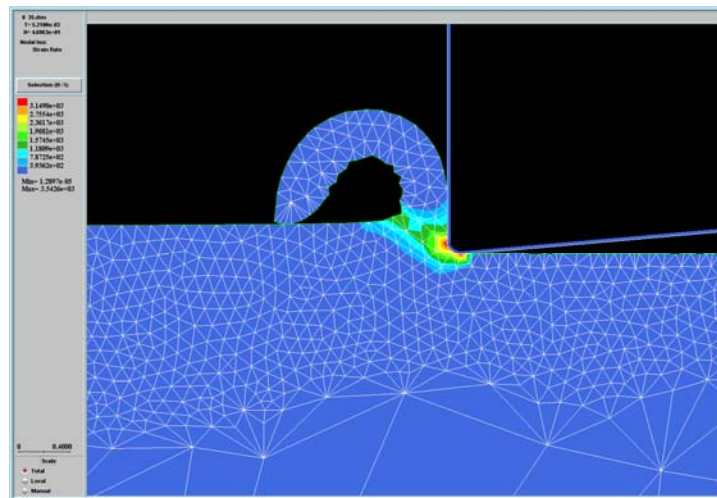


Figure 4.32 The computer simulation model of the 0° side rake angle cutting tool at 35 m/min cutting surface speed.

4.2.1.2 THE 5° SIDE RAKE ANGLE TOOLS

The data from the 5° side rake angle cutting tools showed that as the cutting surface speed increased the shear angle and the cutting ratio decreased. The chip thickness decreased as the cutting surface speed was increased for this side rake angle. The contact length and force both followed the same pattern that the values at the 30 m/min cutting surface speed were greater than the 25 and 35 m/min cutting surface speed shown in Table 4.18. The computer simulation image for the 5° side rake angle cutting tool at 35 m/min as shown in Figure 4.33. There was a visible difference in the side rake angle between the 0 and 5° side rake angle cutting tools. The shear angle shown in the lighter colored area was also greater in the 5° side rake angle than the 0° side rake angle cutting tools. The angle of the side rake angle caused the contact length to decrease, since less material from the chip was forced up the rake face.

Table 4.18 Simulation results for the 5° side rake angle tools.

5° Rake Angle Cutting Tools					
Cutting Speed (m/min)	Chip Thickness (mm)	Contact Length (mm)	Shear Angle (degrees)	Cutting Ratio	Force (lbs)
25	0.303	0.380	34.90	0.660	214
30	0.339	0.383	31.78	0.590	248
35	0.350	0.340	30.93	0.571	191

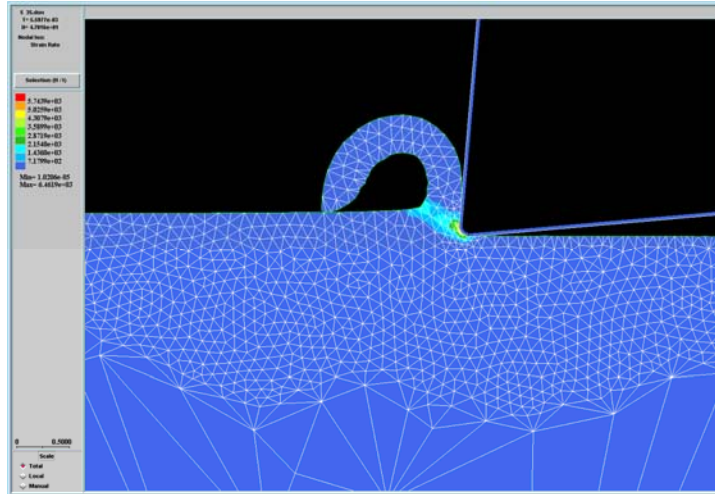


Figure 4.33 The computer simulation model of the 5° side rake angle cutting tool at 35 m/min cutting surface speed.

4.2.1.3 THE 10° SIDE RAKE ANGLE TOOLS

The trends and patterns for the 10° side rake angle cutting tool were the same as the 5° side rake angle cutting tools, as shown in Table 4.19. The increased cutting surface speed decreased the shear angle and cutting ratio. However the increased cutting surface speed increased the chip thickness. The pattern for the contact length and the force showed the values at 30 m/min cutting surface speed are greater than the values at 25 and 35 m/min. In Figure 4.34 the 10° side rake angle cutting tools are shown modeled at 35 m/min cutting surface speed. The shear angle was shown to increase from the previous side rake angles with the cutting tool tip appearing to be underneath the formed chip. The contact length for the 10° side rake angle was shorter than the 0 and 5° side rake angle tools because the 10° side rake angle tools had less interaction with the formed chip before the chip curled away from the rake face.

Table 4.19 Simulation results for the 10° side rake angle tools.

10° Side Rake Angle Cutting Tools					
Cutting Speed (m/min)	Chip Thickness (mm)	Contact Length (mm)	Shear Angle (degrees)	Cutting Ratio	Force (lbs)
25	0.308	0.343	35.81	0.650	192
30	0.336	0.370	33.18	0.595	215
35	0.350	0.336	31.99	0.571	185

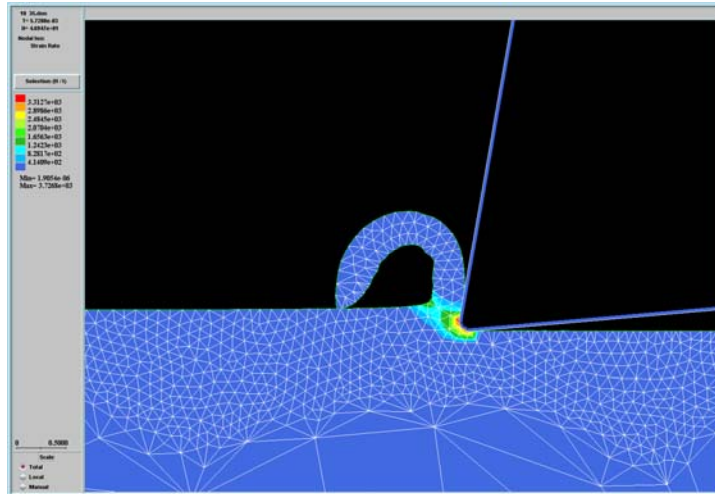


Figure 4.34 The computer simulation model of the 10° side rake angle cutting tool at 35 m/min cutting surface speed.

4.2.1.4 THE 15° SIDE RAKE ANGLE TOOLS

The results from the 15° side rake angle cutting tool do not show any trend or pattern as the cutting surface speed increased. The results for the data at 30 and 35 m/min cutting surface speed were the same except the force. Table 4.20 shows the data for the 15° side rake angle cutting tools. The cutting tool tip in Figure 4.35 appears to be underneath the formed chip more than the 0, 5, and 10° side rake angle cutting tools. This image indicated that the shear angle increased as the side rake angle increased. The contact length was decreased in the 15° side rake angle since the formed chip was curling away from the rake face earlier than the previous side rake angles.

Table 4.20 Simulation results for the 15° side rake angle tools.

15° Side Rake Angle Cutting Tools					
Cutting Speed (m/min)	Chip Thickness (mm)	Contact Length (mm)	Shear Angle (degrees)	Cutting Ratio	Force (lbs)
25	0.282	0.293	40.04	0.710	191
30	0.330	0.330	34.77	0.606	215
35	0.330	0.330	34.77	0.606	185

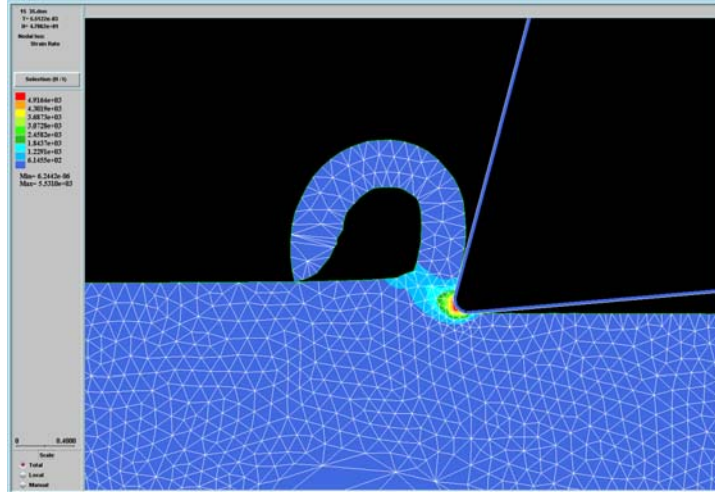


Figure 4.35 The computer simulation model of the 15° side rake angle cutting tool at 35 m/min cutting surface speed.

4.2.2 CUTTING SURFACE SPEED COMPARISON FOR THE SIMULATION DATA

The comparisons made in this section were similar to section 4.1.2. The results for each output are plotted on one graph. The side rake angle cutting tools were plotted with the same symbol throughout this section. The different outputs that were examined are chip thickness, contact length, shear angle, cutting ratio and force.

4.2.2.1 CHIP THICKNESS

The general trend for chip thickness was that as the side rake angle increased the chip thickness decreased. The only cutting surface speed that followed the trend exactly was the 30 m/min cutting surface speed. At the 25 m/min cutting surface speed the chip

thicknesses for the 5° side rake angle cutting tool measured smaller than the 10° side rake angle cutting tool by 0.005 mm. At the 35 m/min cutting surface speed the 5 and 10° side rake angle cutting tool chip thickness are equal. The results are shown in Figure 4.36. As the cutting surface speed increased the chip thickness generally increased.

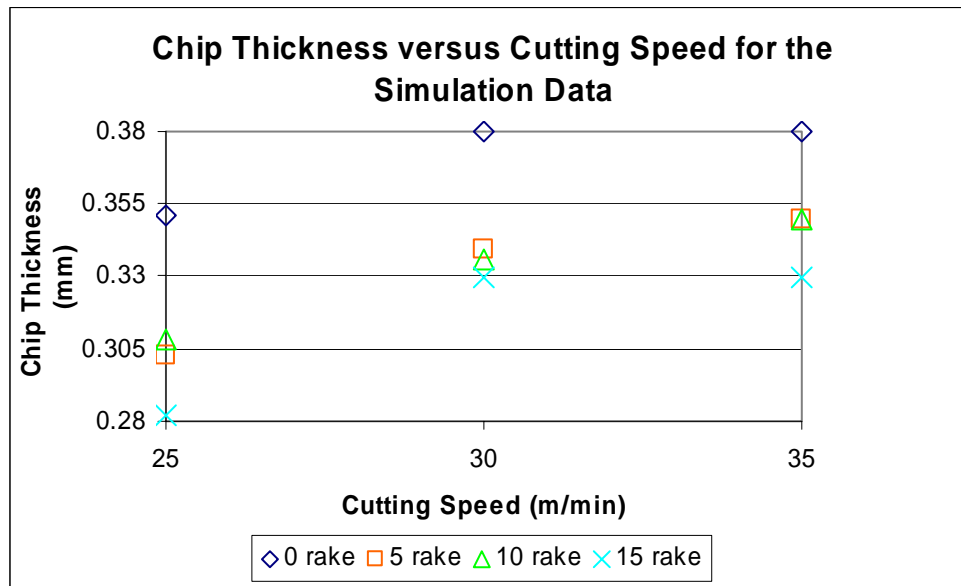


Figure 4.36 Graph of the chip thickness versus cutting surface speed for the simulation results.

4.2.2.2 CONTACT LENGTH

The results for the contact length showed that as the side rake angle increased the contact length decreased. However at the 30 m/min cutting surface speed the contact length for the 5° side rake angle cutting tool was larger than the 0° side rake angle tool by 0.003 mm. The pattern as the cutting surface speed increased the contact length for the 0 and 5° side rake angle cutting tools decreased. The 10 and 15° side rake angle cutting

tools increased from 25 to 30 m/min but decreased from 30 to 35 m/min, as shown in Figure 4.37.

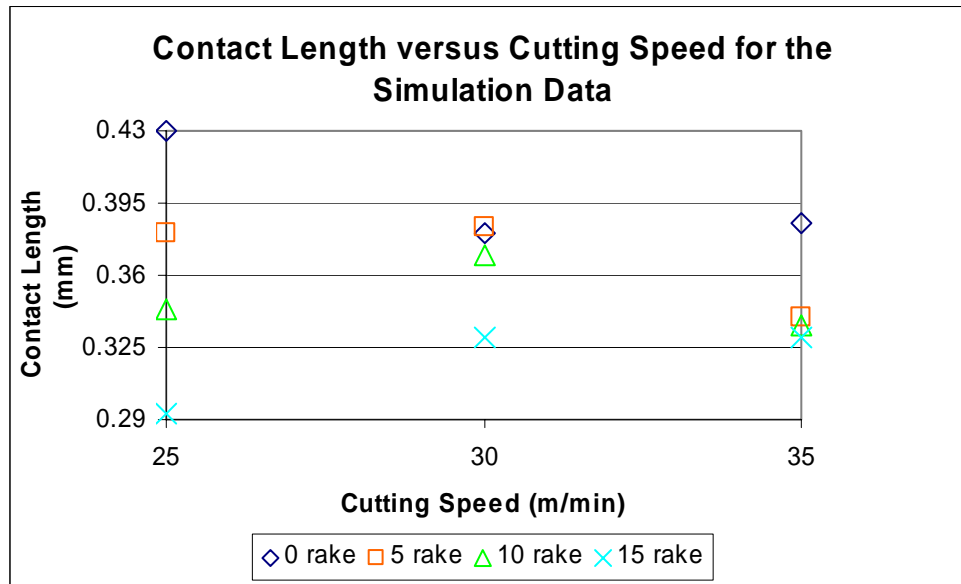


Figure 4.37 Graph of the contact length verse cutting surface speed for the simulation results.

4.2.2.3 SHEAR ANGLE

The trend shown in Figure 4.38 shows that as the side rake angle increased the shear angle increased. Another trend shown in this data was that as the cutting surface speed increased the shear angle decreased. The results for the 0 and 15° side rake angle tools at 30 and 35 m/min are the same value respectively.

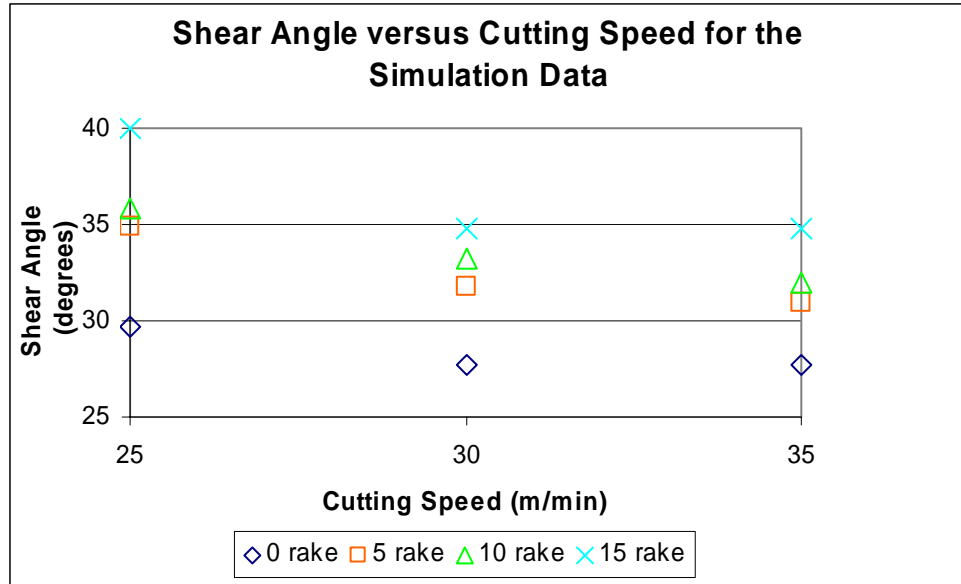


Figure 4.38 Graph of the shear angle verse cutting surface speed for the simulation results.

4.2.2.4 CUTTING RATIO

The cutting ratio trend was the same as the shear angle. The increased side rake angle results in an increased cutting ratio. The values for the 5 and 10° side rake angle cutting tools at 35 m/min are the same. The same trends are shown as the cutting surface speed was increased the cutting ratio decreased. The values for the 0 and 15° side rake angle cutting tools are the same value for the 30 and 35 m/min cutting surface speed respectively, shown in Figure 4.39.

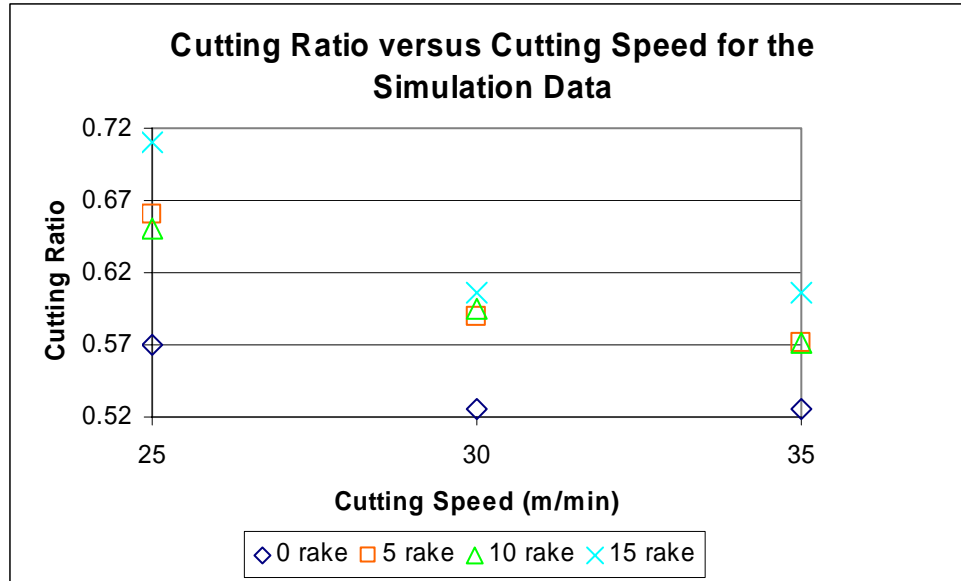


Figure 4.39 Graph of the cutting ratio verse cutting surface speed for the simulation results.

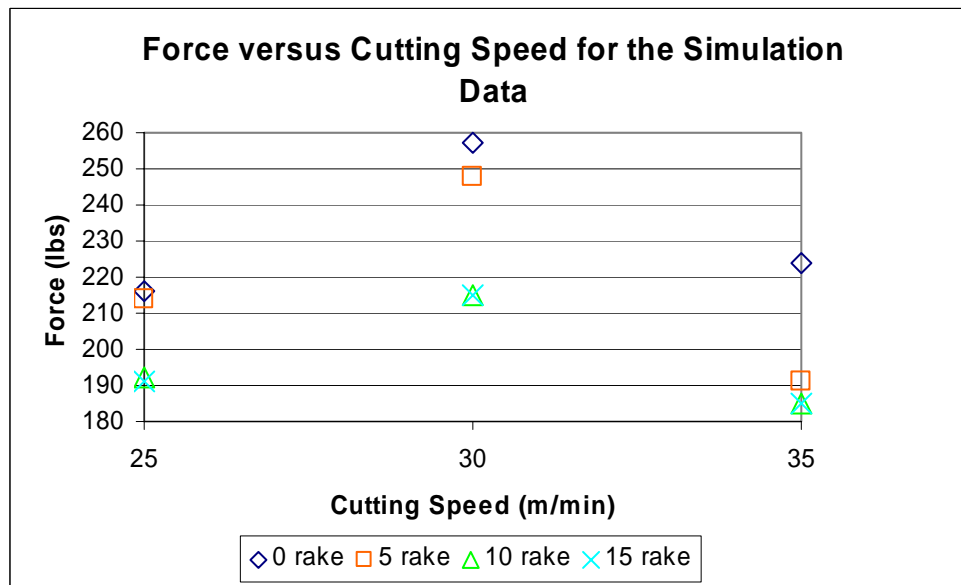


Figure 4.40 Graph of the force verse cutting surface speed for the simulation results.

4.2.2.5 FORCE

The force results are shown in Figure 4.40. The trend that the data followed for the force was that as the side rake angle increased the force decreased. The values show for the 10 and 15° side rake angle cutting tools were similar for the three cutting surface speeds with the 30 and 35 m/min values the same. The force data increased from the 25 to 30 m/min cutting surface speed but decreased from the 30 to 35 m/min cutting surface speed.

4.3 COMPARISON ANALYSIS

To observe any trends with the data the experimental data and simulation data were compared together. The comparisons show what has occurred as the side rake angle of the cutting tool increased with relationship to the cutting surface speed.

This section of results will be looked at in four categories all of which are compared to the side rake angle: Shear Angle, Cutting Ratio, Contact Length, and Force. Since the chip thickness was used in calculating the cutting ratio, the chip thickness will not be analyzed directly in this section. Comparisons between the experimental and simulation data are used to examine trends.

4.3.1 SHEAR ANGLE AND SIDE RAKE ANGLE

The results from the shear angle when compared to the side rake angle showed that a similar trend was followed. The average simulation data was 40 percent larger than the average experimental data for all of the cutting surface speed. To understand the large gap between the results a closer look at the cutting ratio was required. As shown in equation 3.2 the shear angle was calculated from the cutting ratio. The cutting ratio results were analyzed in the following section. However the trend in the data had

promising outcome for further study. The average difference between the experimental and computer simulation results was 13°. The difference decreased 13 percent from the 25 m/min to 35 m/min cutting surface speed. The trends are shown in Figures 4.41-4.43.

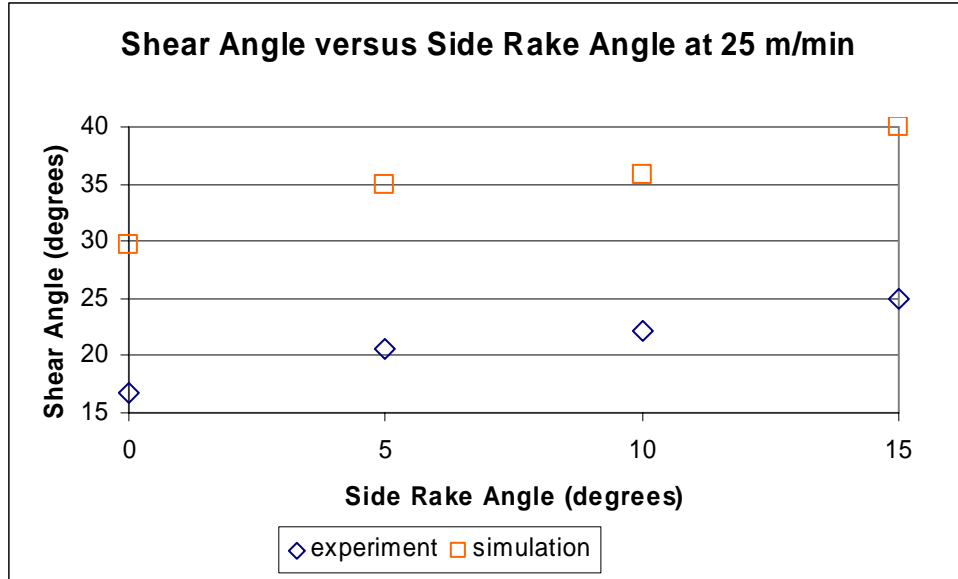


Figure 4.41 A comparison of the shear angle with the side rake angle at 25 m/min cutting surface speed.

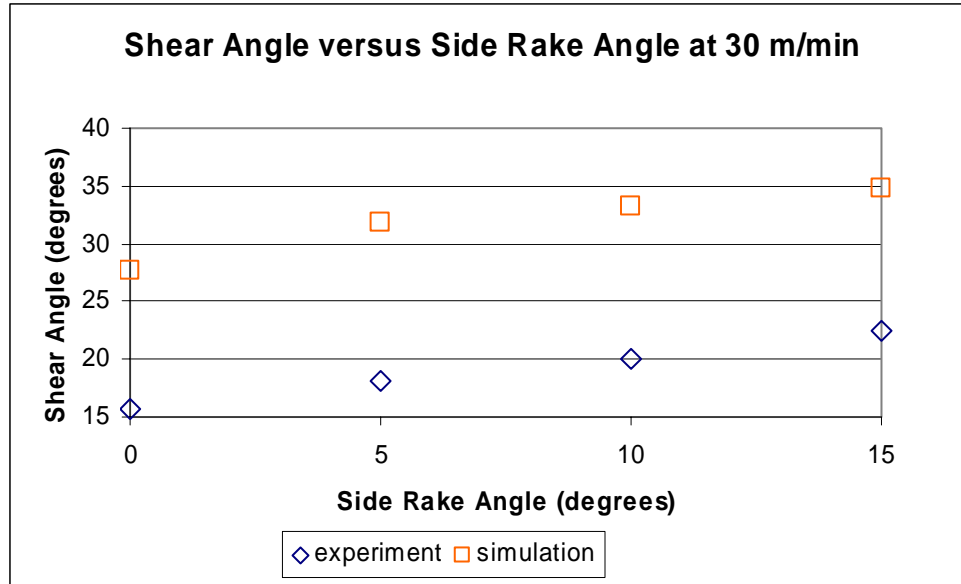


Figure 4.42 A comparison of the shear angle with the side rake angle at 30 m/min cutting surface speed.

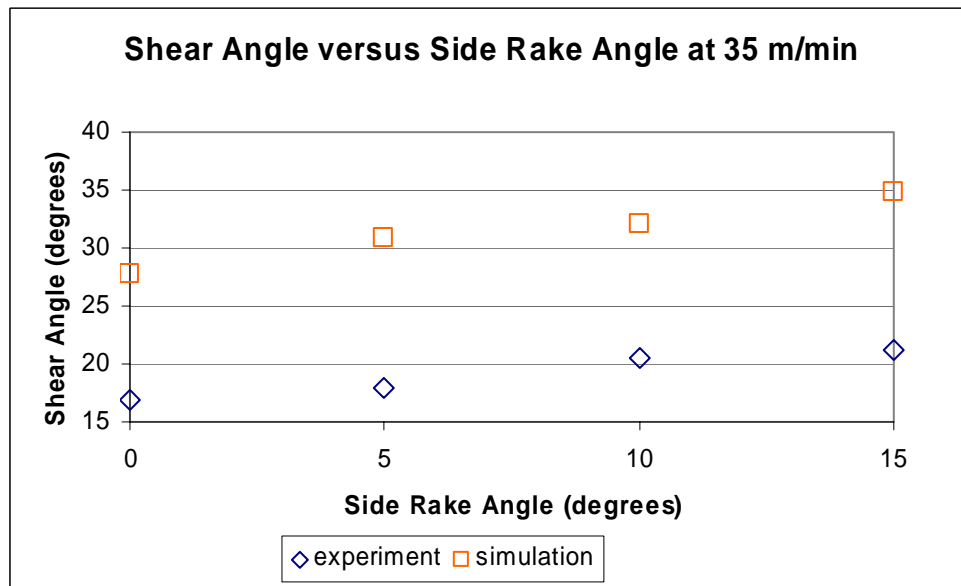


Figure 4.43 A comparison of the shear angle with the side rake angle at 35 m/min cutting surface speed.

4.3.2 CUTTING RATIO AND SIDE RAKE ANGLE

In the Fundamentals of Tool Design book the cutting ratio value for an efficient material remove should be 1.5 (Nee 1998). The simulation data was expected to be more efficient than the experimental data because of the reduced variables in a computer simulation of orthogonal cutting. The simulation cutting ratio at its highest value was still under half of the ideal ratio of 1.5. The data showed that the simulation cutting ratio was 42 percent larger than the experimental data. The cutting ratio equation 3.1 showed that the chip thickness was used to calculate the cutting ratio. Therefore the chip thickness for simulation data was about 42 percent smaller than the experimental data. The difference between the experimental and computer simulation data averaged 0.252 and decreased 16 percent as the cutting surface speed increased from 25 to 35 m/min. The computer simulation model of the chip did not accurately predict the thickness. The material model for the workpiece material did not accurately depict the material flow between the cutting tool and the workpiece. The three cutting surface speed trends as the side rake angle increased the cutting ratio increased. The results for this comparison are shown in Figures 4.44-4.46.

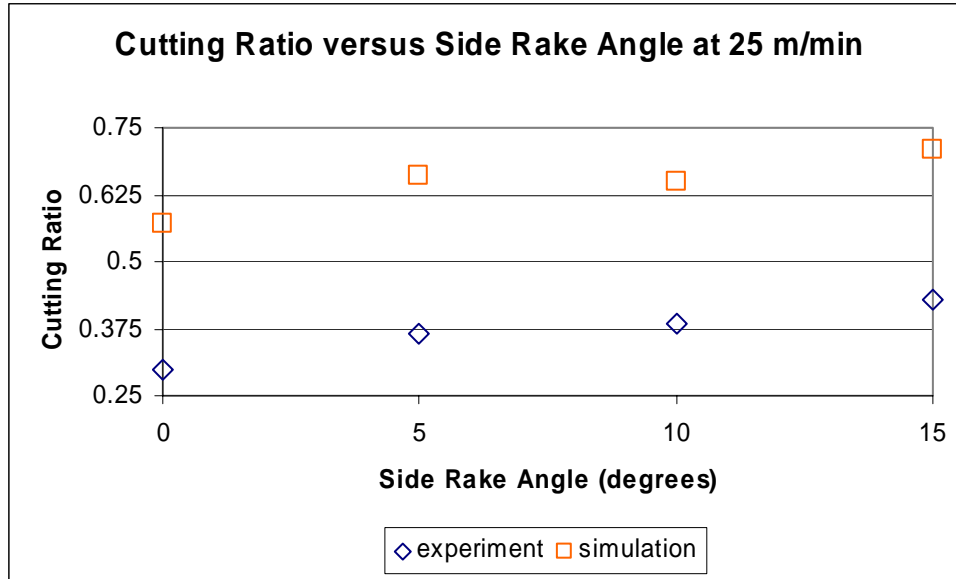


Figure 4.44 A comparison of the cutting ratio with the side rake angle at 25 m/min cutting surface speed.

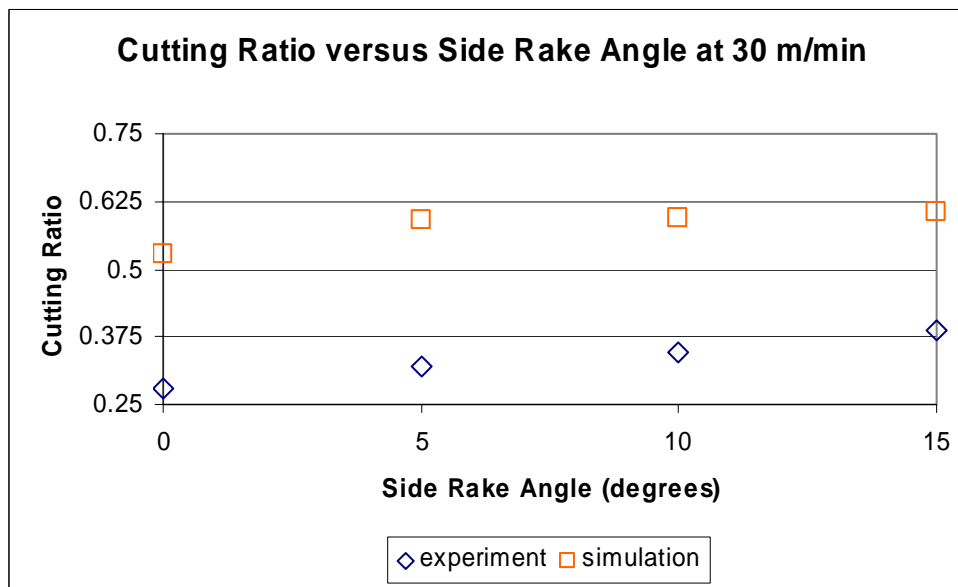


Figure 4.45 A comparison of the cutting ratio with the side rake angle at 30 m/min cutting surface speed.

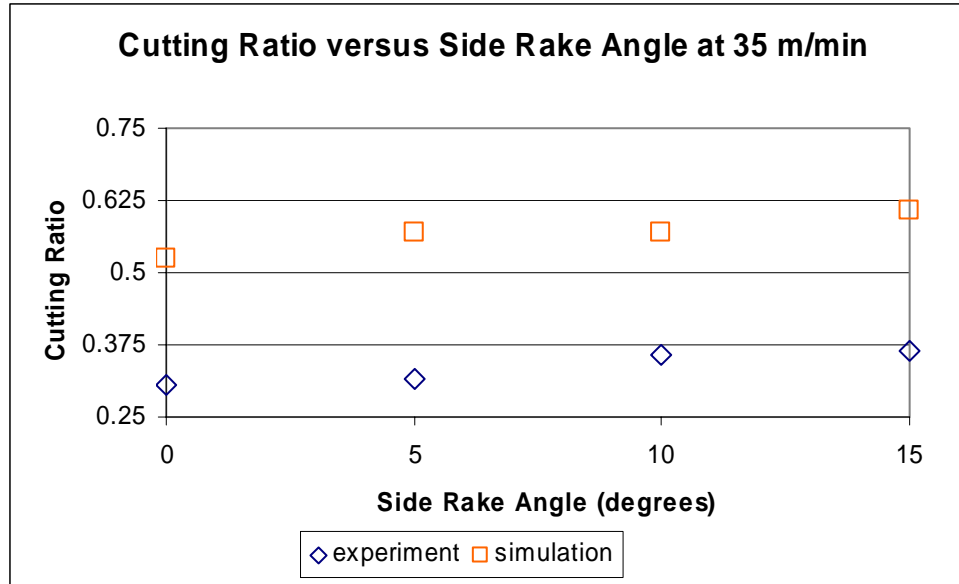


Figure 4.46 A comparison of the cutting ratio with the side rake angle at 35 m/min cutting surface speed.

4.3.3 CONTACT LENGTH AND SIDE RAKE ANGLE

The contact length and the rake angle comparison provide the most promising values and trends. As shown in the Figures 4.47-4.49 the comparisons are in good agreement. The average computer simulation data was 18 percent larger than the average experimental data. The difference between the computer simulation and experimental data was averaged at 0.78 mm, and the difference dropped 48 percent from the 25 to the 35 m/min cutting surface speed. The similar pattern was followed for the 30 and 35 m/min cutting surface speed. The pattern was that the 0, 10, and 15° side rake angle cutting tools experimental value was above the computer simulation, however the 5° side rake angle experimental value was below the simulation. The results from this comparison showed that the simulation model provided a good approximation of the contact length on the cutting tool.

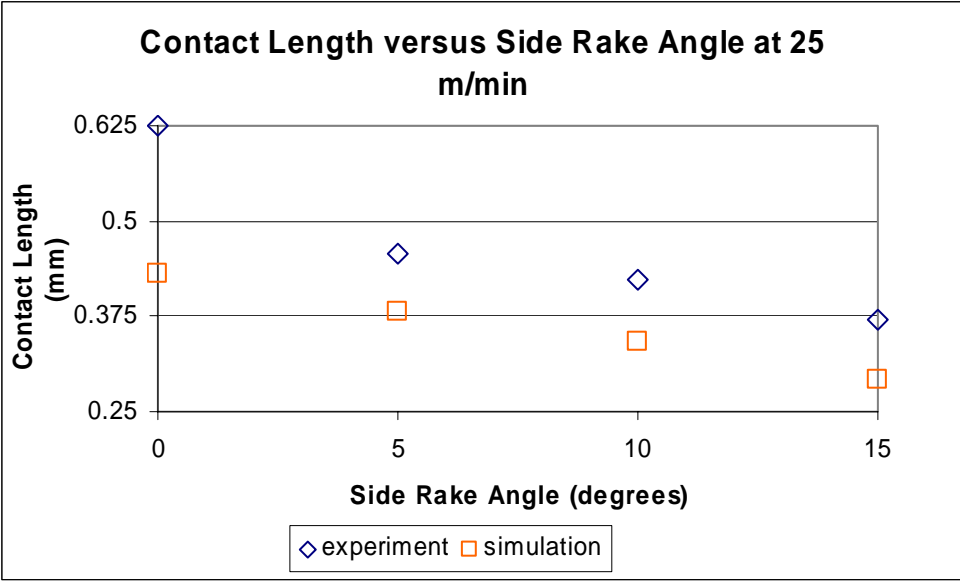


Figure 4.47 A comparison of the contact length with the side rake angle at 25 m/min cutting surface speed.

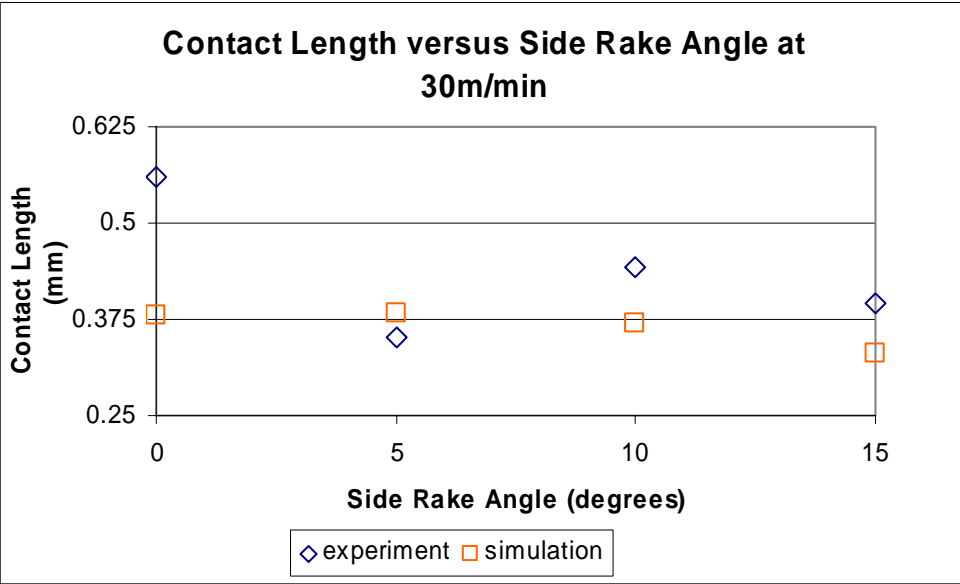


Figure 4.48 A comparison of the contact length with the side rake angle at 30 m/min cutting surface speed.

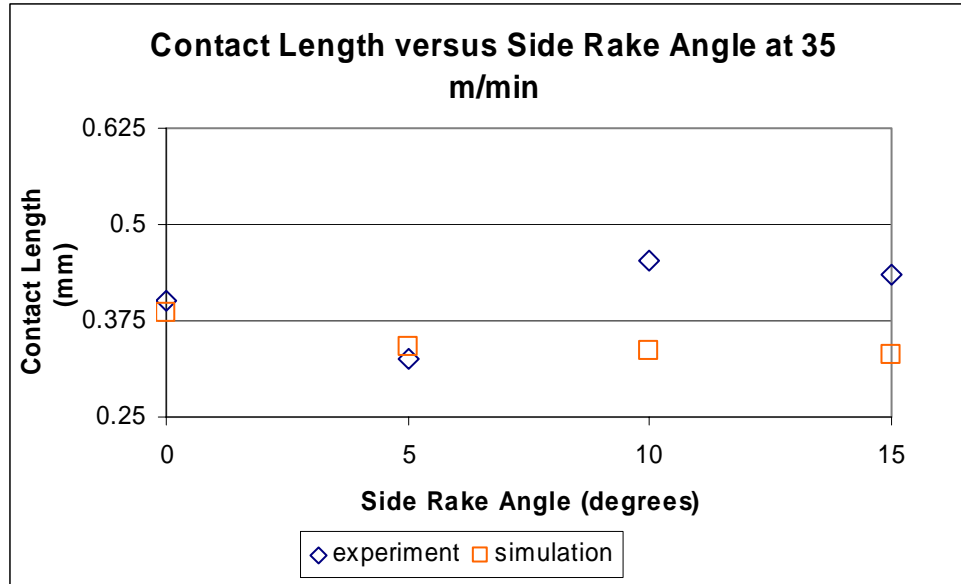


Figure 4.49 A comparison of the contact length with the side rake angle at 35 m/min cutting surface speed.

4.3.4 FORCE AND SIDE RAKE ANGLE

The force comparison between the experimental and simulation data provided good agreement for the 25 and 35 m/min cutting surface speed data shown in Figures 4.50 and 4.52. The simulation data at the 30 m/min cutting surface speed measured larger than the experiment, but the decreased trend was still followed as shown in Figure 4.51. The only explanation for the larger results for the 30 m/min cutting surface speed was the computer simulation data needs to be reevaluated. The simulation data at the 30 m/min cutting surface speed was 18 percent larger than the experimental data at that cutting surface speed. While the simulation data for the 25 and 35 m/min cutting surface speed was 1.5 percent smaller than the experimental data. The average difference between the experimental and computer simulation data was 20 pounds. However the average difference between the experimental and computer simulation data at 25 m/min

was 3.75 pounds. The computer simulation showed promising results to be capable of modeling the forces that occurred in the material removal process.

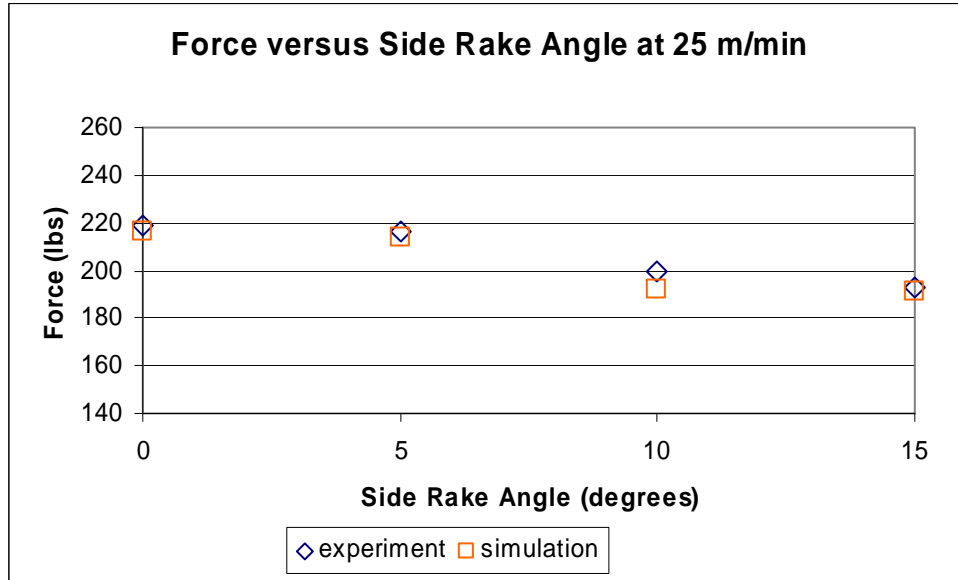


Figure 4.50 A comparison of the force with the side rake angle at 25 m/min cutting surface speed.

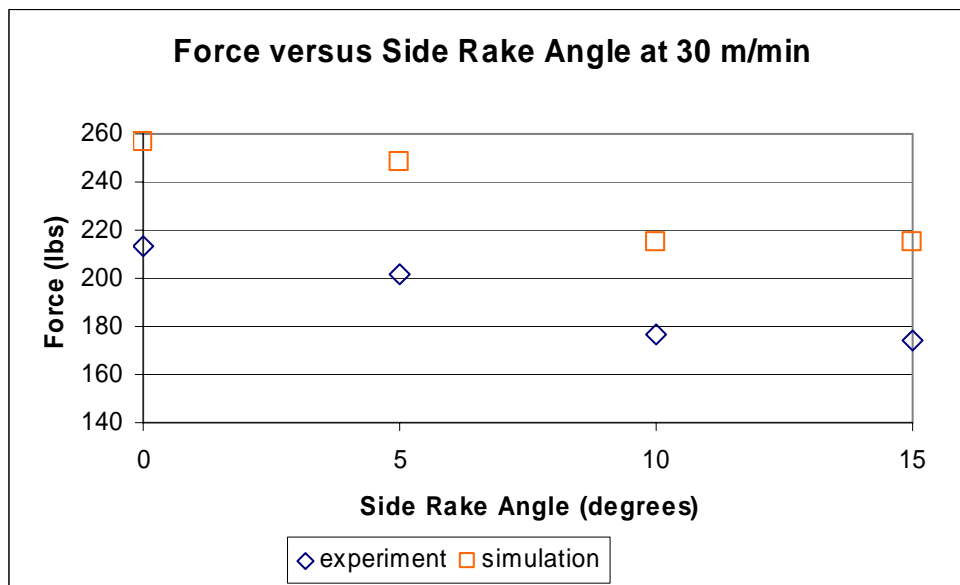


Figure 4.51 A comparison of the force with the side rake angle at 30 m/min cutting surface speed.

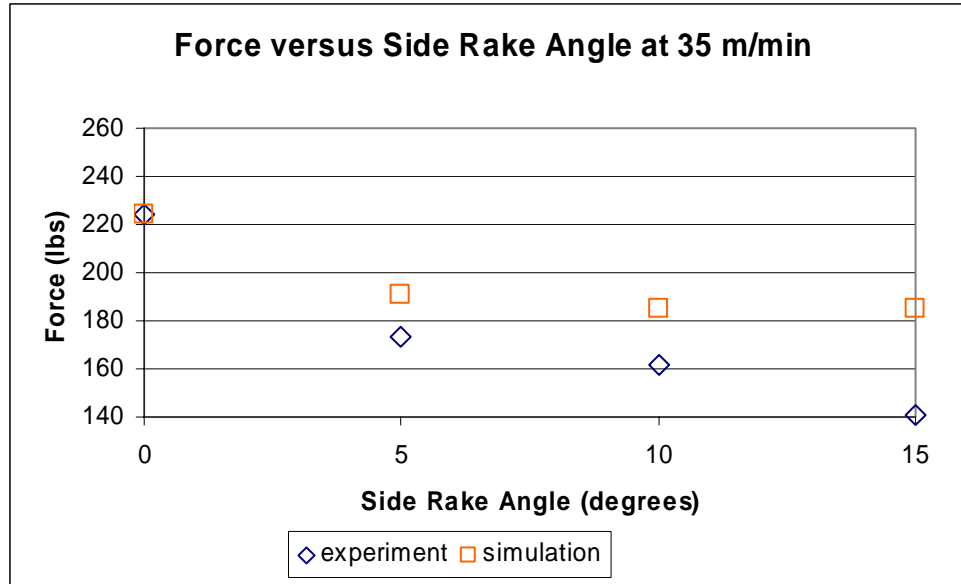


Figure 4.52 A comparison of the force with the side rake angle at 35 m/min cutting surface speed.

CHAPTER 5

CONCLUSIONS AND RECOMMENDATIONS

Tool wear is very critical to the material removal process. There is a large amount of research in tool wear, however Archard's law has not been utilized for predicting tool wear in turning operations. Experimental results collected from the turning process are compared to the computer simulation results. This thesis found that a computer simulation of cutting tools using Archard's law for a wear model can be used to model the turning process.

5.1 CONCLUSION

The null hypothesis states that: There is no significant difference between computer simulation wear and experimental cutting wear in metal cutting. This thesis used a comparison analysis to prove the null hypothesis. The analysis compared several different values from the experimental and simulation results. The comparison analysis provides positive results to continue future research in the computer simulation program to validate the use of this model for tool wear prediction. The null hypothesis is false for the comparison analysis and there is significant difference between the computer simulation and experimental wear. There are several results that provide positive evidence that Archard's law can be used to model tool wear even with the significant differences found. The trend between the experimental and simulation data did have a

positive correlation in all of the results. The contact length and the force values were in close approximation.

The conclusions that are made from the results are listed below:

- The computer simulation predicted the experimental values of chip thickness, cutting ratio, shear angle, and contact length with increased accuracy as the cutting surface speed increased as shown by the decrease in the difference between the values of the same cutting surface speed.
- The computer simulation model for the chip thickness is not an accurate thickness when compared to experimental results. The computer simulation predicted an average of 42 percent below the experimental chip thickness value.
- The trends for the both the experimental and simulation results are seen in Table 5.1.

Table 5.1 The trends from the results of experimental and simulation data as the side rake angle increases from 0 to 15°.

Trends for the results as the cutting tool side rake angle increases		Percent
Shear Angle	Increases	25
Cutting Ratio	Increases	20
Contact Length	Decreases	20
Force	Decreases	19

- Between the 5 and 10° side rake angle the trend for the contact length switches from decreasing as cutting surface speed is increasing to the contact length

increasing as cutting surface speed is increasing. The side rake angle has a greater affect on contact length than cutting surface speed.

- Side rake angle has a greater affect on crater depth then does the cutting surface speed.
- The side rake angle and cutting surface speed have a positive affect on the shear angle and a negative affect on the force.

5.2 RECOMMENDATIONS

Based on the conclusions above further study in tool wear using Archard's law as a wear model is recommended. Upon completing the thesis, the following recommendations for further study and improved research are recommended.

- In order to conduct a better statistical analysis more experimental data is required. However a statistical analysis should not be the only analysis conducted. A comparison of the data needs to be performed as well in order to study trends.
- Simulation is an expanding field of research and future study with Archard's law could add a friction law for coolant. This would provide useful information for what industry is using. Most of the material removal process utilizes coolant to reduce wear and extent tool life.
- Carbide cutting tools would be another area to study using Archard's law. HSS cutting tools are utilized but a carbide cutting tools are more common.
- A study to determine whether there is a correlation between crater depth and chip thickness.

- A study to understand the change in the trend that occurred between the 5 and 10° side rake angle cutting tools for contact length.
- The computer simulation can predict temperature for the material removal process. To capture the temperature at the cutting tool would be a beneficial to compare with the simulation in order to validate the use of Archard's law.

BIBLIOGRAPHY

Drozda, Thomas, J. and Wick, Charles. Tool and Manufacturing Engineers Handbook. vol 1, 4th ed. Dearborn, MI: SME, 1983.

Ezugwu, E.O., Arthur, S.J., and Hines, E.L. "Tool-wear prediction using artificial neural networks." Journal of Materials Processing Technology 49 (1995): 255-264.

Lee, J.H. and Lee, S.J. "One-step-ahead prediction of flank wear using cutting force." International Journal of Machine Tools & Manufacture 39 (1999): 1747-1760.

Li, X.P., Ng, H.H., and Lim, S.C. "A predictive mapping system for tool wear in metal cutting." Journal of Materials Processing Technology 89-90 (1999): 279-286.

Mamalis, A.G., Horváth, M., Branis, A.S., and Manolakos, D.E. "Finite element simulation of chip formation in orthogonal metal cutting." Journal of Materials Processing Technology 110 (2001): 19-27.

Miles, Mike and Kohkonen, Kent. "Tool Wear in Orthogonal Machining." Proceedings of the EMCWA conference, Cincinnati, OH, October 15-17 (2002):181-185.

Movahhedy, M., Gadala, M.S., and Altintas Y. "Simulation of the orthogonal metal cutting process using an arbitrary Lagrangian-Eulerian finite-element method." Journal of Materials Processing Technology 103 (2000): 267-275.

Nee, John G. Fundamentals of Tool Design . 4th ed. Dearborn, MI: SME, 1998.

Oh, Joon-Dong and Warnecke, Gunter, "Mechanically and Thermally Coupled Finite Element Analysis of Chip Formation in Metal Cutting." Proceedings of the NAMRC XXVIII conference, KY (2000).

Shih, Albert J. "Finite element analysis of the rake angle effects in orthogonal metal cutting." International Journal of Mechanical Science 38 (1996): 1-17.

"Turning and Boring Tools, Single Point." Machining Data Handbook (MDH). vol 1, 3rd ed. OH: METCUT Research Associates, Inc, 1980: 15-3.

Yen, Yung-Chang, Sohner, Jorg, Lilly Blaine, and Altan, Taylan, "Estimation of tool wear in orthogonal cutting using the finite element analysis." (2002). The Engineering Research Center for Net Shape Manufacturing. 10 OCT 2002 www.ercnsm.org

APPENDIX

APPENDIX A:

CNC PROGRAM FOR THE OKUMA LATHE

```
$HSSTH.MIN%
XS=5.55 IND=0 ZS=0 ZI=3.0 PG=1 PAS=0 CS=1200
XD=XS
ZL=ZS
PA=PAS
G00 X20 Z20
G50 S2000
DIA =3.=CS5*CS/XD
N10 X=XD+.1 Z=ZL+.1 S=DIA T010101 M3 M42
G96 S=CS
XD=XD-.118
G01 X=XD F.03
ZL=ZL-ZI
Z=ZL F.008
X=XD+.05
G97 S=DIA
G00 X20 M00
X=XD+.1 Z=ZL+.1 S=DIA T020202 M3 M42
G96 S=CS
G01 X=XD Z=ZL+.05 F.008
ZL=ZL-ZI
Z=ZL
X=XD+.05
G97 S=DIA
G00 X20 M00
X=XD+.1 Z=ZL+.1 S=DIA T030303 M3 M42
G96 S=CS
G01 X=XD Z=ZL+.05 F.008
ZL=ZL-ZI
Z=ZL
X=XD+.05
G97 S=DIA
G00 X20 M00
X=XD+.1 Z=ZL+.1 S=DIA T040404 M3 M42
G96 S=CS
G01 X=XD Z=ZL+.05 F.008
```

ZL=ZL-ZI
 Z=ZL
 X=XD+.05
 G97 S=DIA
 G00 X20 M00
 X=XD+.1 Z=ZL+.1 S=DIA T050505 M3 M42
 G96 S=CS
 G01 X=XD Z=ZL+.05 F.01
 Z-12.5
 X=XD+.05
 G97 S=DIA
 PA=PA+1
 G00 X20 Z20 M00
 T111111 M00
 T010101 M00
 (PASS ONE COMPLETE)
 X=XD+.1 Z=ZL+.1 S=DIA T020202 M3 M42
 G96 S=CS
 XD=XD-.118
 G01 X=XD F.03
 ZL=ZL-ZI
 Z=ZL F.008
 X=XD+.05
 G97 S=DIA
 G00 X20 M00
 X=XD+.1 Z=ZL+.1 S=DIA T030303 M3 M42
 G96 S=CS
 G01 X=XD Z=ZL+.05 F.008
 ZL=ZL-ZI
 Z=ZL
 X=XD+.05
 G97 S=DIA
 G00 X20 M00
 X=XD+.1 Z=ZL+.1 S=DIA T040404 M3 M42
 G96 S=CS
 G01 X=XD Z=ZL+.05 F.008
 ZL=ZL-ZI
 Z=ZL
 X=XD+.05
 G97 S=DIA
 G00 X20 M00
 X=XD+.1 Z=ZL+.1 S=DIA T010101 M3 M42
 G96 S=CS
 G01 X=XD Z=ZL+.05 F.008
 ZL=ZL-ZI
 Z=ZL

```

X=XD+.05
G97 S=DIA
G00 X20 M00
X=XD+.1 Z=ZL+.1 S=DIA T050505 M3 M42
G96 S=CS
G01 X=XD Z=ZL+.05 F.01
Z-12.5
X=XD+.05
G97 S=DIA
PA=PA+1
G00 X20 Z20 M00
T111111 M00
T010101 M00
(PASS TWO COMPLETE)
X=XD+.1 Z=ZL+.1 S=DIA T030303 M3 M42
G96 S=CS
XD=XD-.118
G01 X=XD F.03
ZL=ZL-ZI
Z=ZL F.008
X=XD+.05
G97 S=DIA
G00 X20 M00
X=XD+.1 Z=ZL+.1 S=DIA T040404 M3 M42
G96 S=CS
G01 X=XD Z=ZL+.05 F.008
ZL=ZL-ZI
Z=ZL
X=XD+.05
G97 S=DIA
G00 X20 M00
X=XD+.1 Z=ZL+.1 S=DIA T010101 M3 M42
G96 S=CS
G01 X=XD Z=ZL+.05 F.008
ZL=ZL-ZI
Z=ZL
X=XD+.05
G97 S=DIA
G00 X20 M00
X=XD+.1 Z=ZL+.1 S=DIA T020202 M3 M42
G96 S=CS
G01 X=XD Z=ZL+.05 F.008
ZL=ZL-ZI
Z=ZL
X=XD+.05
G97 S=DIA

```

```

G00 X20 M00
X=XD+.1 Z=ZL+.1 S=DIA T050505 M3 M42
G96 S=CS
G01 X=XD Z=ZL+.05 F.01
Z-12.5
X=XD+.05
G97 S=DIA
PA=PA+1
G00 X20 Z20 M00
T111111 M00
T010101 M00
(PASS THREE COMPLETE)
X=XD+.1 Z=ZL+.1 S=DIA T040404 M3 M42
G96 S=CS
XD=XD-.118
G01 X=XD F.03
ZL=ZL-ZI
Z=ZL F.008
X=XD+.05
G97 S=DIA
G00 X20 M00
X=XD+.1 Z=ZL+.1 S=DIA T010101 M3 M42
G96 S=CS
G01 X=XD Z=ZL+.05 F.008
ZL=ZL-ZI
Z=ZL
X=XD+.05
G97 S=DIA
G00 X20 M00
X=XD+.1 Z=ZL+.1 S=DIA T020202 M3 M42
G96 S=CS
G01 X=XD Z=ZL+.05 F.008
ZL=ZL-ZI
Z=ZL
X=XD+.05
G97 S=DIA
G00 X20 M00
X=XD+.1 Z=ZL+.1 S=DIA T030303 M3 M42
G96 S=CS
G01 X=XD Z=ZL+.05 F.008
ZL=ZL-ZI
Z=ZL
X=XD+.05
G97 S=DIA
G00 X20 M00
X=XD+.1 Z=ZL+.1 S=DIA T050505 M3 M42

```

```
G96 S=CS
G01 X=XD Z=ZL+.05 F.01
Z-12.5
X=XD+.05
G97 S=DIA
PA=PA+1
G00 X20 Z20 M00
T111111 M00
T010101 M00
(PASS FOUR COMPLETE)
IF PG=1 GOTO N1000
IF PA=20 GOTO N1010
IF PA<20 GOTO N10
N1000 IF PA<12 GOTO N10
N1010 M02
```

APPENDIX B:

DATA SHEETS FOR EXPERIMENTAL DATA

Table B.1 The data sheet for the 0° side rake angle cutting tool at 25 m/min.

0° Side Rake Angle at 25 m/min					
Pass	X%Load	Z%Load	S%Load	cm ³ removal	cut time
1	17	25	49.5	99.14	0:06:45
2	16	24	50.5	96.99	0:06:36
3	16	24	48	94.83	0:06:24
4	15	24	48.5	92.68	0:06:17
5	16	25	46	90.52	0:06:06
6	16	25	44	88.37	0:05:59
7	16	24	43.5	86.21	0:05:48
8	15	24	42	84.06	0:05:43
9	17	25	41.5	81.90	0:05:33
10	16	24	39.5	79.75	0:05:23
11	16	24	40	77.59	0:05:15
12	16	25	38.5	75.43	0:05:06
Totals				1047.47	1:10:55

Table B.2 The data sheet for the 5° side rake angle cutting tool at 25 m/min

5° Side Rake Angle at 25 m/min					
Pass	X%Load	Z%Load	S%Load	cm ³ removal	cut time
1	15	23	40	99.14	0:06:43
2	16	23	38.5	96.99	0:06:37
3	15	22	36.5	94.83	0:06:23
4	15	22	36.5	92.68	0:06:16
5	15	22	36	90.52	0:06:05
6	16	24	36	88.37	0:06:00
7	15	23	35	86.21	0:05:48
8	15	22	33.5	84.06	0:05:43
9	15	22	31.5	81.90	0:05:32
10	16	24	31	79.75	0:05:24
11	16	22	33	77.59	0:05:15
12	15	23	31.5	75.43	0:05:06
Total				1047.47	1:10:52

Table B.3 The data sheet for the 10° side rake angle cutting tool at 25 m/min.

10° Side Rake Angle at 25 m/min					
Pass	X%Load	Z%Load	S%Load	cm ³ removal	cut time
1	15	23	37.5	99.14	0:06:47
2	15	22	39	96.99	0:06:37
3	16	23	39	94.83	0:06:24
4	15	22	35	92.68	0:06:17
5	15	22	36.5	90.52	0:06:05
6	15	22	36	88.37	0:05:59
7	16	23	37	86.21	0:05:48
8	15	22	35.5	84.06	0:05:42
9	15	22	33	81.90	0:05:33
10	15	23	33	79.75	0:05:24
11	16	23	32.5	77.59	0:05:14
12	15	22	31	75.43	0:05:06
Total				1047.47	1:10:56

Table B.4 The data sheet for the 15° side rake angle cutting tool at 25 m/min.

15° Side Rake Angle at 25 m/min					
Pass	X%Load	Z%Load	S%Load	cm ³ removal	cut time
1	14	22	36	99.14	0:06:42
2	14	22	35	96.99	0:06:37
3	14	21	35.5	94.83	0:06:19
4	15	22	33.5	92.68	0:06:17
5	14	21	34.5	90.52	0:06:05
6	14	21	34	88.37	0:05:59
7	14	21	33	86.21	0:05:48
8	16	22	31.5	84.06	0:05:43
9	14	21	31	81.90	0:05:33
10	14	22	30	79.75	0:05:24
11	14	22	28.5	77.59	0:05:15
12	16	23	28	75.43	0:05:06
Total				1047.47	1:10:48

Table B.5 The data sheet for the 0° side rake angle cutting tool at 30 m/min.

0° Side Rake Angle at 30 m/min					
Pass	X%Load	Z%Load	S%Load	cm ³ removal	cut time
1	17	26	34	72.67	0:04:04
2	17	24	33	70.53	0:03:55
3	17	25	32	68.39	0:03:49
4	16	25	31	66.26	0:03:47
5	17	25	30	64.12	0:03:36
6	16	25	29.5	61.98	0:03:28
7	17	25	29.5	59.85	0:03:21
8	17	25	28	57.71	0:03:14
9	17	26	28	55.57	0:03:07
10	17	24	25	53.44	0:03:00
11	17	25	25.5	51.30	0:02:52
12	16	24	21.5	49.16	0:02:45
13	16	26	22	47.03	0:02:38
14	17	24	21.5	44.89	0:02:31
15	17	25	20.5	42.75	0:02:23
16	17	25	20	40.62	0:02:15
17	30.5	28	21.5	38.48	0:02:08
18	17	24.5	17	36.34	0:02:01
19	18	26	19.5	34.21	0:01:54
20	18	31	22.5	32.07	0:01:47
Total				1047.39	0:58:35

Table B.6 The data sheet for the 5° side rake angle cutting tool at 30 m/min.

5° Side Rake Angle at 30 m/min					
Pass #	X%Load	Z%Load	S%Load	cm ³ removal	cut time
1	16	23	30.5	72.67	0:04:07
2	16	24	31	70.53	0:03:56
3	16	24	30.5	68.39	0:03:50
4	16	24	30.5	66.26	0:03:43
5	16	24	30	64.12	0:03:36
6	16	25	28	61.98	0:03:28
7	16	24	26.5	59.85	0:03:20
8	17	24	25.5	57.71	0:03:14
9	16	23	24.5	55.57	0:03:07
10	16	25	23	53.44	0:03:00
11	16	24	22	51.30	0:02:53
12	16	24	21	49.16	0:02:45
13	16	23	20.5	47.03	0:02:38
14	16	25	19.5	44.89	0:02:30
15	16	24	19	42.75	0:02:23
16	16	24	18	40.62	0:02:16
17	16	24	17	38.48	0:02:09
18	16	24	16	36.34	0:02:01
19	17	24	15	34.21	0:01:54
20	17	24	14.5	32.07	0:01:47
Total				1047.39	0:58:37

Table B.7 The data sheet for the 10° side rake angle cutting tool at 30 m/min.

10° Side Rake Angle at 30 m/min					
Pass	X%Load	Z%Load	S%Load	cm ³ removal	cut time
1	16	23	30	72.67	0:04:04
2	15	23	29	70.53	0:03:57
3	16	23	28	68.39	0:03:48
4	16	22	28	66.26	0:03:42
5	16	23	25.5	64.12	0:03:37
6	15	23	24	61.98	0:03:28
7	16	24	24	59.85	0:03:21
8	16	23	23	57.71	0:03:14
9	16	23	22.5	55.57	0:03:07
10	15	23	22	53.44	0:02:59
11	16	24	21	51.30	0:02:53
12	16	23	20	49.16	0:02:45
13	16	23	19.5	47.03	0:02:39
14	15	23	18.5	44.89	0:02:30
15	17	24	17.5	42.75	0:02:23
16	16	23	17	40.62	0:02:16
17	16	23	16	38.48	0:02:08
18	16	23	15	36.34	0:02:01
19	16	24	14	34.21	0:01:54
20	17	23	14	32.07	0:01:46
Total				1047.39	0:58:32

Table B.8 The data sheet for the 15° side rake angle cutting tool at 35 m/min.

15° Side Rake Angle at 30 m/min					
Pass #	X%Load	Z%Load	S%Load	cm ³ removal	cut time
1	15	22	27.5	72.67	0:04:04
2	15	22	24.5	70.53	0:03:56
3	15	22	24.5	68.39	0:03:49
4	16	23	24	66.26	0:03:42
5	15	22	23	64.12	0:03:36
6	15	22	22.5	61.98	0:03:27
7	15	22	21.5	59.85	0:03:21
8	16	23	20.5	57.71	0:03:14
9	15	22	20	55.57	0:03:06
10	15	22	19	53.44	0:03:00
11	15	22	18	51.30	0:02:53
12	16	23	18	49.16	0:02:45
13	15	22	17	47.03	0:02:38
14	15	22	16	44.89	0:02:30
15	15	22	15.5	42.75	0:02:22
16	17	23	15	40.62	0:02:15
17	15	22	14	38.48	0:02:09
18	16	23	13	36.34	0:02:01
19	17	22	12	34.21	0:01:54
20	16	23	11.5	32.07	0:01:47
Total				1047.39	0:58:29

Table B.9 The data sheet for the 0° side rake angle cutting tool at 35 m/min.

0° Side Rake Angle at 35 m/min					
Pass	X%Load	Z%Load	S%Load	cm ³ removal	cut time
1	18	26	47.5	98.21	0:04:43
2	16	24	43.5	96.22	0:04:38
3	16	24	41	94.23	0:04:31
4	16	24	40	92.25	0:04:25
5	17	25	41	90.26	0:04:22
6	16	24	38	88.27	0:04:15
7	16	23	38	86.28	0:04:08
8	16	23	38	84.29	0:04:04
9	17	24	37.5	82.30	0:03:57
10	16	24	35.5	80.31	0:03:50
11	16	23	34.5	78.32	0:03:45
12	16	24	33.5	76.33	0:03:40
Total				1047.27	0:50:18

Table B.10 The data sheet for the 5° side rake angle cutting tool at 35 m/min.

5° Side Rake Angle at 35 m/min					
Pass	X%Load	Z%Load	S%Load	cm ³ removal	cut time
1	16	24	42.5	98.21	0:04:42
2	16	24	40	96.22	0:04:38
3	16	23	39.5	94.23	0:04:31
4	16	23	39.5	92.25	0:04:25
5	16	23	38	90.26	0:04:22
6	16	24	38.5	88.27	0:04:15
7	16	23	37	86.28	0:04:09
8	16	23	35.5	84.29	0:04:03
9	16	23	34.5	82.30	0:03:58
10	16	24	34	80.31	0:03:50
11	16	23	33.5	78.32	0:03:45
12	16	23	32.5	76.33	0:03:40
Total				1047.27	0:50:18

Table B.11 The data sheet for the 10° side rake angle cutting tool at 35 m/min.

10° Side Rake Angle at 35 m/min					
Pass #	X%Load	Z%Load	S%Load	cm ³ removal	cut time
1	16	23	38.5	98.21	0:04:42
2	16	23	40	96.22	0:04:38
3	16	24	39.5	94.23	0:04:31
4	16	23	38.5	92.25	0:04:24
5	16	23	37	90.26	0:04:21
6	16	23	37.5	88.27	0:04:15
7	16	24	36	86.28	0:04:09
8	16	23	34.5	84.29	0:04:04
9	16	23	34.5	82.30	0:03:57
10	16	23	33.5	80.31	0:03:50
11	16	24	33.5	78.32	0:03:45
12	16	23	32.5	76.33	0:03:40
Total				1047.27	0:50:16

Table B.12 The data sheet for the 15° side rake angle cutting tool at 35 m/min.

15° Side Rake Angle at 35 m/min					
Pass #	X%Load	Z%Load	S%Load	cm ³ removal	cut time
1	15	23	38.5	98.21	0:04:43
2	16	22	37.5	96.22	0:04:39
3	15	22	35	94.23	0:04:32
4	16	23	36	92.25	0:04:25
5	15	22	35.5	90.26	0:04:21
6	15	22	33	88.27	0:04:15
7	16	22	32.5	86.28	0:04:09
8	16	23	31.5	84.29	0:04:03
9	16	22	31	82.30	0:03:58
10	16	22	30	80.31	0:03:50
11	16	22	29.5	78.32	0:03:45
12	16	23	29	76.33	0:03:40
Total				1047.27	0:50:20

Table B.13 The raw data for the force calculations.

<i>Cutting speed(m/min)</i>	<i>Rake angle (degrees)</i>	<i>Current before cut (amps)</i>	<i>Max Current (amps)</i>	<i>Diameter (inches)</i>	<i>Volts from data plate</i>
25	0	7.9	36.60	3.612	170
	5	7.9	36.10	3.612	170
	10	7.9	34.00	3.612	170
	15	7.9	33.20	3.612	170
30	0	8.17	41.57	3.010	170
	5	8.17	39.80	3.010	170
	10	8.17	35.88	3.010	170
	15	8.17	35.50	3.010	170
35	0	8.56	49.50	3.128	170
	5	8.56	40.20	3.128	170
	10	8.56	38.30	3.128	170
	15	8.56	34.30	3.128	170

APPENDIX C:

CHIP THICKNESS MEASUREMENTS

Table C.1 Chip Thickness measurements taken from experimental data chips.

0° Side Rake Angle at 25 m/min													inch	mm	
Pass 1	0.025	0.031	0.028	0.025	0.024	0.025	0.026	0.023	0.023	0.023	0.025	0.023	0.025	0.0255	0.648
Pass 3	0.025	0.026	0.025	0.028	0.024	0.028	0.025	0.035	0.028	0.028	0.028	0.028	0.022	0.0266	0.676
Pass 4	0.027	0.023	0.027	0.022	0.025	0.032	0.029	0.026	0.023	0.023	0.026	0.023	0.026	0.0260	0.660
Pass 6	0.029	0.025	0.028	0.033	0.023	0.028	0.023	0.033	0.023	0.023	0.027	0.023	0.027	0.0272	0.691
Pass 8	0.036	0.023	0.020	0.035	0.022	0.031	0.024	0.026	0.025	0.025	0.022	0.025	0.022	0.0264	0.671
Pass 12	0.029	0.029	0.023	0.033	0.027	0.028	0.027	0.024	0.025	0.025	0.023	0.025	0.023	0.0268	0.681
Average													0.0264	0.671	
5° Side Rake Angle at 25 m/min													Inch	mm	
Pass 1	0.023	0.029	0.019	0.022	0.015	0.016	0.024	0.025	0.026	0.025	0.017	0.026	0.017	0.0216	0.549
Pass 3	0.017	0.021	0.017	0.018	0.017	0.017	0.024	0.020	0.016	0.020	0.022	0.016	0.022	0.0189	0.480
Pass 4	0.023	0.021	0.024	0.022	0.024	0.022	0.020	0.019	0.021	0.019	0.027	0.021	0.027	0.0223	0.566
Pass 6	0.029	0.024	0.021	0.024	0.020	0.019	0.021	0.024	0.022	0.022	0.020	0.022	0.020	0.0224	0.569
Pass 8	0.022	0.021	0.013	0.023	0.023	0.026	0.022	0.022	0.023	0.022	0.017	0.023	0.017	0.0212	0.538
Pass 12	0.026	0.024	0.025	0.022	0.026	0.026	0.022	0.024	0.026	0.024	0.024	0.026	0.024	0.0245	0.622
Average													0.0218	0.554	

Table C.1 continued

10° Side Rake Angle at 25 m/min													inch	mm
Pass 1	0.022	0.018	0.021	0.017	0.019	0.022	0.025	0.019	0.015	0.017	0.0195	0.495		
Pass 3	0.025	0.022	0.022	0.021	0.022	0.021	0.019	0.018	0.018	0.021	0.0209	0.531		
Pass 4	0.021	0.023	0.020	0.021	0.020	0.015	0.017	0.019	0.015	0.024	0.0195	0.495		
Pass 6	0.023	0.022	0.024	0.022	0.023	0.021	0.021	0.021	0.022	0.023	0.0222	0.564		
Pass 8	0.022	0.021	0.023	0.023	0.024	0.022	0.019	0.022	0.020	0.022	0.0218	0.554		
Pass 12	0.020	0.021	0.019	0.021	0.019	0.020	0.021	0.015	0.017	0.021	0.0194	0.493		
Average													0.0206	0.522
15° Side Rake Angle at 25 m/min													inch	mm
Pass 1	0.019	0.020	0.022	0.020	0.019	0.018	0.024	0.017	0.021	0.019	0.0199	0.505		
Pass 3	0.021	0.018	0.016	0.019	0.017	0.017	0.015	0.018	0.017	0.018	0.0176	0.447		
Pass 4	0.019	0.019	0.021	0.018	0.018	0.018	0.021	0.020	0.019	0.019	0.0192	0.488		
Pass 6	0.017	0.017	0.018	0.016	0.016	0.018	0.016	0.021	0.017	0.016	0.0172	0.437		
Pass 8	0.019	0.019	0.016	0.017	0.020	0.019	0.018	0.016	0.018	0.019	0.0181	0.460		
Pass 12	0.020	0.017	0.018	0.017	0.018	0.020	0.021	0.021	0.018	0.020	0.0190	0.483		
Average													0.0185	0.470

Table C.1 continued

0° Side Rake Angle at 30 m/min													inch	mm
Pass 2	0.027	0.033	0.025	0.035	0.024	0.035	0.028	0.034	0.027	0.029	0.029	0.029	0.0297	0.754
Pass 4	0.031	0.021	0.028	0.028	0.021	0.029	0.025	0.023	0.028	0.025	0.025	0.025	0.0259	0.658
Pass 6	0.029	0.027	0.025	0.028	0.026	0.027	0.026	0.025	0.026	0.034	0.026	0.034	0.0273	0.693
Pass 9	0.031	0.027	0.029	0.025	0.023	0.026	0.032	0.025	0.024	0.026	0.026	0.026	0.0268	0.681
Pass 12	0.024	0.021	0.022	0.025	0.027	0.024	0.026	0.023	0.028	0.023	0.023	0.023	0.0243	0.617
Pass 20	0.046	0.038	0.048	0.048	0.028	0.024	0.029	0.031	0.031	0.034	0.034	0.034	0.0357	0.907
Average													0.0283	0.718
5° Side Rake Angle at 30 m/min													inch	mm
Pass 2	0.024	0.022	0.024	0.024	0.026	0.026	0.021	0.025	0.026	0.024	0.026	0.024	0.0242	0.615
Pass 4	0.025	0.024	0.022	0.020	0.026	0.024	0.024	0.022	0.023	0.023	0.023	0.023	0.0233	0.592
Pass 6	0.025	0.027	0.015	0.026	0.026	0.025	0.027	0.025	0.023	0.028	0.023	0.028	0.0247	0.627
Pass 9	0.024	0.029	0.026	0.023	0.024	0.019	0.023	0.022	0.026	0.028	0.028	0.0244	0.620	
Pass 12	0.027	0.025	0.026	0.027	0.023	0.025	0.027	0.023	0.022	0.021	0.021	0.0246	0.625	
Pass 20	0.025	0.029	0.028	0.028	0.030	0.027	0.027	0.030	0.027	0.026	0.026	0.0277	0.704	
Average													0.0248	0.630

Table C.1 continued

10° Side Rake Angle at 30 m/min													inch	mm			
Pass 2	0.020	0.022	0.021	0.022	0.021	0.022	0.021	0.022	0.021	0.022	0.021	0.022	0.023	0.025	0.024	0.0221	0.561
Pass 4	0.022	0.023	0.022	0.022	0.021	0.022	0.021	0.022	0.021	0.022	0.021	0.022	0.026	0.021	0.020	0.0216	0.549
Pass 6	0.023	0.025	0.021	0.023	0.021	0.023	0.022	0.022	0.023	0.022	0.022	0.020	0.020	0.026	0.023	0.0228	0.579
Pass 9	0.022	0.027	0.022	0.027	0.022	0.027	0.028	0.022	0.023	0.022	0.022	0.022	0.022	0.023	0.024	0.0240	0.610
Pass 12	0.019	0.022	0.021	0.022	0.021	0.020	0.021	0.024	0.025	0.020	0.020	0.020	0.022	0.022	0.022	0.0216	0.549
Pass 20	0.026	0.025	0.022	0.025	0.022	0.027	0.025	0.025	0.024	0.026	0.025	0.026	0.026	0.026	0.024	0.0250	0.635
Average													0.0229	0.580			
15° Side Rake Angle at 30 m/min													inch	mm			
Pass 2	0.022	0.020	0.017	0.020	0.017	0.021	0.017	0.018	0.022	0.025	0.017	0.021	0.025	0.016	0.020	0.0198	0.503
Pass 4	0.022	0.021	0.017	0.020	0.017	0.020	0.021	0.025	0.019	0.020	0.021	0.025	0.018	0.023	0.0206	0.523	
Pass 6	0.023	0.021	0.019	0.021	0.019	0.017	0.020	0.018	0.021	0.020	0.020	0.020	0.021	0.019	0.0199	0.505	
Pass 9	0.022	0.022	0.019	0.022	0.019	0.021	0.021	0.021	0.022	0.019	0.021	0.022	0.022	0.022	0.0211	0.536	
Pass 12	0.022	0.022	0.019	0.022	0.019	0.021	0.020	0.020	0.020	0.016	0.020	0.020	0.020	0.019	0.0199	0.505	
Pass 20	0.023	0.022	0.023	0.022	0.023	0.020	0.021	0.023	0.020	0.023	0.021	0.020	0.020	0.023	0.0218	0.554	
Average													0.0205	0.521			

Table C.1 continued

0° Side Rake Angle at 35 m/min													inch	mm	
Pass 1	0.030	0.025	0.029	0.025	0.033	0.026	0.023	0.025	0.025	0.026	0.025	0.025	0.025	0.0267	0.678
Pass 3	0.029	0.025	0.020	0.032	0.025	0.032	0.028	0.028	0.027	0.030	0.027	0.030	0.028	0.0276	0.701
Pass 4	0.027	0.022	0.028	0.026	0.028	0.023	0.029	0.029	0.030	0.025	0.030	0.025	0.021	0.0259	0.658
Pass 6	0.029	0.024	0.026	0.025	0.024	0.023	0.029	0.029	0.027	0.025	0.027	0.025	0.026	0.0258	0.655
Pass 8	0.022	0.028	0.023	0.031	0.028	0.022	0.020	0.020	0.026	0.021	0.026	0.021	0.033	0.0254	0.645
Pass 12	0.021	0.025	0.026	0.023	0.022	0.026	0.027	0.027	0.025	0.025	0.025	0.025	0.031	0.0251	0.638
Average													0.0261	0.663	
5° Side Rake Angle at 35 m/min													inch	mm	
Pass 1	0.029	0.021	0.023	0.027	0.030	0.028	0.029	0.029	0.018	0.027	0.018	0.027	0.020	0.0252	0.640
Pass 3	0.029	0.028	0.028	0.030	0.025	0.024	0.032	0.032	0.024	0.030	0.024	0.030	0.020	0.0270	0.686
Pass 4	0.028	0.020	0.022	0.030	0.029	0.029	0.028	0.028	0.023	0.026	0.023	0.026	0.025	0.0260	0.660
Pass 6	0.023	0.023	0.021	0.026	0.021	0.020	0.026	0.026	0.028	0.028	0.028	0.028	0.024	0.0240	0.610
Pass 8	0.022	0.020	0.023	0.024	0.027	0.026	0.023	0.023	0.026	0.021	0.026	0.021	0.025	0.0237	0.602
Pass 12	0.025	0.022	0.023	0.026	0.027	0.024	0.024	0.024	0.025	0.030	0.025	0.030	0.023	0.0249	0.632
Average													0.0251	0.638	

Table C.1 continued

10° Side Rake Angle at 35 m/min													inch	mm
Pass 1	0.021	0.022	0.024	0.021	0.019	0.021	0.024	0.020	0.025	0.018	0.0215	0.546		
Pass 3	0.023	0.022	0.028	0.022	0.021	0.018	0.022	0.024	0.024	0.019	0.0223	0.566		
Pass 4	0.028	0.024	0.026	0.023	0.024	0.023	0.023	0.022	0.022	0.024	0.0239	0.607		
Pass 6	0.021	0.016	0.022	0.020	0.020	0.023	0.021	0.025	0.018	0.025	0.0211	0.536		
Pass 8	0.026	0.019	0.021	0.022	0.024	0.027	0.025	0.021	0.020	0.022	0.0227	0.577		
Pass 12	0.022	0.020	0.025	0.024	0.022	0.018	0.021	0.024	0.022	0.021	0.0219	0.556		
Average													0.0222	0.565
15° Side Rake Angle at 35 m/min													inch	mm
Pass 1	0.019	0.020	0.021	0.021	0.021	0.020	0.017	0.024	0.022	0.018	0.0203	0.516		
Pass 3	0.023	0.019	0.024	0.020	0.024	0.024	0.023	0.020	0.020	0.022	0.0219	0.556		
Pass 4	0.022	0.024	0.020	0.019	0.023	0.023	0.024	0.026	0.022	0.023	0.0226	0.574		
Pass 6	0.021	0.022	0.021	0.022	0.022	0.022	0.021	0.019	0.023	0.022	0.0215	0.546		
Pass 8	0.022	0.022	0.017	0.026	0.024	0.022	0.021	0.020	0.023	0.020	0.0217	0.551		
Pass 12	0.025	0.021	0.019	0.020	0.025	0.025	0.025	0.024	0.023	0.023	0.0230	0.584		
Average													0.0218	0.555

APPENDIX D:
CHIP PICTURES COMPLETE



Figure D.1 Chip images for the 0° side rake angle cutting tool at 25 m/min.



Figure D.2 Chip images for the 5° side rake angle cutting tool at 25 m/min.

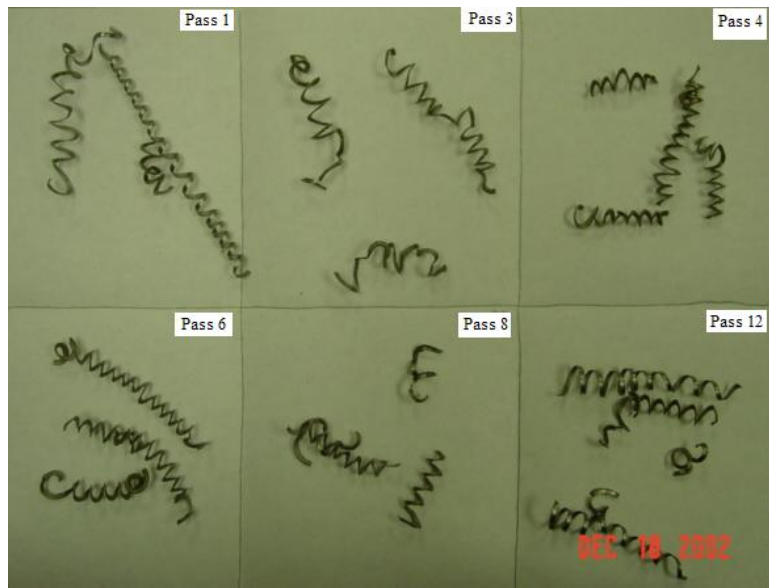


Figure D.3 Chip images for the 10° side rake angle cutting tool at 25 m/min.

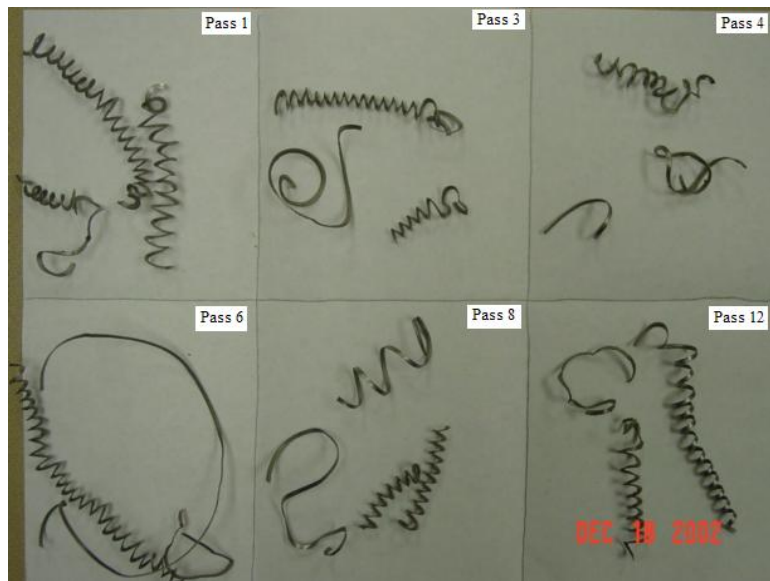


Figure D.4 Chip images for the 15° side rake angle cutting tool at 25 m/min.



Figure D.5 Chip images for the 0° side rake angle cutting tool at 30 m/min.



Figure D.6 Chip images for the 5° side rake angle cutting tool at 30 m/min.

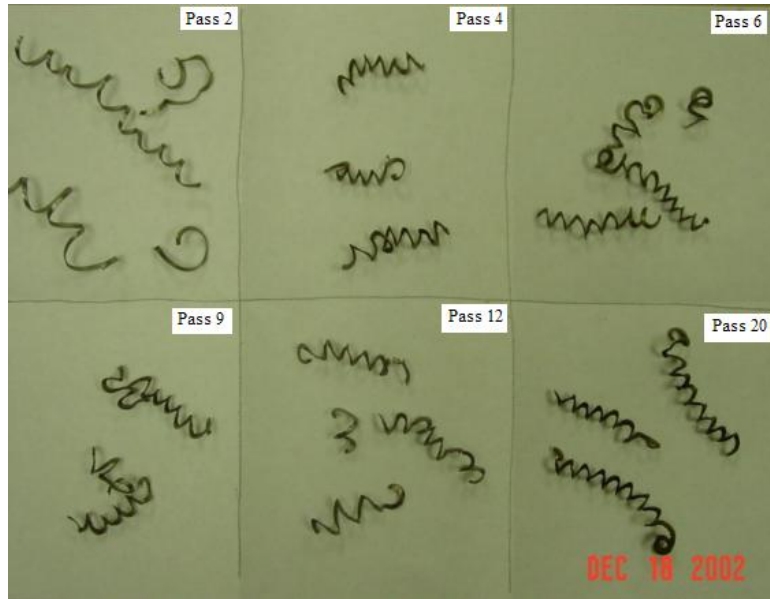


Figure D.7 Chip images for the 10° side rake angle cutting tool at 30 m/min.

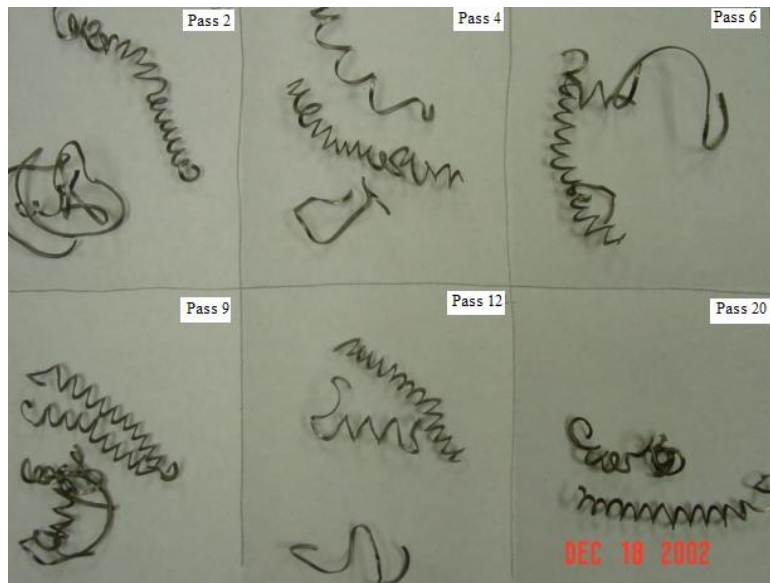


Figure D.8 Chip images for the 15° side rake angle cutting tool at 30 m/min.



Figure D.9 Chip images for the 0° side rake angle cutting tool at 35 m/min.



Figure D.10 Chip images for the 5° side rake angle cutting tool at 35 m/min.



Figure D.11 Chip images for the 10° side rake angle cutting tool at 35 m/min.

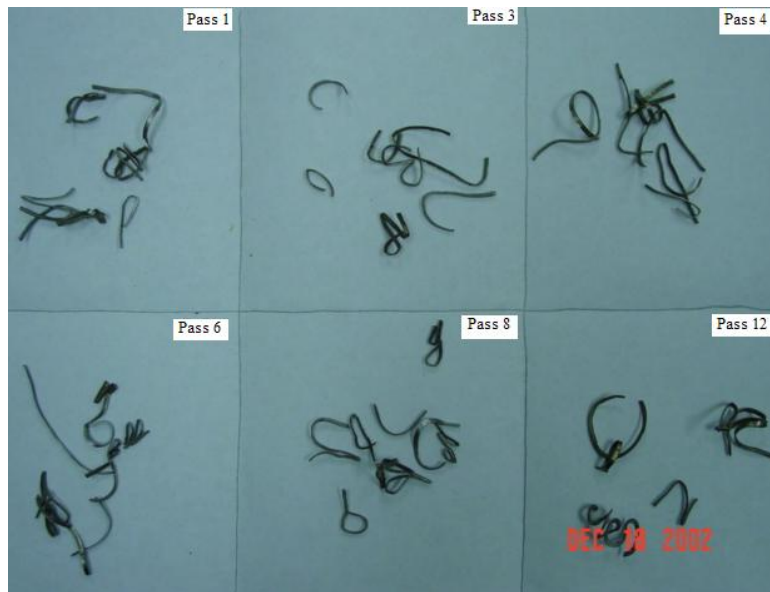


Figure D.12 Chip images for the 15° side rake angle cutting tool at 35 m/min.

APPENDIX E:

EXPERIMENTAL AND SIMULATION RAW DATA

Table E.1 Raw data for the experimental results.

<i>Cutting speed (m/min)</i>	<i>Rake Angle (degrees)</i>	<i>Shear Angle (degrees)</i>	<i>Cutting ratio</i>	<i>Contact length (mm)</i>	<i>Force (lbs)</i>	<i>Chip Thickness (mm)</i>	<i>Crater Depth (mm)</i>
25	0	16.72	0.300	0.625	219	0.671	0.0508
	5	20.52	0.364	0.456	216	0.554	0.0686
	10	22.18	0.386	0.423	200	0.522	0.0762
	15	24.99	0.429	0.371	193	0.470	0.0432
30	0	15.67	0.281	0.559	213	0.718	0.0305
	5	18.15	0.320	0.352	202	0.630	0.0508
	10	20.00	0.347	0.444	177	0.580	0.0280
	15	22.55	0.387	0.396	174	0.521	0.0254
35	0	16.92	0.304	0.400	224	0.663	0.0356
	5	17.93	0.316	0.325	173	0.638	0.0152
	10	20.54	0.357	0.453	162	0.565	0.0076
	15	21.19	0.364	0.435	141	0.554	0.0305

Table E.2 Raw data for the simulation results.

<i>Cutting speed (m/min)</i>	<i>Rake angle (degrees)</i>	<i>Shear angle (degrees)</i>	<i>Cutting ratio</i>	<i>Contact length (mm)</i>	<i>Force (lbs)</i>	<i>Chip Thickness (mm)</i>
25	0	29.68	0.570	0.430	216	0.351
	5	34.90	0.660	0.380	214	0.303
	10	35.81	0.650	0.343	192	0.308
	15	40.04	0.710	0.293	191	0.282
30	0	27.76	0.526	0.380	257	0.380
	5	31.78	0.590	0.383	248	0.339
	10	33.18	0.595	0.370	215	0.336
	15	34.77	0.606	0.330	215	0.330
35	0	27.76	0.526	0.385	224	0.380
	5	30.93	0.571	0.340	191	0.350
	10	31.99	0.571	0.336	185	0.350
	15	34.77	0.606	0.330	185	0.330

APPENDIX F:
TOOL WEAR IMAGES

Table F.1 The 25 m/min cutting speed before and after tool wear images.

25 m/min cutting speed				
	Rake Face		Flank Face	
Rake angle (°)	Before	After	Before	After
0				
5				
10				
15				

Table F.2 The 30 m/min cutting speed before and after tool wear images.

30 m/min cutting speed				
	Rake Face		Flank Face	
Rake angle (°)	Before	After	Before	After
0				
5				
10				
15				

Table F.3 The 35 m/min cutting speed before and after tool wear images.

35 m/min cutting speed				
	Rake Face		Flank Face	
Rake angle (°)	Before	After	Before	After
0				
5				
10				
15				

APPENDIX G:
COMPUTER SIMULATION IMAGES

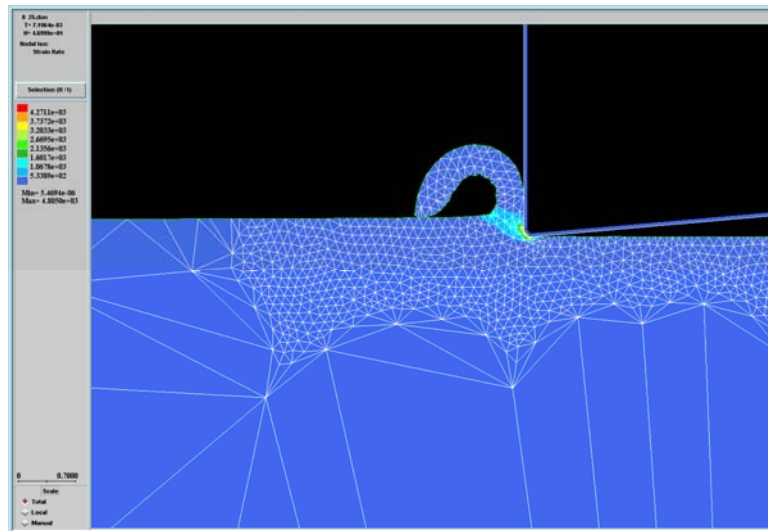


Figure G.1 The computer simulation image for the 0° side rake angle cutting tool at 25 m/min.

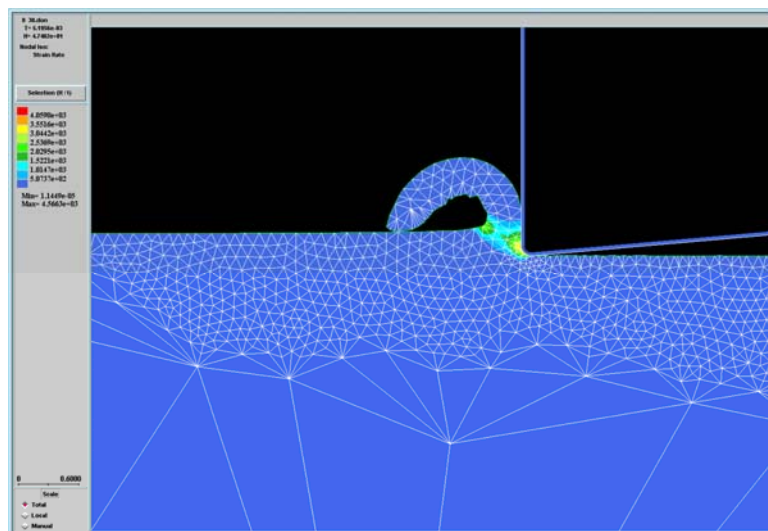


Figure G.2 The computer simulation image for the 0° side rake angle cutting tool at 30 m/min.

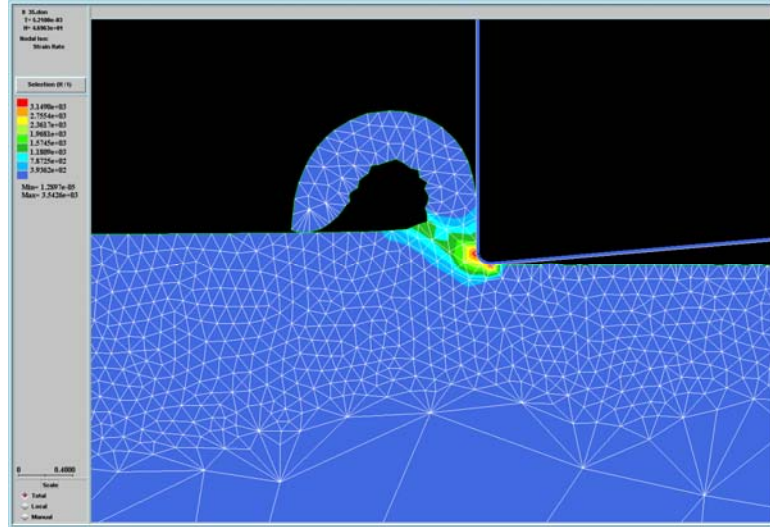


Figure G.3 The computer simulation image for the 0° side rake angle cutting tool at 35 m/min.

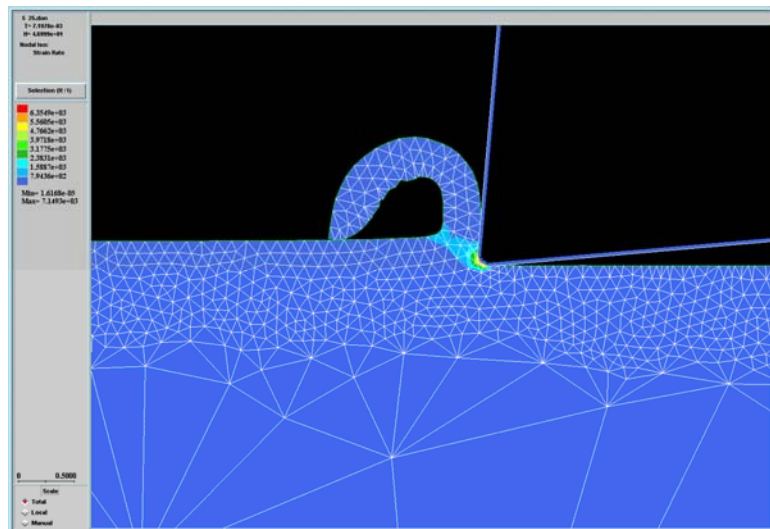


Figure G.4 The computer simulation image for the 5° side rake angle cutting tool at 25 m/min.

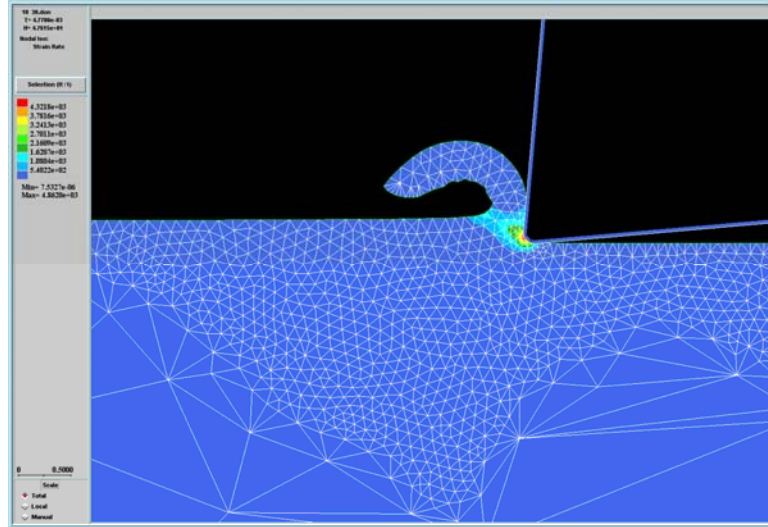


Figure G.5 The computer simulation image for the 5° side rake angle cutting tool at 30 m/min.

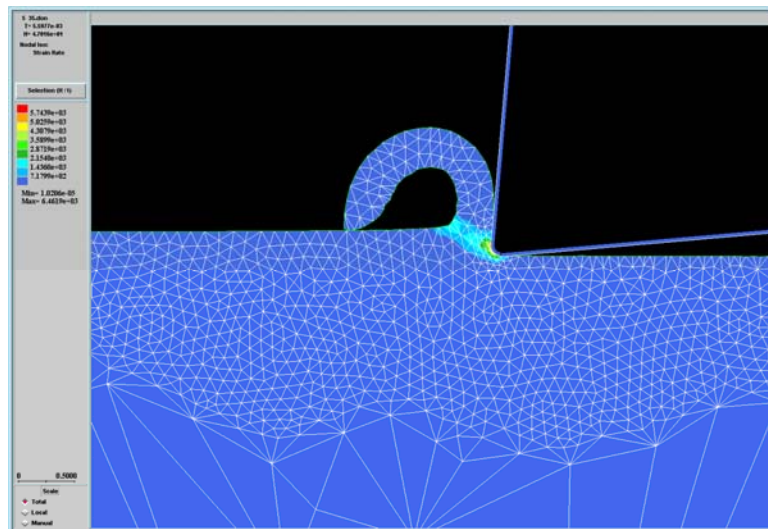


Figure G.6 The computer simulation image for the 5° side rake angle cutting tool at 35 m/min.

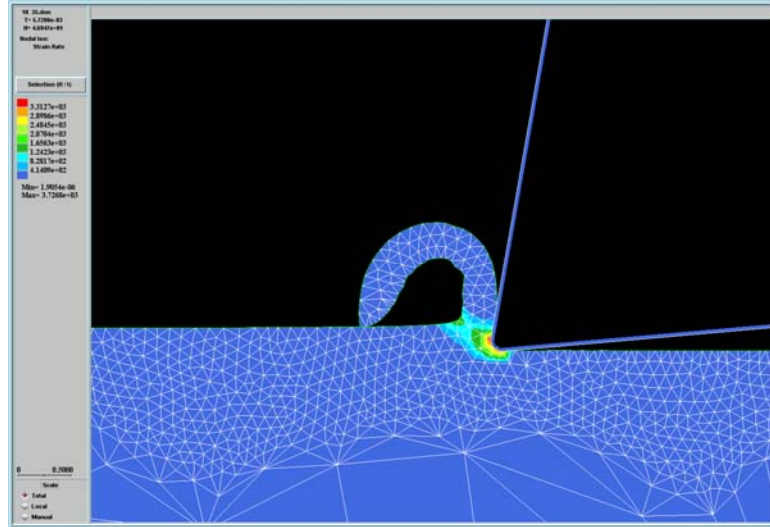


Figure G.9 The computer simulation image for the 10° side rake angle cutting tool at 35 m/min.

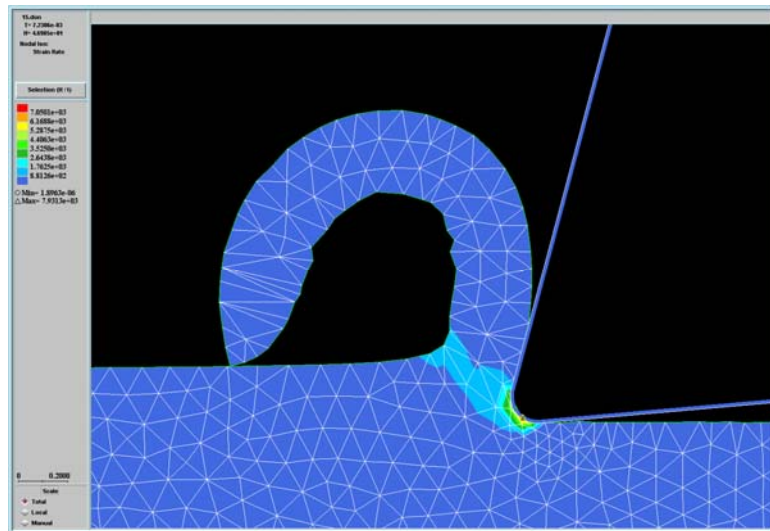


Figure G.10 The computer simulation image for the 15° side rake angle cutting tool at 25 m/min.

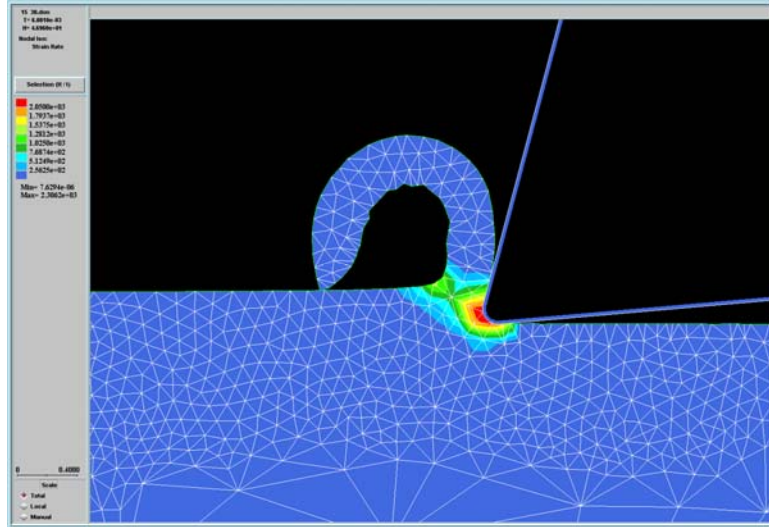


Figure G.11 The computer simulation image for the 15° side rake angle cutting tool at 30 m/min.

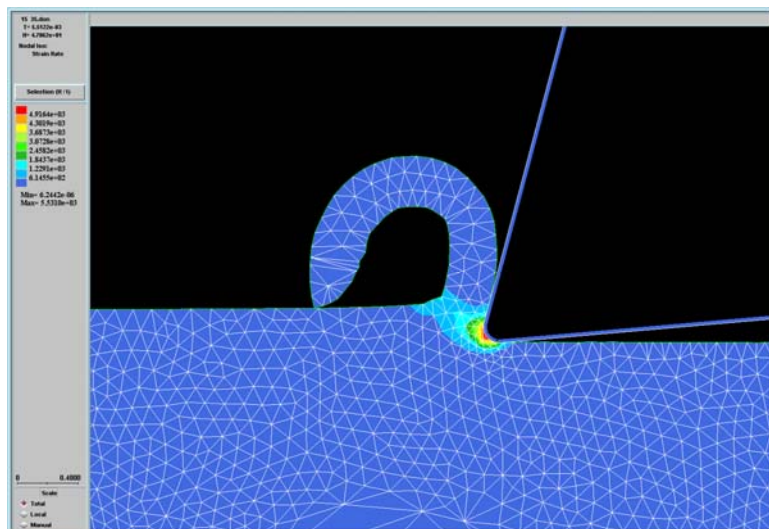


Figure G.12 The computer simulation image for the 15° side rake angle cutting tool at 35 m/min.